Unravelling the Role of Ascorbic Acid and ER Stress in SEPN1-Related Myopathy

Thesis

Unravelling the role of ascorbic acid and ER stress in SEPN1-related myopathy

Thesis submitted by Diego Pozzer

Istituto di Ricerche Farmacologiche Mario Negri IRCCS, Milan, Italy

for the degree of

Doctor of Philosophy

The Open University, UK, Discipline of Life and Biomolecular Sciences

September 2019

Abstract

Selenoprotein N1 (SEPN1) is a member of the selenocysteine-containing protein family, that is localised in the endoplasmic reticulum (ER) and ubiquitously expressed throughout the body.

Mutations in the human *SEPN1* gene were identified as the genetic cause of a muscle disease referred as SEPN1-related myopathy (SEPN1-RM), in which the main clinical features are axial weakness, scoliosis, a variable degree of spinal rigidity, respiratory failure and insulin resistance.

The selective muscle phenotype of the human SEPN1 loss of function, the redox nature of SEPN1, and the fact that SEPN1-depleted cells show oxidative stress support the idea that SEPN1 may be involved in protecting muscle ER redox homeostasis.

Ascorbic acid is an important antioxidant that is localized in the cytoplasm and in the endoplasmic reticulum lumen, since it is a cofactor needed in the folding of pro-collagen. Malnutrition characterized by low intake of ascorbic acid affects skeletal muscles, in terms of fatigue and myalgia.

Thus, both ascorbic acid and SEPN1 deficiency bring to the development of a myopathic condition, which can be explained by the fact that the two molecules have overlapping functions and intracellular localization.

To test the hypothesis that the anti-oxidant vitamin ascorbic acid protects SEPN1 knock out (KO) muscles from the consequences of SEPN1 loss of function we developed a mouse model mutant of SEPN1, which is also dependent on exogenous ascorbic acid. Our findings showed that a limited intake of ascorbic acid triggers ER

stress and exacerbates SEPN1-related myopathic phenotype suggesting a protective role of the ascorbic acid in SEPN1 KO muscle. We also found that the highly active diaphragm muscle shows impaired force production and ER stress in SEPN1 KO mice and that the ablation of the ER stress mediator C/EBP homologous protein (CHOP) prevents diaphragm dysfunction and attenuates ER stress in SEPN1 KO mice.

Lipotoxicity, meaning an overload of fatty acids, is among the conditions able to trigger ER stress. By feeding SEPN1 KO mice with a high-fat diet, we observed that the myopathic phenotype is not only restricted to the diaphragm, but also to the hind limb muscles of SEPN1 KO mice. These mice developed myopathic features that were characterised by the insurgence of ER stress.

These findings suggest that ER stress is a novel pathogenic mechanism underlying SEPN1-RM and therefore reveal a therapeutic target for this disease, for which no treatment is currently available.

Preface

In this thesis it is reported the work that I've carried out during my PhD program from October 2015 to October 2019 under the supervision and direction of Dr. Ester Zito (director of the studies) and Prof. David Ron and Stefan Marciniak (external supervisors) at the Istituto di Ricerche Farmacologiche Mario Negri IRCCS.

Declaration

This PhD research project has not been submitted in whole or in part for a degree or diploma or other qualification to any other university. The experimental work described herein was performed by myself, Diego Pozzer, and also includes some work carried out in collaboration with the members of the laboratory of Signal Transduction and with:

- Dr. William Invernizzi, head of "Neurochemistry and behaviour Lab" at the Istituto di Ricerche Farmacologiche Mario Negri IRCCS in Milan, who is an expert in ascorbic acid measurements.
- Prof. Bert Blaaw, Associate Professor at the Università degli Studi di Padova and group leader at VIMM (Venetian Institute of Molecular Medicine), who took care of the measurements of the muscle force.

Acknowledgments

First of all, I would like to thank my supervisor Dr. Ester Zito. In her lab I learned the traits that a good researcher should develop, such as the importance of creating a proper hypothesis with clear goals and the need of planning in details every aspect of an experiment.

Special thanks to my external supervisors, Dr. David Ron and Dr. Stefan Marciniak, who, throughout the four years of PhD, gave me opinions and support.

Dr. William Invernizzi and Prof. Bert Blaauw have been extremely kind to me, sharing their knowledge and expertise in the HPLC and muscle force measurements respectively.

Heartfelt gratitude to my previous and present lab mates, with honourable mentions to Alex, Ersilia and Simona, and to all of the friends that I made here in the Institute.

I understood that a positive working environment is crucial to sustain the challenges that this job arises constantly, and should be always pursued from all the members of the lab.

List of Abbreviations

2DG = H^3-2-deoxyglucose

ASC and AA = Ascorbic Acid

ATF6 = Activating Transcription Factor 6

ATP = Adenosine TrisPhosphate

BIP = Binding Immunoglobulin Protein

CHOP = C/EBP homologous protein

CFTD = congenital fiber type disproportion

CHOP = C/EBP homologous protein

CRU = Calcium Release Unit

DHA = DeHydroAscorbic acid

DHPR = DiHydroPyridine Receptor

EC-Coupling = Excitation-Contraction coupling

ECM = Extra-Cellular Matrix

eIF2-α = eukaryotic Initiation Factor 2-alpha

ER = Endoplasmic Reticulum

ERAD = ER-Associated protein Degradation

ERO1 = ER Oxidoreductin 1

ERp44 = Endoplasmic Reticulum resident protein 44

FADH = Flavin Adenine Dinucleotide (reduced)

GADD34 = Growth Arrest and DNA Damage-inducible protein 34

GLUT = GLUcose Transporter

GPX = Glutathione PeroXidase

GSH = Glutathione

HFD = High-Fat Diet

IMM = Inner Mitochondrial Membrane

IP3R1 = Inositol 1,4,5-trisphosphate Receptor isoform 1

IRE1 = Inositol-Requiring Enzyme 1

JSR = Junctional Sarcoplasmic Reticulum

KD = Keshan Disease

GULO = l-GULOno-lactone oxidase

MB-DRM = Desmin-Related Myopathy with Mallory Body-like inclusions

MmD = Multi-minicore Disease

NADH = Nicotinamide Adenine Dinucleotide (reduced)

NADPH = Nicotinamide Adenine Dinucleotide Phosphate (reduced)

NOX4 = NADPH Oxidase 4

OMM = Outer Mitochondrial Membrane

OxPhos = Oxidative Phosphorylation

PDI = Protein Disulfide Isomerase

PERK = Protein kinase r-like ER Kinase

PP1 = Protein Phosphatase 1

PRDX4 = PeRoxireDoXin-4

ROS = Reactive Oxygen Species

RyR1 = Ryanodine Receptor 1

SECIS = SElenoCysteine Insertion Sequence

SelK = Selenoprotein K

SEPN1-RM = SEPN1-Related Myopathy

SERCA2 = Sarco-Endoplasmic Reticulum Calcium ATPase 2

SR = Sarcoplasmic Reticulum

SRE = Selenocysteine codon Redefinition Element

SVCT = Sodium dependent Vitamin C Transporter

Trx = ThioRedoXin

TrxRs = Thioredoxin Reductases

T-tubule = Transverse tubule

UPR = Unfolded Protein Response

WMD = White Muscle Disease

XBP1 = X Box Binding Protein 1

Index

Chapter 1 – Introduction

1.1 - Selenium

1.1.1 - An introduction to selenium

Selenium is a chemical metalloid element, discovered in 1817 by Jöns Jacob Berzelius, towards which the interest has grown over the years, due to some contradictory conclusions regarding its impact on human health.

The main source of selenium comes from food, particularly cereals, meat, fish and dairy products, although it is believed that the worldwide difference in the amount of selenium among living beings reflects the levels of selenium in the soils (Rayman, 2008) (Figure 1).

The recommended amount of daily intake of selenium is 53 µg per day for women and 60 µg per day for men (Rayman, 2004) but up to 800 µg per day of selenium showed no adverse effects (Weekley and Harris, 2013).

Selenium is incorporated in mammals primarily as selenocysteine, an amino acid incorporated in the selenoproteins (Figure 2).

Name	Molecular structure	Molecular formulae	Distribution
Selenium, elemental	[COMPLEX STRUCTURE]	Se^0	Soil
Hydrogen selenide Selenide	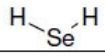	H_2Se; Se^{2-}	Mammals
Selenate	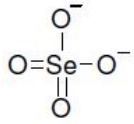	$SeO4_{2-}$	Soil, plants and mammals
Selenite	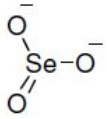	SeO_3^{2-}	Soil, plants and mammals

Figure 1 - Inorganic forms of selenium and their distribution (Rocha et al., 2016).

Name	Molecular structure	Molecular formulae	Distribution
Selenocysteine	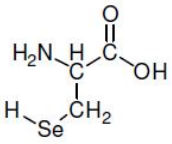	$C_3H_7NO_2Se$	Plants
Seleno-homocysteine	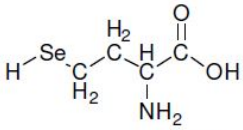	$C_4H_9NO_2Se$	Plants and mammals
Seleno-methionine	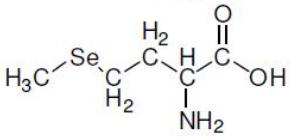	$C_5H_{11}NO_2Se$	Plants and mammals
Methyl selenocysteine	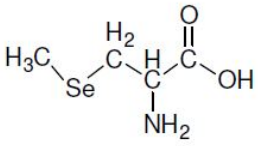	$C_4H_9NO_2Se$	Plants

Figure 2 - Organic forms of selenium (Rocha et al., 2016).

1.1.2 – Selenium and its correlation with human pathologies

Many evidences suggest that deficiency of selenium is linked to the onset of several human diseases. Among these, diseases of endocrine and cardiovascular system together with cancer are those more connected with a selenium deficiency (Figure 3).

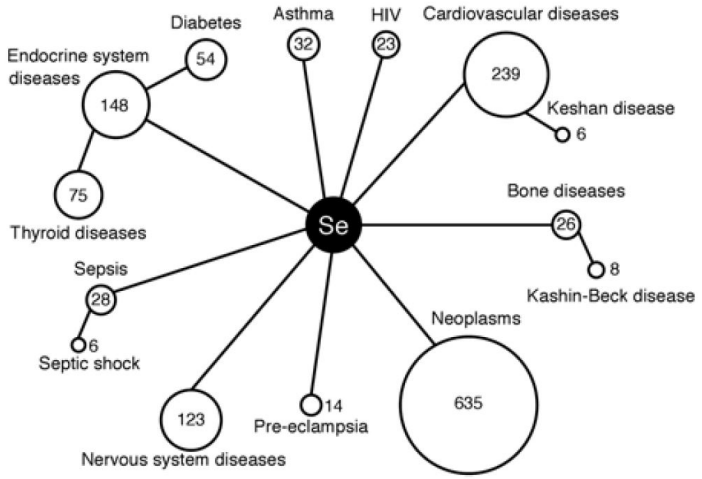

Figure 3 - Number of publications regarding the connection between selenium dis-levels and human diseases (Vinceti et al., 2016).

1.1.3 – Emblematic example of a disease due to low intake of selenium: Keshan disease

Keshan disease (KD) is an endemic cardiomyopathy characterised by multifocal cardiac necrosis that is endemic in an area of China known as Keshan (from which the name of the disease). This disease is caused by a dietary deficiency of selenium whose levels are particularly low in the soil of Keshan. Quantitative analysis of selenium levels in human samples (scalp hair, blood, urine) and locally grown cereals have shown a direct correlation between low levels of selenium in the biological samples of affected individuals and low levels of selenium in soil (Chen et al., 1980). For example, the hair levels of selenium in KD patients was under 0.12 ppm that is almost half of the levels of healthy populations (that is around 0.20 ppm) (Ge et al., 1983).

Oral supplementation with sodium selenite resulted in prevention of the disease, highlighting that low levels of selenium is the primary cause of KD (Chen et al., 1980).

Deficiency of selenium exerts its pathological effects through the impairment of the function of selenoproteins. Indeed, not only the amount of selenium in blood and urine was lower in KD patients but also the levels of glutathion peroxidases (GPXs), the most important class of selenoproteins, were decreased (Levander and Beck, 1997).

The incidence of KD was variable among the different seasons of the year and importantly not all of the selenium deficient inhabitants became ill suggesting that a second factor was necessary to develop KD (Yang, 1985). In fact, viral infections from Coxsackie virus B4, a single-RNA stranded pathogenic enterovirus that causes myocarditis, was found in KD victims (Levander and Beck, 1997). *In vivo* studies on animal models confirmed the implication of Coxsackievirus in the development of the heart damage of KD patients: selenium-deficient mice infected with Coxsackie virus B4 developed more severe heart problems than the control group fed a standard selenium diet and infected with the virus (Bai, 1980).

In addition, a deficiency of the anti-oxidant vitamin E had very similar effects on mice infected with the Coxsackie virus B3/20 (a myocarditic strain of the aforementioned virus), suggesting a potential overlapping function of selenium and vitamin E (Lippman et al., 2009) (Hoekstra, 1975).

1.1.4 – Selenium and myopathies in animals

The correlation between the amount of selenium and muscle pathologies has been known since the middle of the last century.

Livestock that are raised in selenium-poor soils develop the “white muscle disease” (WMD), a muscle pathology characterised by progressive muscular weakness affecting mainly highly active muscles, such as diaphragm, masticatory muscles and myocardium

(Delesalle et al., 2017). Muscles biopsies from WMD-affected animals present pale striations (Figure 4 and 5), hence the name of the disease, and blood serum from affected animals contains low levels of GPX. This disease is caused by a deficiency of selenium and/or vitamin E, for this it is classified as a "nutritional myopathy" and the affected animals can be treated by adding supplements of sodium selenite and vitamin E to the diet.

As for KD, WMD is also due to a simultaneous deficiency of vitamin E, which has antioxidant functions, and selenium indicating that the accumulation of oxygen radicals in the muscle may be the pathogenic cause of the disease (Finno and Valberg, 2012) (Delesalle et al., 2017).

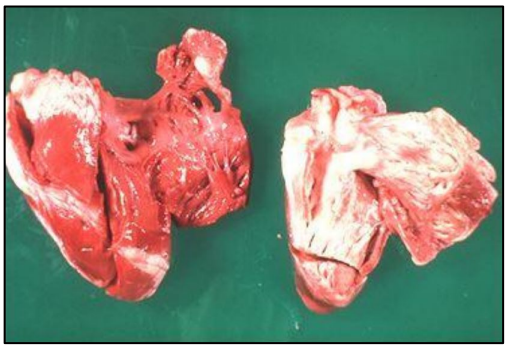

Figure 4 - WMD muscle (on the right) have a paler color than the wild type (on the left).

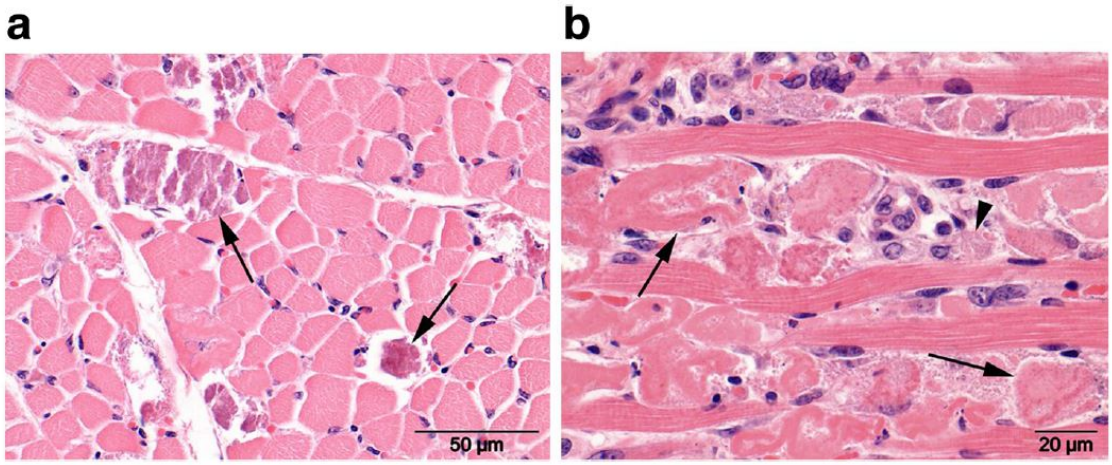

Figure 5 - H&E staining of a skeletal muscle from a WMD animal. a) Transverse section showing multifocal mineralization (black arrows) b) Longitudinal section depicting the fragmentation of the skeletal muscle and macrophages infiltration (arrowhead) (Delesalle et al., 2017).

1.1.5 – Selenium and myopathies in human

Another interesting indication of the correlation between selenium deficiency and myopathy comes from the observation of human patients under prolonged parenteral nutrition. In many cases, in fact, the muscle weakness of these patients was associated with a severe selenium deficiency in blood. Twenty-two post-operative patients under total parenteral nutrition from 10 to 40 days were diagnosed with a clinical selenium responsive syndrome characterised by severe muscle pain (Abrams et al., 1992). Low levels of selenium have been also connected to the sarcopenia (loss of muscle mass) as a consequence of aging. The "in CHIANTI" study ("Invecchiare in Chianti", meaning

Aging in Chianti, an area of Tuscany, Italy) tried to shed some light on the mechanisms underlying aging, hypothesizing that poor muscle strength in the elderly is caused by low selenium levels in plasma (Lauretani et al., 2007). In this study the data obtained from a cohort of 1155 patients of equal or more than 65 years old highlighted a connection between low selenium levels and poor grip strength. However a causative effect between low selenium level and muscle weakness was missing in this study (Lauretani et al., 2007).

1.2 – Selenoproteins

1.2.1 – History of selenoproteins

Selenocysteine (Figure 6) was recognized, after a long time, as the 21st amino acid (Chambers et al., 1986; Zinoni et al., 1986) since It's encoded by an UGA codon, which is usually one of the three stop codons (Kryukov et al., 2003).

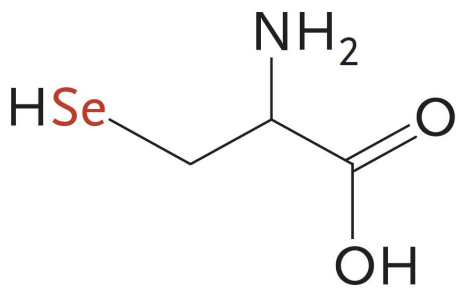

Figure 6 - Chemical structure of the selenocysteine (Loscalzo, 2014).

Selenocysteine is incorporated into proteins as a result of a genetic code expansion, because the translation of selenoproteins involves the decoding of a UGA codon that would otherwise be a termination codon. The UGA codon is decoded by means of species-specific mechanisms guided by a secondary structure in the 3'-UTR of selenoprotein mRNA and requiring the involvement of a stem loop structure of the selenocysteine insertion sequence (SECIS) (Figure 7)(Lescure et al., 2009) and other factors such as a selenocysteine-specific elongation factor, selenophosphatase synthetase and a SECIS binding protein (Figure 8) (Kryukov et al., 2003).

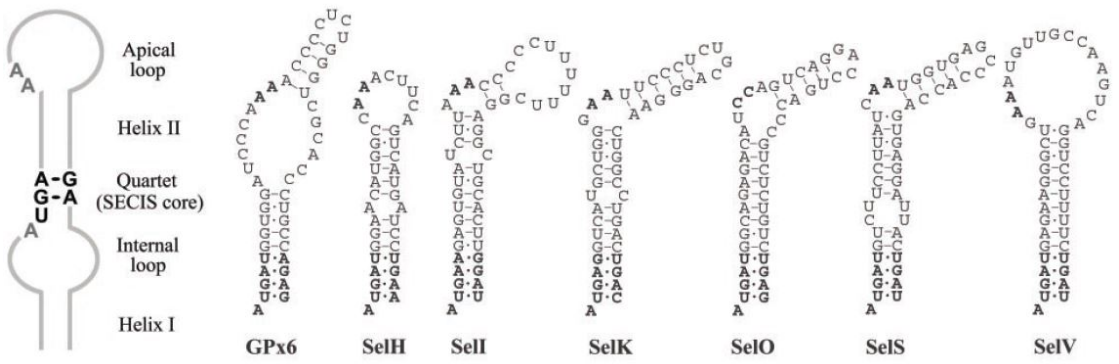

Figure 7 - SECIS consensus and SECIS structure in some selenoproteins (Kryukov et al., 2003).

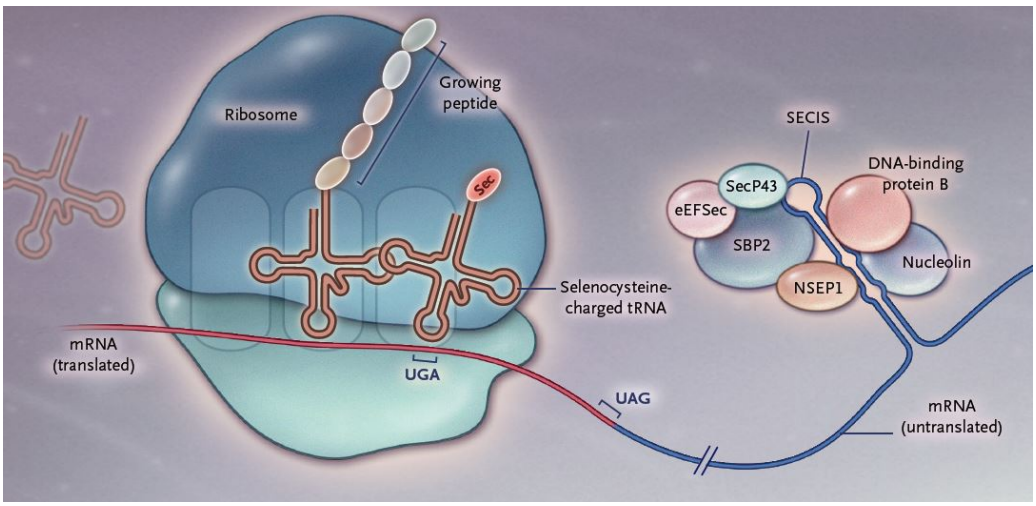

Figure 8 – Graphical representation of the SECIS element at the 3' untranslated region of the mRNA, together with other six elements which regulate the selenocysteine incorporation: Sec-specific elongation factor (eEFSec), selenocysteine-insertion sequence binding protein 2 (SBP2), nuclease sensitive element-binding protein 1 (NSEP1), SecP43, DNA-binding protein B and nucleolin (Loscalzo, 2014).

The importance of these factors in the selenoprotein synthesis is demonstrated by the fact that genetic mutations in selenocysteine-insertion sequence binding protein (SBP2), one of the elements of the SECIS complex, give rise to loss of function of all selenoproteins and a multisystemic syndrome characterised by growth retardation and abnormal thyroid function (Dumitrescu et al., 2010). Compromised bones, inner ear and muscles are other clinical features of this pathology (Fradejas-Villar, 2018).

The selenol group (-SeH, also called selenohydryl group or SeC), found in selenocysteinyl residue of selenoproteins, is an analogue of the thiol group (-SH, also called sulfhydryl group) of cysteine with a higher nucleophilicity (Johansson et al., 2005) (Rocha et al., 2016) (Figure 9 and 10).

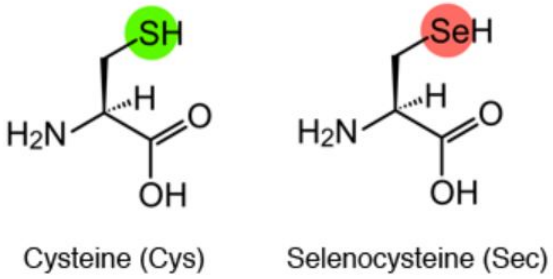

Figure 9 - Chemical structure of cysteine and selenocysteine.

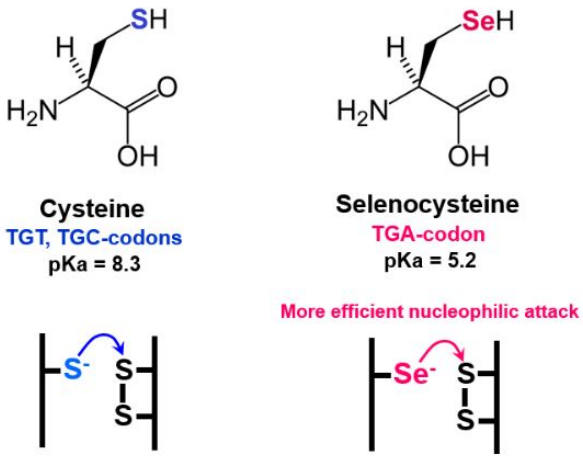

Figure 10 – Graphical representation of the nucleophilic attack of the cysteine and selenocysteine on an oxidized proteinaceous target.

1.2.2 – Mammalians selenoproteins

The human selenoproteome consists of 25 selenoproteins containing at least one selenocysteine which is involved in the biological function of the selenoprotein (Addinsall et al., 2018) (Shchedrina et al., 2010). In 2016, a new nomenclature was suggested for the selenoproteins (Table1): the root symbol SELENO followed by a letter identify selenoproteins whose function is still not known whereas selenoproteins with a known function will continue to be identified with the old name (Gladyshev et al., 2016). For the purpose of this thesis, Selenoprotein N will be indicated with the classical symbol SEPN1.

Symbol	Name	Synonyms	Subcellular location
SELENOF	Selenoprotein F	Selenoprotein 15, SEP15	ER lumen
SELENOH	Selenoprotein H	SELH, C11orf31	Nucleus
SELENOI	Selenoprotein I	SELI, EPT1	Unknown
SELENOK	Selenoprotein K	SELK	ER and plasma membrane
SELENOM	Selenoprotein M	SELM, SEPM	ER lumen
SELENON (SEPN1)	Selenoprotein N	SEPN1, SELENON	ER membrane
SELENOO	Selenoprotein O	SELO	Unknown
SELENOP	Selenoprotein P	SEPP1, SeP, SELP, SEPP	Secreted
SELENOS	Selenoprotein S	SELS, SEPS1, VIMP	ER and plasma membrane
SELENOT	Selenoprotein T	SELT	ER membrane
SELENOV	Selenoprotein V	SELV	Unknown

SELENOW	Selenoprotein W	SELW, SEPW1	Cytosol
TXNRD1	Thioredoxin reductase 1	TR1, TRXR1	Cytosol, nucleus
TXNRD2	Thioredoxin reductase 2	TRXR2, TR3,	Mitochondria
TXNRD3	Thioredoxin-glutathion reductase	TGR, TRXR3, TR2	Cytosol
GPX1	Glutathione peroxidase 1	GSHPX1	Cytosol, mitochondria
GPX2	Glutathione peroxidase 2	GSHPX-G1	Cytosol
GPX3	Glutathione peroxidase 3	Plasma glutathione peroxidase	Secreted
GPX4	Glutathione peroxidase 4	Phospholipid hydroperoxide, Glutathion peroxidase, PHGPX	Cytosol, mitochondria, nucleus
GPX6	Glutathione peroxidase 6		Unknown
DIO1	Iodothyronine deiodinase 1	D1	Plasma membrane
DIO2	Iodothyronine deiodinase 2	D2	ER membrane
DIO3	Iodothyronine deiodinase 3	D3	Plasma membrane
MSRB1	Methionine sulfoxide reductase B1	SELR, SELX, SEPX1	Cytosol, nucleus
SEPHS2	Selenophosphate synthetase 2	SPS2	Cytosol

Table 1 - New nomenclature of the 25 selenoproteins (Gladyshev et al., 2016) (Shchedrina et al., 2010) *together with their subcellular localization.*

GPXs are the first identified selenoproteins in mammals in 1970's (Fohe and Gzler, 1973). These enzymes are involved in the defence of the cell from the oxidative damage of H_2O_2 or organic hydroperoxide, which are reduced to water or corresponding alcohols by using glutathione (GSH) as source of reducing equivalents ($H_2O_2 + 2GSH \rightarrow 2H_2O + GS\text{-}SG$).

Another important class of selenoproteins is represented by the Thioredoxin reductases (TrxRs), whose function is to catalyse the reduction of thioredoxin (Trx). Together with Trx and nicotinamide adenine dinucleotide phosphate (NADPH), TrxR is part of the thioredoxin system that reduces disulfide bonds in proteins (Shchedrina et al., 2010). Briefly, electrons flow from NADPH to thioredoxin reductase and then to thioredoxin and finally reduce a disulphide bond in a thiol of a proteinaceous substrate (Holmgren A, Lu J 2010). The enzymatic mechanism of TrxR relies on an electron transfer relay with Trx: the nucleophilic selenolate anion of the selenocysteine in TrxR attacks a cysteine on Trx to form a selenenyl-sulfide intermediate that is later resolved by the resolving cysteine in the catalytic site of TrxR (Lu et al., 2009) (Figure 11).

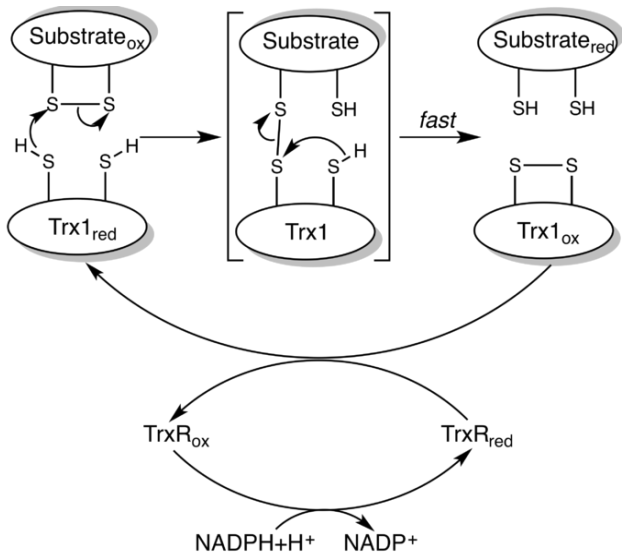

Figure 11 - Catalytic mechanism of the thioredoxin system. A disulfide bridge in Trx is reduced by electrons donated by TrxR. Reduced-Trx transfers electrons to a disulphide bond of the final substrate that is reduced in a free thiol (image courtesy of Wikipedia).

Iodothyronine deiodinases (or selenodeiodinases) are integral membrane selenoproteins (DIO1 and DIO3 are located in the plasma membrane, DIO2 in the endoplasmic reticulum). DIO2 activates the thyroid hormone, while DIO3 inactivates it. DIO1 is able to activate and inactivate thyroid hormone depending on which iodine is removed from the iodothyronine molecule (Marsili et al., 2016).

Since both hypo- and hyperthyroidism impair muscle function (Dentice et al., 2010) (Dentice et al., 2014), Iodothyronine deiodinases have been studied to evaluate their effect on muscle. DIO2 and DIO3 are important to regulate satellite cells differentiation during muscle regeneration after an injury (Marsili et al., 2016).

Selenoprotein W (SELENOW) is the smallest selenoprotein containing a Cys-X-X-SeC motif and is mostly present in skeletal muscle and brain of mammals (Loflin et al., 2006). SELENOW is required for the differentiation of myoblasts in myotubes (Noh et al., 2010) and its loss is associated with KD and WMD (see chapter 1.1.3 and 1.1.4) (Papp et al., 2010; Whanger, 2000).

Selenoprotein S is one of the seven ER resident selenoproteins (Figure 12) and is highly expressed in skeletal muscle. The impairment of the muscle strength of SELENOS knock-out mice suggests an important role of SELENOS in the muscle contraction (Addinsall et al., 2018).

Selenoproteins have been linked to ER stress. In rat cardiomyocytes, overexpression of selenoprotein K (SelK), one of the ER resident selenoproteins, decreased the production of ROS (Lu et al., 2006). Thus, SelK plays an important role in the oxidative stress provoked by accumulation of hydrogen peroxide.

Another ER selenoprotein, SelS, is involved in the regulation of ER stress. SelS is one of the component of the endoplasmic reticulum-associated degradation (ERAD)

machinery (Lilley and Ploegh, 2004), which is devoted to the transport of unfolded and misfolded proteins to the cytosol, for further degradation. For this reason, SelS could be crucial to limit the accumulation of proteins inside the ER, hence to avoid the insurgence of ER stress.

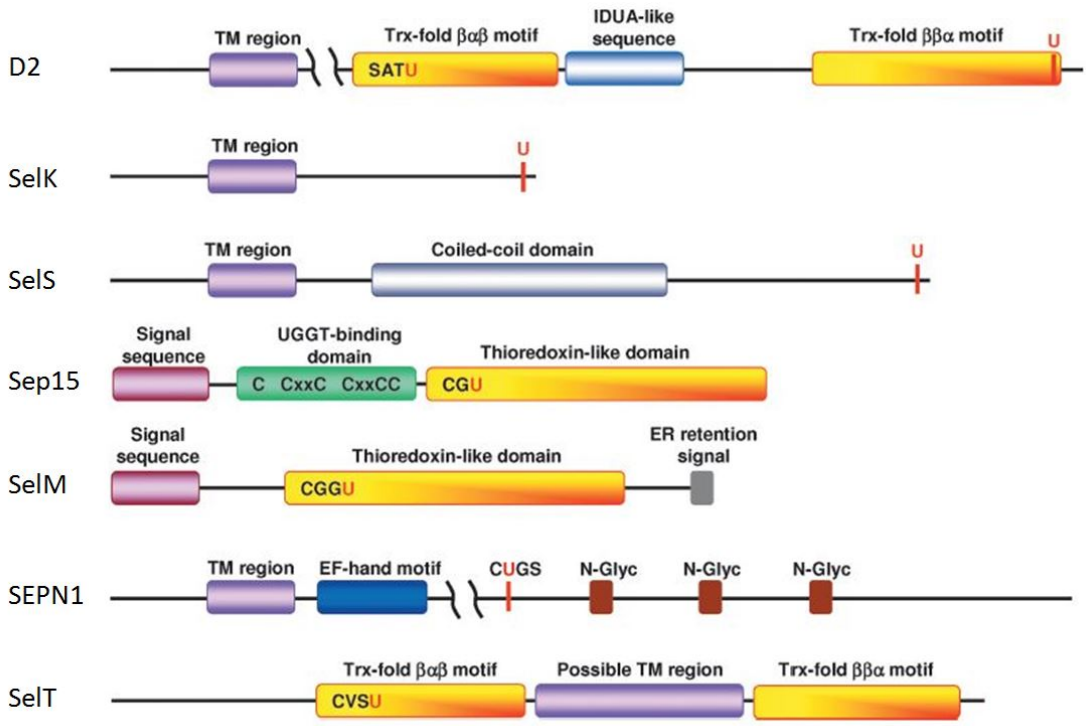

Figure 12 - Schematic representation of the mammalian ER selenoproteins and their domains. D2, SelK, SelS and SelN contain the transmembrane (TM) region at the N-terminal (violet box). Thioredoxin-like fold known for D2, Sep15, SelM and SelT are indicated (yellow boxes). Sec (U) location is depicted in red. N-terminal signal peptide in Sep15 and SelM is indicated in pink. EF-hand motif (blue box) in SelN (blue box), coiled-coil domain in SelS (light grey box), ER retention signal in SelM (grey box), UGGT-binding domain in Sep15 (green box) and Iduronidase alpha-L (IDUA)-like sequence in D2 (light blue) are also reported (Shchedrina et al., 2010).

1.3 – Selenoprotein N

1.3.1 – Selenoprotein N (SEPN1): a general introduction

In 1999, bioinformatics analyses in search for SECIS sequence brought SEPN1 to the light (Lescure et al., 1999).

SEPN1 gene is located on chromosome 1p35-p36. The coding sequence is characterised by 13 exons and the selenocysteine UGA codon is on the exon 10 (Moghadaszadeh et al., 2001). Two alternatively spliced transcript variants encoding two distinct SEPN1 isoforms have been found but the shorter transcript is predominant in the majority of cells (Lin et al., 2008; Makałowski et al., 1994; Petit et al., 2003; Schmid and Jelinek, 1982).

Although mutations in other selenoproteins, such as GPXs, TrxRs and deiodinases, have been linked to different types of disease, SEPN1 was the first identified selenoprotein whose mutations are associated to a genetic pathology, referred as "SEPN1-related myopathy" (SEPN1-RM).

1.3.2 – SEPN1-related myopathy

All of the pathological mutations so far identified in *SEPN1* are localised in the 3' (in the SECIS sequence), in the selenocysteine codon redefinition element (SRE) and in the coding sequence. They consist of micro-deletions or insertions leading to frameshift, splice site mutations that cause aberrant pre-messenger RNA splicing or single-nucleotide changes including missense mutations that are centred around the selenocysteine (Figure 13) (Allamand et al., 2006; Castets et al., 2012).

Mutations in the *SEPN1* gene were originally identified as the genetic cause of rigid spine muscular dystrophy (RSMD1), and have subsequently been associated with other neuromuscular disorders: the classic form of multi-minicore disease (MmD), rare cases of desmin-related myopathy with Mallory body-like inclusions (MB-DRM) and congenital fiber type disproportion (CFTD) (Lescure et al., 2009). These four early-onset autosomal recessive pathologies show clinical and morphological overlaps, including predominantly axial weakness, an early development of scoliosis, respiratory failure and a variable degree of spinal rigidity (Figure 14). At ultra-structural level, electron micrographs from muscle biopsy of affected individuals show zones of Z-lines streaming, sarcomere disorganization and area of mitochondria depletion, referred to as minicores (Figure 15) (Ferreiro et al. 2002). For these similarities at clinical and ultrastructural level, the aforementioned pathologies are now grouped and called SEPN1-RM.

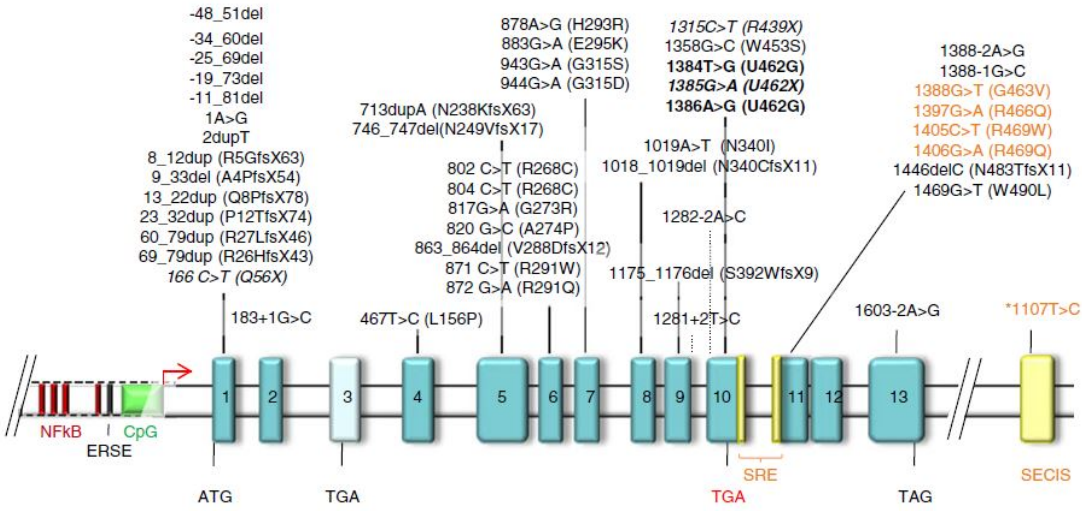

Figure 13 – Graphical representation of SEPN1 exons and mutations found in SEPN1-RM patients. Exon 3, which is subject to alternative splicing, is in light blue. Mutations in the selenocysteine codon are in bold, nonsense mutations are in italics and mutations in SRE/SECIS regions are in orange. In the 5' region, before SEPN1 promoter, nuclear factor kappa-light-chain-enhancer of activated B cells (NFkB), ER-stress element (ERSE) and CpG islands are depicted (Castets et al., 2012).

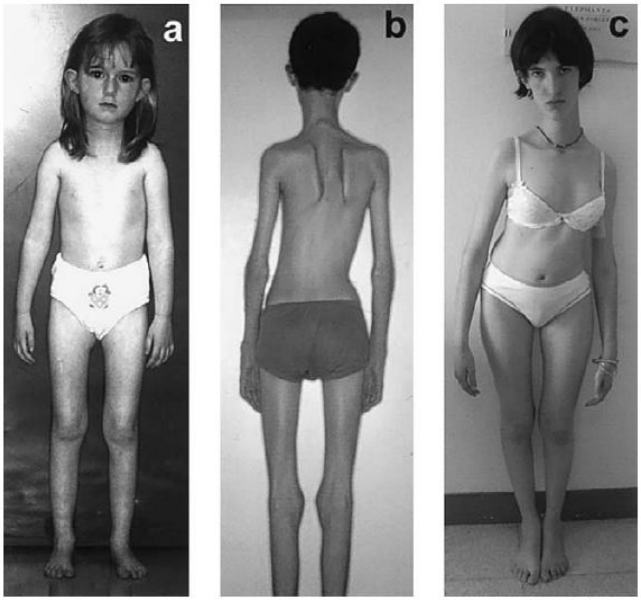

Figure 14 – Representative pictures of SEPN1-RM patients: Slender neck with lack of sternocleidomastoid bulk and flat thorax (patient "a", 5,5 years old). Scoliosis, lateral trunk deviation and an unusual appearance of lower limbs (patient "b", 15 years old, and "c", 17 years old) (Ferreiro et al. 2002).

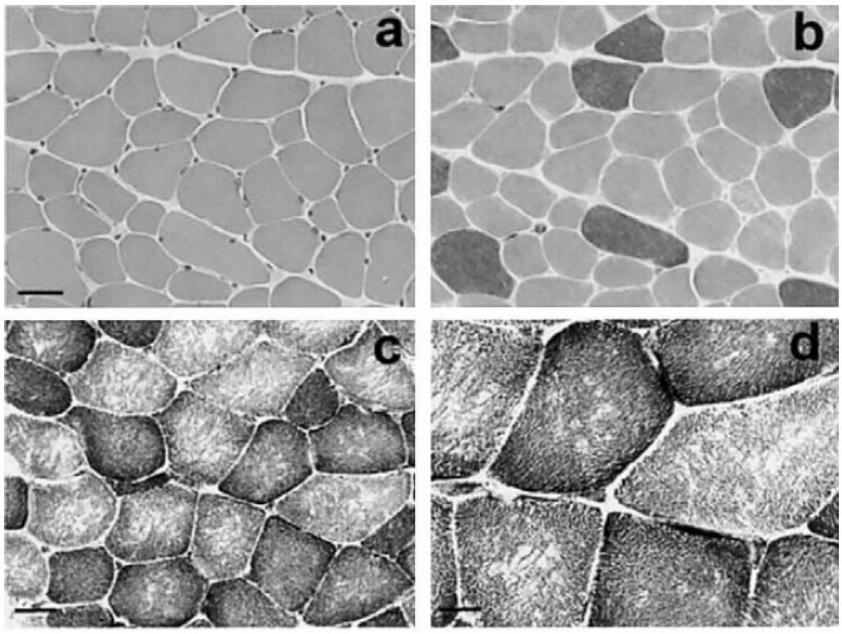

Figure 15 - Transverse muscle sections with minicores. a,b) left deltoid of a 5 years old patient stained with H&E (a) or myosin adenosine trisphosphatase, pH 9.4 (b), scale bar = 40 µm. Lighter (type I) fibers are predominant compared to the dark (type II) fibers. c,d) right deltoid of a 14 years old patient stained with nicotinamide adenine dinucleotide-tetrazolium reductase (NADH-TR) ("c", scale bar = 25 µm) or succinate dehydrogenase ("d", scale bar = 12,5 µm). Both the stainings show minicores, the white areas/dots lacking oxidative activity (Ferreiro et al. 2002).

The spinal stiffness is a defining feature of SEPN1-RM together with an early respiratory failure which represents a common life-threatening condition even in ambulant SEPN1-RM patients. Recently studies point to weakness and dysfunction of the diaphragm as the cause of the respiratory failure and suggest nocturnal non-invasive ventilation as a mean of stabilizing the respiratory function in SEPN1-RM patients (Caggiano et al., 2017). In addition, glucose intolerance and insulin resistance was reported in a cohort of SEPN1-RM patients suggesting that insulin resistance may be an overlooked aspect of SEPN1-RM (Clarke et al., 2006).

1.3.3 – SEPN1 characterisation

SEPN1 is an ER membrane protein ubiquitously expressed throughout the body (Petit et al., 2003). Human SEPN1 is composed by 590 amino acids with a molecular mass of 68 KDa and its structure has not been solved yet. Bioinformatics analyses predict 4 sites of glycosylation, a calcium-binding domain (EF-hand) and 3 trans-membrane domains in SEPN1. However unpublished results of protease accessibility assays suggest that SEPN1 is a type II membrane protein with only one transmembrane domain (Figure 16). Most of the protein is located inside the ER lumen, while a short tail at the N-terminal faces the cytosol. On the ER side of SEPN1, the selenocysteine is close to a cysteine residue and this dyad of amino acids resembles the catalytic active site of TrxR (Castets et al., 2012).

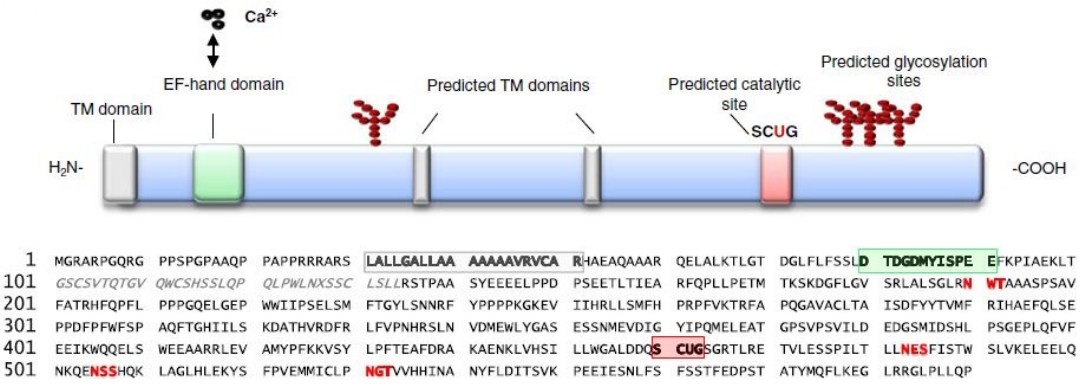

Figure 16 – Bioinformatics prediction of different domains in SEPN1. TM =Transmembrane motif, EF-hand domain = calcium binding site, SCUG = Possible catalytic site containing the selenocysteine. Below, the amino acid sequence is presented. The gray box depicts the transmembrane domain, the green box the EF-hand domain and the red box the SCUG site. Red bold letters indicates the glycosylation sites (Castets et al., 2012).

SEPN1 function is still not known, partly because of the difficulty in obtaining a pure protein necessary to test its activity. However, biochemical studies have shown a role of SEPN1 in redox and calcium homeostasis.

SEPN1-devoid myotubes have an excess of oxidized proteins and treatment of these cells with the anti-oxidant N-acetyl-cysteine decreases the protein oxidation (Arbogast et al., 2009). In addition, SEPN1 co-immunoprecipitates with Ryanodine Receptor 1 (RyR1), a calcium release channel of the ER whose genetic mutations are also associated to muscle diseases (central core and minicore diseases). RyR1 from SEPN1 mutants shows a reduced ability to bind its ligand and modulator ryanodine suggesting that SEPN1 interacts with RyR1 and modulates its activity in a redox-dependent manner (Jurynec et al., 2008).

Following studies have hypothesized that the CU domain of SEPN1 may be involved in an electron transfer chain with a proteinaceous substrate and have developed a "trapping mutant" of SEPN1 to identify proteinaceous interactors of SEPN1 that interact with SEPN1 in a redox-dependent manner. In the list of these SEPN1 interactors sarcoplasmic reticulum calcium ATPase isoform 2 (SERCA2), a calcium pump of the ER, stands out. In addition, functional studies showed that the rate of calcium uptake in the ER was impaired in SEPN1 KO cells and recovered only in SEPN1 KO cells expressing a redox active SEPN1 suggesting that SEPN1 interacts with SERCA2 and regulates its activity in a redox-dependent manner (Marino et al., 2015). On the same line, the overexpression of ER oxidoreductin 1 (ERO1), a protein disulfide oxidase of the ER whose activity is associated to the stoichiometric production of H_2O_2, was shown to be detrimental in SEPN1-devoid myoblast cell line suggesting that SEPN1 may counteract ERO1 detrimental effect on cells (Marino et al., 2015).

1.3.4 – SEPN1: data from animal models

Given the lack of a purified SEPN1 that would have allowed *in vitro* mechanistic studies, the functional studies on SEPN1-mutant cells together with the phenotypical characterisation of SEPN1 loss-of-function animal models have been important to infer SEPN1 function.

In temporal order the first studies for the assessment of SEPN1 function were conducted on zebrafish. *Sepn1*-antisense morpholino oligonucleotide injected in zebrafish induced alterations in muscle architecture and compromised the fish motility (Figure 17) (Deniziak et al., 2007).

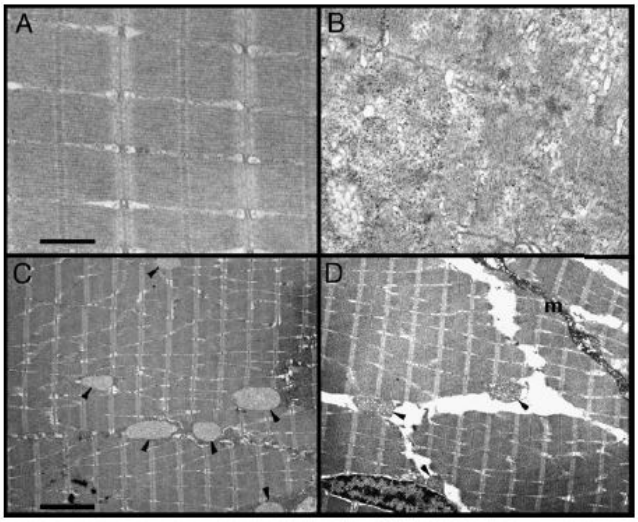

Figure 17 - Altered myofibrillar ultrastructure in Sepn1 morphant. A). Electron micrograph of WT muscle showing a well-organized triad. B) Electron micrograph of Sepn1 morphant muscle showing that the muscle structure severely perturbed and the triad is not detectable. C) Electron micrograph of WT muscle showing that mitochondria (arrowheads) are regularly interposed among myofibrills. D) Electron micrograph of Sepn1 morphant showing that peripheral mitochondria (arrowheads) are suspended in myofibril-free space. Image from (Deniziak et al., 2007).

Another zebrafish study started from the observation of overlapping muscle phenotypical features between patients with RyR1 mutations and those with SEPN1

mutations and showed that the same overlapping phenotypical features were seen between *Ryr1* morphants and *Sepn1* morphants in zebrafish. In addition, this study supported a model in which SEPN1 interacts with RyR and modifies the redox state of RyR, which is critical for the regulation of the calcium flow (Jurynec et al., 2008).

The first SEPN1 KO mouse model was engineered and studied in 2011. This model is characterised by the excision of exon 3 in *Sepn1,* thus leading to *Sepn1* transcripts that are not stable and undergo degradation. SEPN1 KO offspring were recovered at the expected mendelian frequency suggesting that the lack of SEPN1 does not trigger developmental defects in mice (Rederstorff et al., 2011).

During adulthood, SEPN1 KO mice do not show any overt muscle phenotype in normal cage condition. However, when these mice were forced to increased muscle activity (regular every other day session of forced swimming for 3 months) the lack of SEPN1 gave rise to phenotypical features which resemble those of SEPN1-RM patients such as progressive stiffness, sarcopenia of trunk and limb muscles and kyphosis.

Immuno-histochemical and morphometric analysis of SEPN1 KO mice hind limb muscles revealed lack of atrophy, necrosis and fibrosis, as well lack of changes in the ratio oxidative to glycolytic fibers, whereas the back muscles of SEPN1 KO mice resulted atrophic.

Although the hind limb muscles of SEPN1 KO mice were spared from any overt phenotype, regeneration of these muscles resulted impaired and satellite cells were reduced after injections of cardiotoxin (a myonecrotic agent)(Figure 18) suggesting the importance of SEPN1 in muscle regeneration (Castets et al., 2011).

A different SEPN1 KO mouse was generated in Beggs' laboratory that, as the previous mouse model, doesn't express *SEPN1* in any tissues. In this model exon 9 in the *Sepn1* gene was replaced by a Neomycin cassette, causing a frameshift that lead to a

truncated SEPN1 protein. Since exon 9 encodes for the selenocysteine residue, the abnormal SEPN1 protein is non-functional. As for the previously described SEPN1 KO model, also in this case the levels of *Sepn1* transcripts were greatly reduced compared to the WT mice. Interestingly, an abnormal lung development together with enlarged alveoli and decreased tissue elastance was seen in this SEPN1 KO mice, suggesting the possibility that SEPN1 loss may affect not only muscle but also lung function (Moghadaszadeh et al., 2013). It is not known if abnormal lungs were also developed by SEPN1 KO mice in the previously described mice model, since the non-muscle tissues that were analysed did not include lungs.

The Beggs' SEPN1 KO mouse does not show an overt muscle phenotype. However histochemical analyses on SEPN1 KO muscles suggest that the combined deficiency of the anti-oxidant vitamin E and daily running sessions lead to minicores, which are areas of mitochondria depletion, and a defining feature of SEPN1-RM muscle biopsies (Moghadaszadeh et al., 2013).

Minicores on sections of gastrocnemii of SEPN1 KO mice were also observed after muscle injection of an adenovirus driving ERO1 expression, suggesting that an excess of the ER stress responsive protein disulphide oxidase ERO1 is detrimental for the muscle architecture of SEPN1 KO mice (Marino et al., 2015).

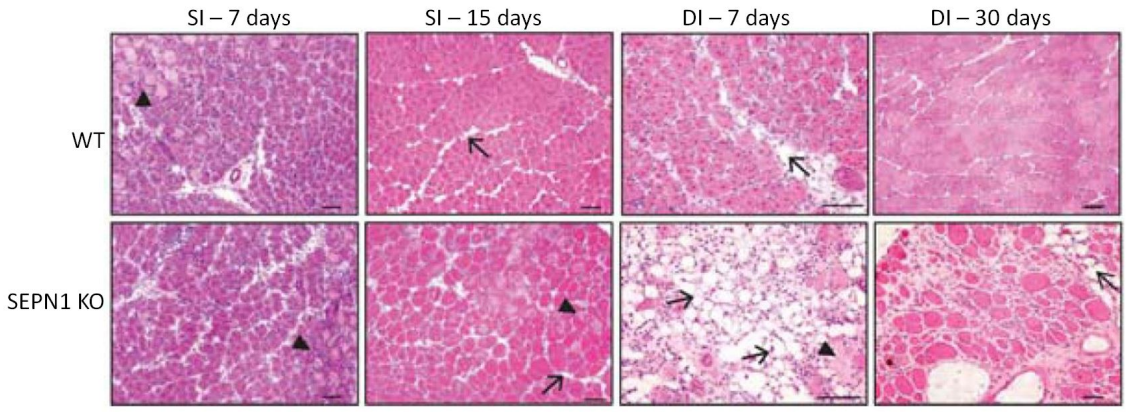

Figure 18 – Representative H&E stainings of tibialis anterior from mice injected with single (SI) or double (DI) injections of cardiotoxin, after 7, 15 or 30 days from the injection. The lack of SEPN1 impaired the regeneration of muscle fibers mainly after a second injection of cardiotoxin. Black arrows indicate adipocytes, black arrowhead necrotic fibers (Castets et al., 2011).

1.4 – Endoplasmic reticulum stress and unfolded protein response

The endoplasmic reticulum (ER) is the largest organelle in the cell and is the compartment in which the proteins destined for the secretory pathway and cell surface are folded. The proteins enter in an unfolded state, and only leave when they are correctly folded and assembled. It is predicted that about 20% of the proteins encoded by the human genome enter the secretory pathway. The process of folding in the ER requires enzymes to catalyse the steps that are critical to reach the functional protein conformation, and chaperones to prevent misfolding and the aggregation of folding intermediates. Highly secretory cells and tissues of multi-cellular organisms, such as those involved in the immune and endocrine systems, have become specialized for secretion and are therefore particularly reliant on ER integrity and protein folding.

ER protein misfolding occurs when the load of proteins in the ER exceeds the capacity of the folding machinery and results in ER stress. ER stress is sensed by three stress receptors in mammals: inositol-requiring enzyme 1 (IRE1), protein kinase R-like ER kinase (PERK), and activating transcription factor 6 (ATF6) (Ron and Walter, 2007).

These sensors are ER transmembrane proteins with a stress-sensing luminal portion and a cytoplasmic effector domain. When these three stress receptors sense ER stress, generally following the dissociation of the chaperone binding immunoglobulin protein (BIP) from the three receptors, they activate a homeostatic response, the Unfolded Protein Response (UPR), that swings into action by attenuating protein translation and promoting the transcription of chaperones to rectify the accumulation of misfolded

proteins in ER, thus generally relieving ER stress. Phylogenetically, the most conserved of the three receptors is IRE1, that is a kinase and endoribonuclease that promotes the unconventional splicing of an intronic region of X box binding protein 1 (XBP1) that subsequently becomes a transcription factor of the genes involved in protein folding and ERAD (Figure 19).

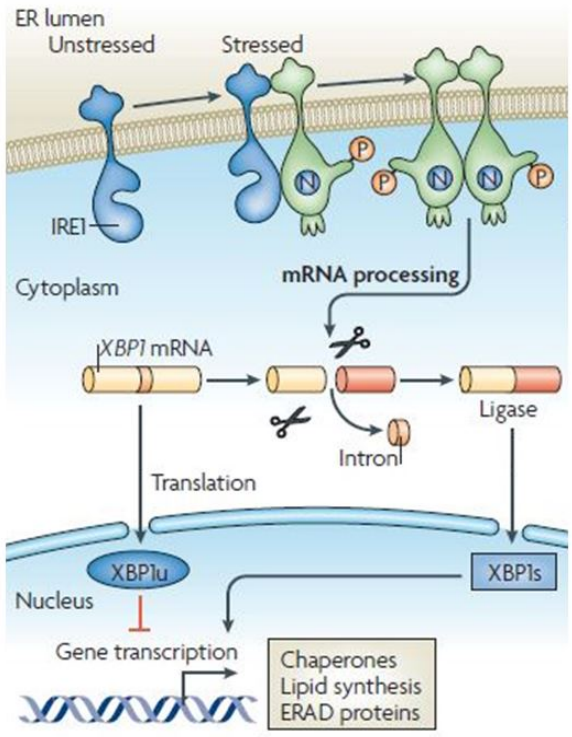

Figure 19 - IRE1 pathway. Following ER stress IRE1 dimerizes and exerts its endoribonucleolytic activity on XBP1 mRNA. Spliced XBP1 mRNA (XBP1s) encodes for a transcriptional factor that translocates to the nucleus. The unspliced XBP1 mRNA encodes an inhibitor of the UPR (XBP1u). (Ron and Walter, 2007).

Following ER stress, PERK dimerizes in the ER membrane and auto-phosphorylates its cytosolic protein kinase domain. The activated PERK attenuates protein synthesis by phosphorylating eukaryotic initiation factor 2-alpha (eIF2-α) (Figure 20). The ER stress-activated ATF6 traffics to the Golgi, where it is proteolytically cleaved from its transmembrane domain, and subsequently reaches the nucleus where it acts as a transcription factor for chaperones such as BIP/GRP78 and GRP94 (Figure 21). The ER stress response therefore acts by inhibiting protein translation through the PERK pathway and favouring protein degradation and the induction of chaperones through

the IRE1 and ATF6 branches. This coordinated action of protein degradation and the induction of chaperones relieves ER stress and re-establishes homeostasis and suggest an important role of the UPR as a survival pathway for ER stressed cell (Ron and Walter, 2007).

However, a form of unrelieved chronic ER stress may occur and lead to cell death. All three arms of the UPR contribute to the transcriptional activation of the apoptotic gene C/EBP homologous protein (CHOP). CHOP deletion protects severely stressed cells against death, which suggests that CHOP has evolved (in vertebrates) to associate ER stress with apoptotic death (Marciniak et al., 2004).

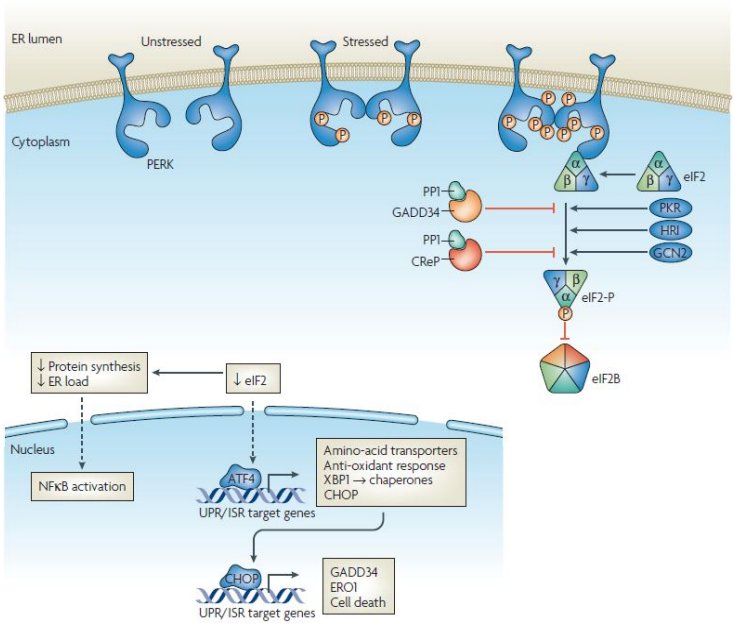

Figure 20 - PERK pathway. ER stress is sensed by PERK on the ER membrane. PERK dimerizes and becomes active by auto-phosphorylation of its cytosolic domain. Activated PERK inhibits elf2 by phosphorylating its α subunit. The decrease of activated elf2 lowers the amount of newly synthesized proteins (Ron and Walter 2007).

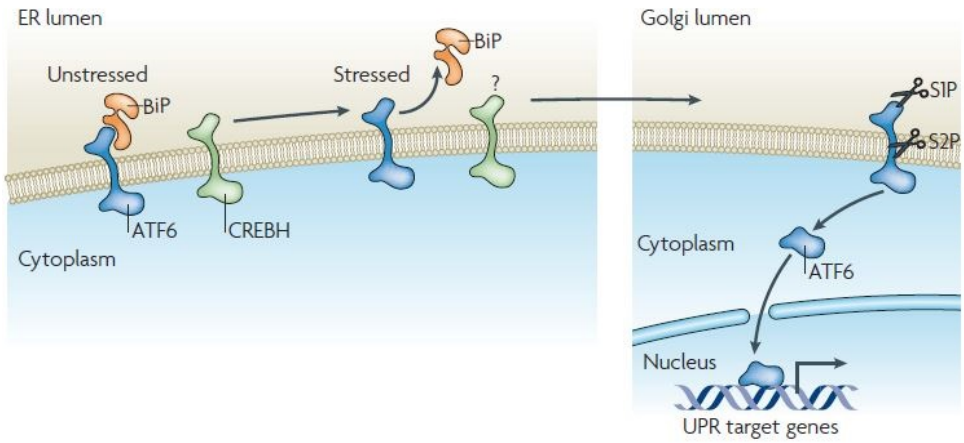

Figure 21 - ATF6 pathway. BiP proteins detach from ATF6 during ER stress causing ATF6 to translocate to Golgi. Here, ATF6 is cleaved by the lumenal site 1 protein (SBP1) and the intra-membrane site 2 proteases (SBP2). The cleaved portion of ATF6 moves from the cytoplasm to the nucleus where it acts as a transcription factors of UPR target genes (Ron and Walter, 2007).

However, the relationships between CHOP and the apoptosis machinery are unlikely to be the only reason that explains why CHOP-devoid cells are protected from death. Indeed, comparisons of wild-type and CHOP-/- cells indicate that the latter experiences less ER stress when confronted with the same perturbation of protein folding in their ER and therefore suggest a connection between CHOP and ER stress.

The same study revealed growth arrest and DNA damage-inducible protein (GADD34) and ERO1 as transcriptional targets of CHOP and showed that they might be involved in the failure of the homeostasis. GADD34 recruits protein phosphatase 1 (PP1) to dephosphorylate eif2-alpha and thus promotes reactivation of the protein synthesis, that may be detrimental for example in case of genomic mutations that give rise to misfolded proteins (Marciniak et al., 2004).

ERO1, the main protein disulfide oxidase of the ER, is also a transcriptional target of CHOP and a failure to activate ERO1 further explains the less oxidizing conditions observed in the ER of stressed CHOP-/- cells and may contribute to their ability to survive to high levels of ER stress (Marciniak et al., 2004).

The enzymatic activity of ERO1 as protein disulphide oxidase is associated with a stoichiometric production of H_2O_2: one molecule of H_2O_2 is generated for each disulfide bond introduced on new client proteins, thus burdening cells with a potentially toxic oxidant that must be disposed of safely (Pollard et al., 1998). This connection highlights the dual nature of ERO1: from one side is an important enzyme that is involved in protein folding from the other side generates H_2O_2 that at high concentrations is toxic for cells.

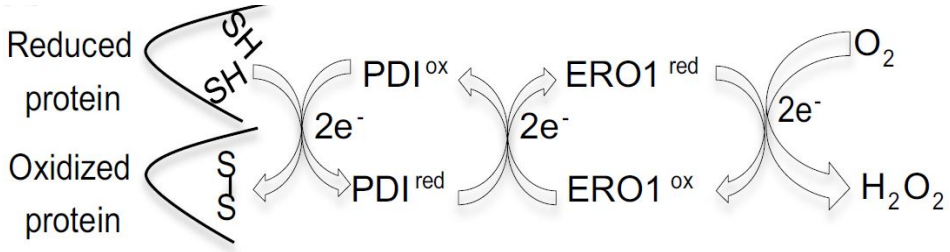

Figure 22 – Cartoon depicting the reaction of disulphide bond formation of client proteins involving the enzymatic activity of ERO1 and PDI. The electrons move from the oxidized, disulphide bonded protein to PDI and then ERO1. The final acceptor of electrons in the reaction is the molecular oxygen that is oxidized to H_2O_2 (Zito, 2015).

1.5 – Skeletal muscle

1.5.1 – Skeletal muscle

Skeletal muscle accounts for 40% of total body weight and contains more than half of all body proteins (Frontera and Ochala, 2015).

Skeletal muscle is composed by myofibers (muscle fibers characterised by the fusion of several muscle cells) surrounded by connective tissue which characterise the extracellular matrix (ECM). The size of each muscle is determined by the number and the size of the myofibers.

Epimysium is the outer connective tissue surrounding the whole skeletal muscle. Inside, groups of myofibers are kept together by another layer of connective tissue named perimysium. Lastly, the single muscle fiber is surrounded by its own plasmamembrane, the sarcolemma, and by the endomysium.

Each myofiber is composed by thousands of myofibrils inside the cytoplasm that are composed by myofilaments of actin (thin filaments) and myosin (thick filaments), which form units called sarcomeres. Sarcomeres, the basic contractile units of the skeletal muscle, are parallel subunits repeated along the myofibril and are aligned with the sarcomeres in the next myofibril, depicting a pattern that causes the fibers to appear striped, hence the term “striated” for the skeletal muscle (Figure 23).

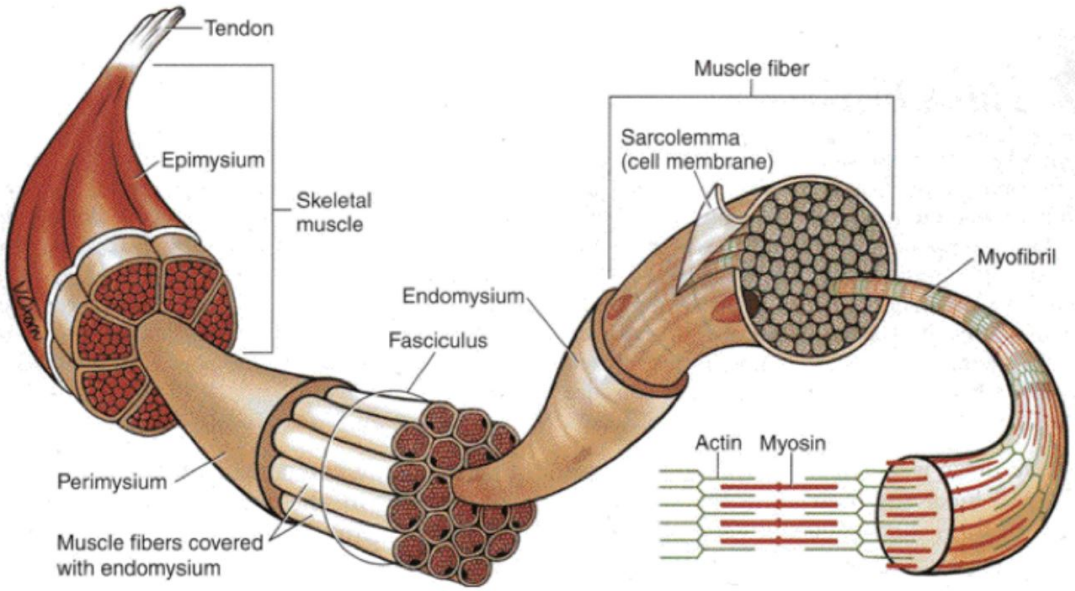

Figure 23 – General skeletal muscle architecture. From epimysium to endomysium, different layers of connective tissue wrap thousands of myofibers (Kraemer, W.J., Fleck, S.J. & Deschenes, M.R., 2012).

1.5.2 – Skeletal muscle and its ER

An important component of the sarcomere is the "sarcoplasmic reticulum", SR. Indeed, inside muscle fibers there is not only ER but also an extensive myofibril-associated network of membranes termed SR, which is a differentiated domain of the muscle ER dedicated to calcium handling. SR originates from ER during the early stage of muscle differentiation when the ER enlarged in volume and myofibrils surrounding it like a net. The SR is specialized to serve muscle contraction through two distinct actions: one is the uptake and storage of calcium ions which is mediated by the calcium ATPase SERCA, distributed over the extensive free SR. The second function is the rapid release of calcium that occurs at the level of the junctional SR (JSR) that is in close contact with the transverse tubule (T tubule), invaginations of the plasmamembrane carrying an electrical signal. The JSR-T tubule association forms the triad or Calcium release Unit

(CRU) and contain the complex for the excitation-contraction coupling (EC-coupling). The EC-coupling links the action potential, carried along a T-tubule, to SR calcium release via the Ryanodine Receptors (RyRs). In conclusion muscle fibers contain ER, that is dedicated to protein synthesis, folding and transport, the free SR, whose surface has a high density of SERCA, and therefore allows calcium refill in the SR lumen after muscle contraction, and in direct continuity with the free SR there is the JSR, that is involved in calcium efflux following an action potential (Volpe et al. 1992; Kaisto 2003)(Porter 1945; Franzini-Armstrong 2018).

To meet metabolic demand during contraction and relaxation, skeletal muscle fibers require a large amount of adenosine triphosphate (ATP), mostly supplied by mitochondria that populate the slow-twitch (type I) fiber and fast twitch (type II) fibers with some differences in abundance and distribution. Type I fibers are highly oxidative and have the highest mitochondrial content including triadic and longitudinal mitochondria whereas type II fibers have not only less but almost exclusively triadic mitochondria (Figure 24). In the mitochondrial cristae, the respiratory complexes involved in the oxidative phosphorylation (OxPhos) system are located. The OxPhos converts the energy derived from nutrients in ATP. The efficiency of this oxidative metabolism critically depends on the Krebs cycle (that metabolizes sugars) and β-oxidation (that metabolizes fatty acids), respectively for the generation of reduced nicotinamide adenine dinucleotide (NADH) and reduced flavin adenine dinucleotide (FADH2), which feed electrons to the electron transport chain. Electrons flow is coupled with the translocation of protons across the inner mitochondrial membrane (IMM), generating a transmembrane electrochemical gradient, which is finally exploited by ATP synthase to generate ATP. Oxidative metabolism is controlled by calcium ions which activate several key metabolic enzymes, including pyruvate

dehydrogenase, alpha-ketoglutarate, isocitrate dehydrogenase, as well as complexes I, III, IV and V of the electron transport chain. Therefore, mitochondrial calcium is an important regulator of ATP production. In murine skeletal muscles, both ER and SR are closely associated to mitochondria and about a quarter of the outer surface of mitochondria is very close to the JSR. Studies of electron microscopy indicate that the outer mitochondrial membrane (OMM) is on an average of 130 nm from the site of RyR-mediated calcium release. These measurements support the concept of short-term formation of high calcium microdomains that allow efficient calcium exchange between ER/SR and mitochondria and suggests that ER/SR calcium levels may influence ATP production in mitochondria (Glancy et al., 2013).

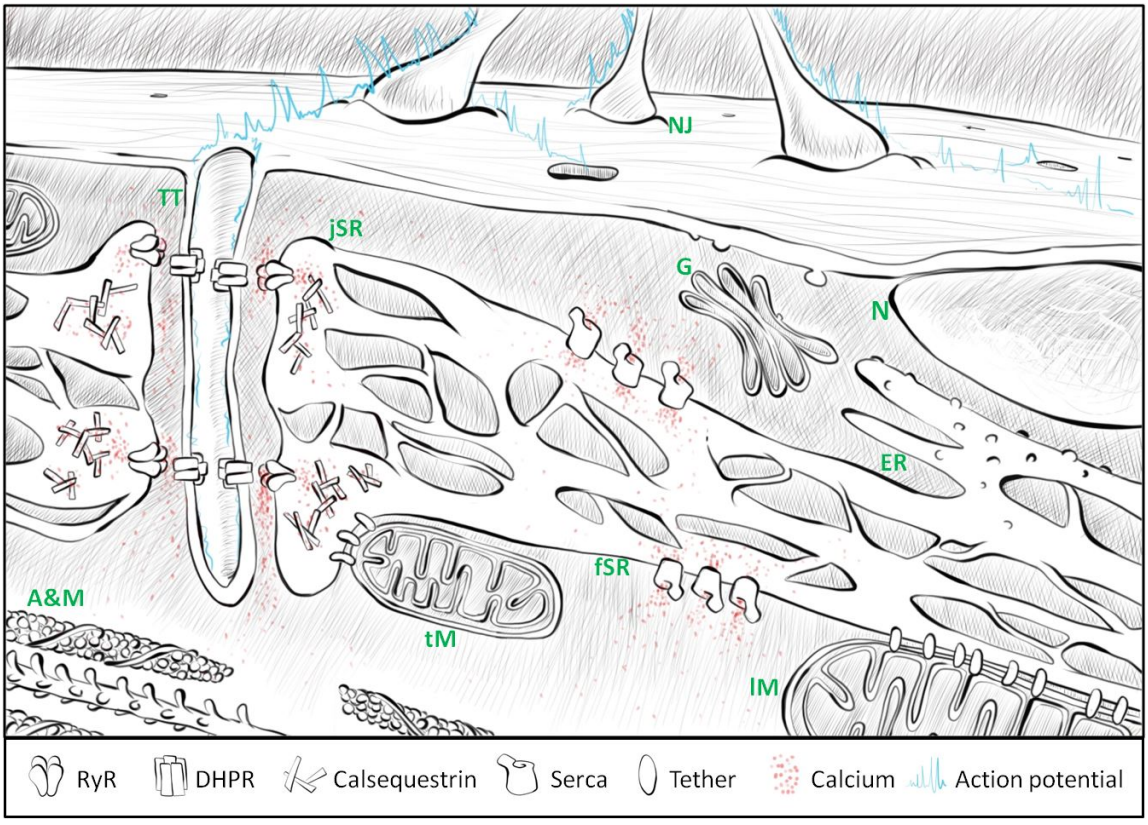

Figure 24 - Cartoon of the spatial organization of ER and SR domains. An action potential is transmitted from the motoneuron to the neuromuscular junction (NJ), and from NJ to the T-tubules (TT). The TT depolarization is sensed by the dihydropyridine receptor (DHPR), which is in close physical contact with RyR1 on the jSR that is also connected to triadic mitochondria (tM). As a consequence, RyR1 opens and calcium leaves the SR. SERCA pumps are mostly distributed on the free SR (fSR) and promote calcium re-uptake in fSR, that is in contact with longitudinal mitochondria (lM). More distal to the TT, close to nuclei (N) and Golgi (G) there is a canonical ER that fulfils the function of protein synthesis and folding and is prone to ER stress.

1.5.3 – ER stress in skeletal muscle

The relevance of ER stress and the consequent UPR in skeletal muscle are suggested by the fact that these are among the primary processes triggered by altered environmental cues such as long-distance running or a simple dietary alteration in skeletal muscle (Wu et al., 2011) (Deldicque et al., 2010).

Skeletal muscle is interesting with respect to the UPR because it has a limited role in protein secretion. However, muscle contraction and relaxation are finely regulated by changes in the intracellular calcium (Ca^{2+}) concentration that also influences protein folding into the ER.

Changes in redox status of both cytoplasmic and luminal cysteines affect the activity of calcium channels and pumps that play a crucial role in the excitation contraction coupling but are also important regulators of ER/SR calcium levels. For example, mixed disulfides between the ER-localised oxidoreductase endoplasmic reticulum resident protein 44 (ERp44) and cysteines on the third luminal loop of Inositol 1,4,5-trisphosphate receptor isoform 1 (IP3R1) inhibit the activity of this ligand-regulated

calcium release channel (Higo et al., 2005), and cysteine-dependent interactions between the oxidoreductase ERp57 and the fourth luminal loop of SERCA 2b inhibit calcium reuptake into the ER by this ATP-driven pump (Li and Camacho, 2004). Similarly, RyR1 activity is also regulated in a redox-dependent manner; for example, H_2O_2-mediated oxidation generated by SR-localised NADPH oxidase isoform 4 (NOX4) affects the redox state of regulatory RyR1 thiols, leading to a leaky RyR1 and affecting muscle performance (Sun et al., 2011).

This suggests that altered redox poise in skeletal muscle may affect the activity of calcium channels and pumps and therefore from one side enfeebles the mechanism of excitation-contraction coupling and from the other side impairs the calcium levels of the ER, that are important for the chaperone activity, therefore triggering ER stress.

1.6 – Ascorbic acid

1.6.1 – Ascorbic acid: an introduction

Ascorbic acid (ASC) is an organic compound with two enantiomeric isoforms: L-ascorbate is the most common while D-ascorbate can be produced synthetically but has no biological function.

The biosynthetic pathway of ASC in animals starts from glucose, which is converted into ASC as a result of a four-step enzyme-mediated reaction. The organ in which this biosynthetic reaction takes place has changed in different species during evolution: it is the kidney in amphibians but the liver in mammals, possibly because a larger organ is a more appropriate mean of producing such a fundamental substance in more complex organisms. However, the biosynthesis of ASC has disappeared in guinea pigs, monkeys and humans since the gene of L-gulono-lactone oxidase (the last enzyme in the biosynthetic pathway of ASC) (GULO) has acquired mutations that have led to it becoming a pseudogene, thus leaving these species incapable of synthesising their own ASC. As a consequence humans are auxotroph for ASC and for them ASC is the vitamin C (Chatterjee, 1973; Drouin et al., 2011)(Figure 25 and Figure 26).

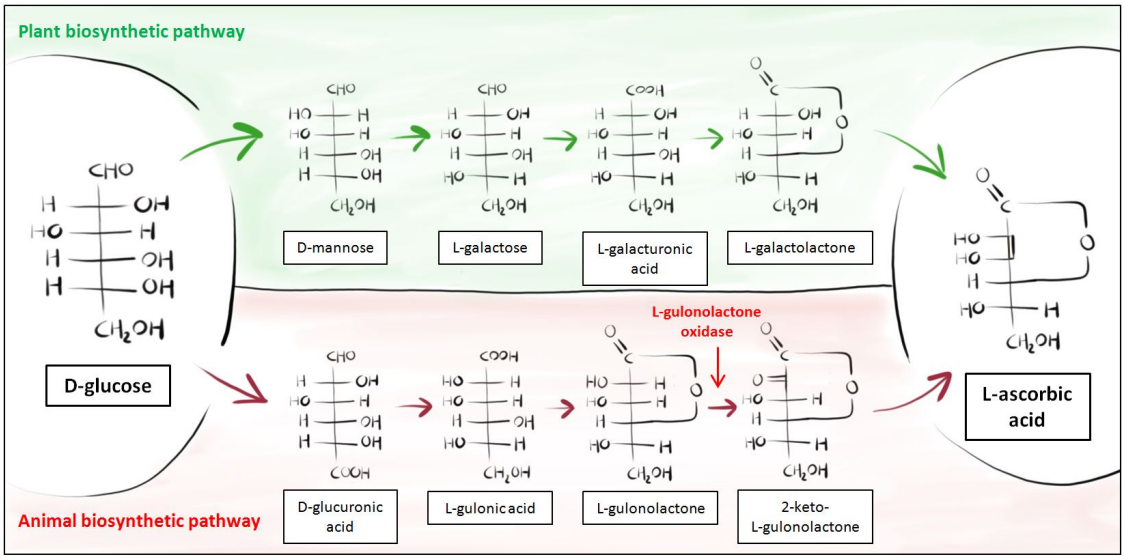

Figure 25 - Differences in the biosynthetic pathway of ASC between plant and animal kingdoms. Plants are prototroph for ASC, human and other primates do not have a functional L-gulonolactone oxidase (GULO) and are therefore auxotroph for ASC.

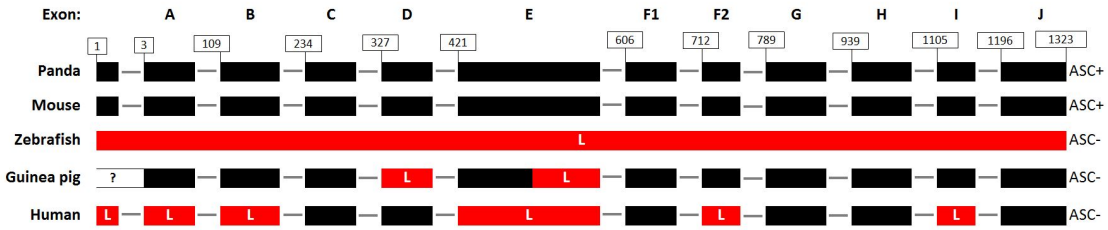

Figure 26 - Schematic graphical representation of exon-intron structures of animal Gulo genes. The conserved 11 exons of Gulo among vertebrates are depicted by capital letter. Black boxes depict homologous exons, exons that have accumulated too many mutations or completely missing are depicted in red marked as "L" (lost). ASC+ indicates species that are prototroph for ASC and ASC- species that are auxotroph for ASC.

Nutritional deficiency of ASC causes scurvy and it occurs when ASC plasma concentrations are less than 0.2 mg/dL. Scurvy is characterised by symptoms such as follicular hyperkeratosis, bleeding gums, pethechiae and impaired wound healing due to connective tissue defects, although less serious symptoms such as gingival inflammation and fatigue are the earliest markers in vitamin C-deficient humans who are still not completely scorbutic (Levine et al., 1996).

Chronic low levels of ASC in the diet bring to arthalgia (joint pain) in knees, ankles and wrists, with the possibility of bleeding in the joint areas. Muscle pain is also a common feature (Fain, 2005). In a guinea pigs study it was postulated that a diet poor in ASC impairs skeletal muscles ability to recover after injuries (Boyle and Irving, 1951).

1.6.2 – ASC metabolism and uptake

After ingestion, the body receives both ASC and ascorbate, which inter-converts depending on pH status. As an anti-oxidant, ASC can undergo an oxidative reaction that leads to the loss of two electrons and the formation of oxidised dehydroascorbic acid (DHA). This may occur as a result of food processing techniques or within the gastrointestinal tract, after which it can be reduced back to ASC by means of various mechanisms (Calcutt, 1951; Wells and Xu, 1994; Wilson, 2002). The results of pharmacokinetic experiments suggest that, after oral ingestion, plasma vitamin C concentrations are strictly controlled by intestinal absorption, tissue transport and renal reabsorption, whereas higher plasma concentrations can only be reached by means of intravenous administration, which by-passes intestinal absorption (Levine et al., 2011).

ASC is transported inside cells by the sodium-dependent vitamin C transporters SVCT1, SVCT2 and SVCT3, which are localised on the cell membrane. Given its chemical

similarity to glucose, DHA is taken up by some members of the glucose transporter (GLUT) family (Rumsey et al., 2000).

The findings of early studies of isolated microsomes by Banhegyi and Benedetti suggested that ASC and DHA are both taken up by the ER, but DHA uptake is preferred (Bánhegyi et al., 1998). The same authors and others later showed that the transport of DHA into the ER is mediated by ER membrane-localised GLUT10, the gene which is mutated in patients with arterial tortuosity syndrome (Callewaert et al., 2008; Gamberucci et al., 2017; Segade, 2010). It has also been shown that SVCT2 is localised on the ER membrane and can mediate the uptake of ASC (Figure 27.) (Muñoz-Montesino et al., 2014).

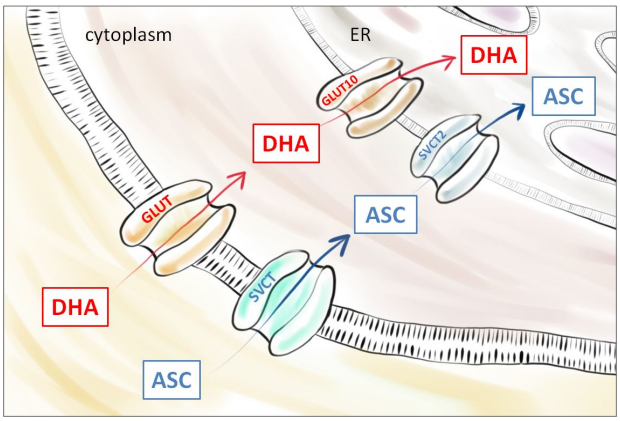

Figure 27 - Graphical representation of ASC and DHA transporters. DHA is actively transported inside the cell by GLUT transporters and inside the ER by GLUT10. ASC enters the cell through SVCT1, SVCT2 channels: once in the cytoplasm it's transported in the ER by SVCT2.

1.6.3 – Antioxidant properties of ASC

The need to ensure that the ER has an efficient anti-oxidant system is highlighted by the fact that it contains enzymes that generate H_2O_2: ERO1 is induced during the ER stress response and its activity is associated with a stoichiometric production of H_2O_2 (Zito, 2015). In addition, there are other sources of H_2O_2 inside the ER (such as the

membrane-localised NOX4) or the close vicinity to mitochondria which, given their phosphorylative oxidation, are one of the main sources of cellular H_2O_2 production.

Like ERO1 and peroxiredoxin-4 (PRDX4) (in enzymatic way), DHA (in non-enzymatic way) is involved in the re-oxidation of protein disulfide isomerase (PDI) during oxidative protein folding, which suggests that the protein folding is in some way related to ASC metabolism. However, *in vitro* assays indicate that this reaction is too slow to be the main pathway for the intra-cellular reduction of DHA to ASC. In addition, it has been shown that ASC can reduce the sulphenic groups generated by an H_2O_2 attack on a protein thiol through a 2-electron oxidation (Tavender et al., 2010; Zito, 2013). After the 2-electron oxidation of ASC to DHA, DHA may follow one of two routes: hydrolysis to 2-3 diketo-l-gulonate (which cannot be converted back to ASC and therefore represents a net loss of cellular ASC) (Figure 28) or enzymatic re-conversion to its reduced form through the glutathione-ascorbate cycle (however, although this is present in plants, it is not known whether it exists in the ER of animal cells) (Bode et al., 1990; Noctor and Foyer, 1998). Once again in relation to its properties as a reductant, ASC is necessary to keep ferrous iron in a reduced state at the active site of ER luminal Fe(II)/2OG-dependent dioxygenases (*e.g.*, prolyl hydroxylases and lisyl hydroxylases), that are enzymes involved in the hydroxylation of collagen, an important modification for the formation of the compact triple helix of collagen. This modification is crucial since it makes collagen competent for the secretion and therefore it can be deposited in the ECM (Myllyharju, 2008)(Figure 29).

ASC, by means of its oxidized form DHA, and ER stress appear to be somehow linked. In fact, ASC can decrease oxidative stress and accumulation of unfolded proteins inside the ER lumen, by re-oxidizing PDI and countering the effects of H_2O_2 accumulation.

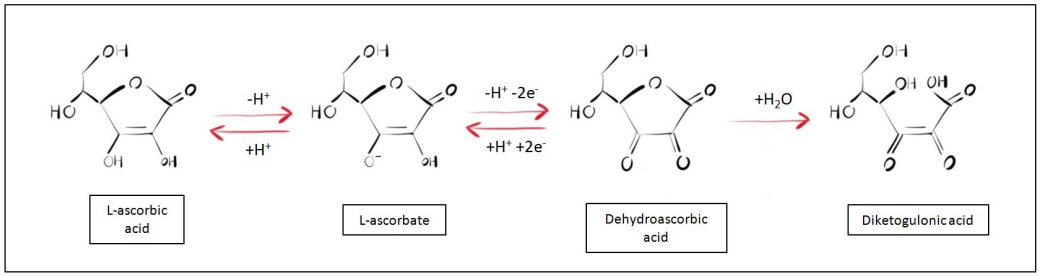

Figure 28 - Different states of ASC. The natural occurring form of ASC is the L-ascorbic acid, which exerts the anti-scorbutic function. This form is present at acidic pH. If the pH is more basic (pH ~ 7) ASC is present as a mono-anion, L-ascorbate. In an oxidant environment, L-ascorbate is oxidised to dehydroascorbic acid (DHA), which can be hydrolyzed to the inactive (without any anti-scorbutic properties) 2,3-diketogulonate.

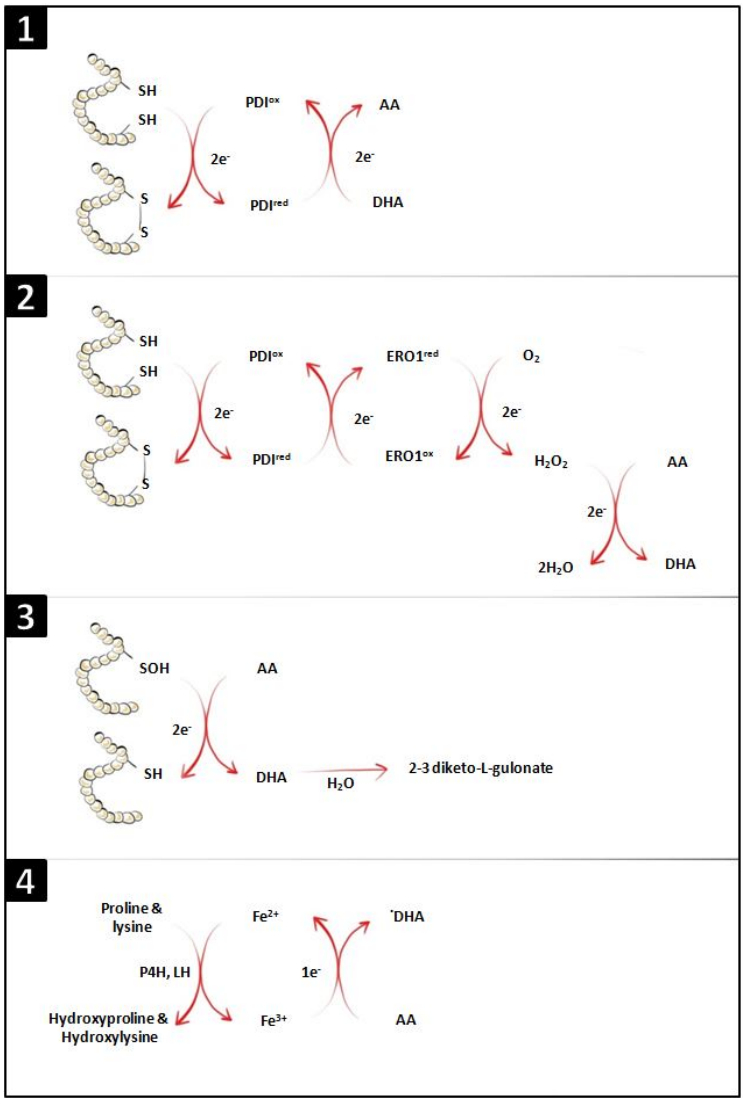

Figure 29 - Redox reactions involving ASC. DHA and ERO1 are respectively involved in the non-enzymatic and enzymatic reaction of PDI-re-oxidation during oxidative protein folding (1 and 2). ASC may reduce protein sulphenylation due to an H_2O_2 attack on a protein thiol. Following the oxidation of ASC to DHA, DHA is subject to hydrolysis at 2-3 diketo-l-gulonate, which cannot be converted back to ASC and therefore represents a net loss of intra-cellular ASC (3). Inside the ER, ASC is required to maintain the reduction of ferrous iron at the active site of ER luminal Fe(II)/2OG-dependent dioxygenases (e.g., prolyl and lisyl hydroxylases, P4H and LH), which are enzymes involved in the hydroxylation of collagen (4).

ASC is transported and present in almost all tissues. Regarding skeletal muscle, ASC is transported by the high-affinity, low capacity transporter SVCT2 (Low et al., 2009). It has been estimated that skeletal muscle contains relatively little ASC in comparison to other tissues (approximately 3-4mg/100g of muscle) (Savini et al., 2005), but the large amount of skeletal muscle means that it stores almost 70% of the total AA in the body suggesting an important function of this vitamin in this specific tissue (Omaye et al., 1987).

Chapter 2 - Rationale and specific aims

The loss of function of SEPN1 in humans gives rise to myopathy, but the lack of an obvious muscle phenotype in SEPN1 knock-out mice (SEPN1 KO) (Rederstorff et al., 2011) and the sensitivity of this model to oxidative stress lead us to postulate that the redox function of SEPN1 is compensated in the endoplasmic reticulum of the murine muscle. The consequences of the absence of SEPN1 on the muscle function will be evaluated with different approaches. The role of ascorbic acid in covering the function of SEPN1, the impact of the loss of SEPN1 in diaphragm and the effect of external factors able to trigger ER stress such as a high-fat diet.

SPECIFIC AIMS:

- To investigate if ASC can mimic SEPN1 function in the ER. This arrangement would explain why mice, which are still able to synthesize ASC, are protected against the absence of SEPN1. To test the hypothesis that ASC is a redundant factor of SEPN1, a mouse model dependent on exogenous ASC for survival will be generated and crossed with SEPN1 knock-out mice in order to obtain compound mice that are devoid of SEPN1 and dependent on exogenous ASC. These compound mutants will be used to evaluate the effect of the lack of SEPN1 on the stress of the endoplasmic reticulum (ER stress) and muscle phenotype.

- Different muscles (hind limb muscles and diaphragm) of SEPN1 KO mice will be analysed for the presence of pathological signs and ER stress.
- Environmental cues as high fat diet, that is known to trigger ER stress in muscle, will be scrutinized to study the effects on the muscle phenotype of SEPN1 KO mice.

Chapter 3 - Results

3.1 –Role of Ascorbic Acid in SEPN1-RM

3.1.1 – Preliminary data

It was already observed that the ER-resident ASC may be involved in an electron redox reaction that, by relieving ER proteins of their hyperoxidised state, converts ascorbate into an unstable oxidised dehydroascorbate derivative with a consequent net loss of ASC (Zito et al., 2012). In order to test the ASC metabolism in SEPN1 deficient myoblast, we stably lowered SEPN1 levels by means of lentiviral shRNA in C2C12 cells, a myoblast cell line. The resulting SEPN1 Knock down (KD) cells had 70% less SEPN1 and we compared these cells with mock infected cells (WT). To explore the turnover of ASC in WT and SEPN1 KD C2C12 cells we used a quantitative high-performance liquid chromatography (HPLC)-based method that selectively measures the reduced form of ASC (Fig.30).

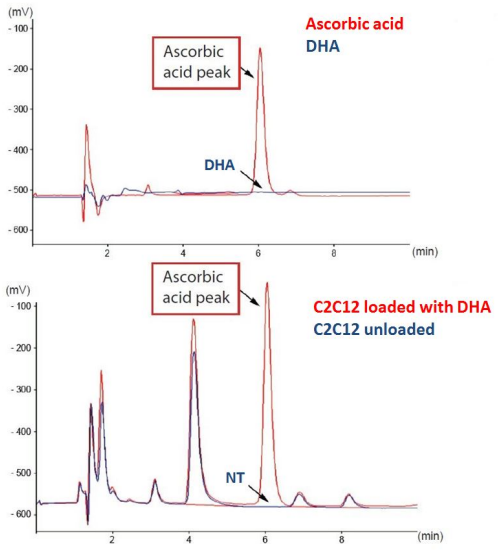

Figure 30 - HPLC traces of ASC. The upper traces show a peak signal for the standard ASC that is not detected for the standard DHA indicating that the method is specific for the detection of ASC and does not detect its oxidized form, DHA. The lower traces show a peak signal of ASC in C2C12 cells loaded with DHA, indicating a conversion of the latter to reduced form of ASC inside the cells.

After a short pulse of DHA (DHA was used as is more efficiently taken up than ASC) in WT and SEPN1 KD C2C12 cells, the levels of ASC were measured in both cells. The decay of ASC was observed to be faster in the SEPN1 KD cells than in the WT cells (Fig. 31) suggesting a more rapid turnover of ASC in SEPN1 KD cells.

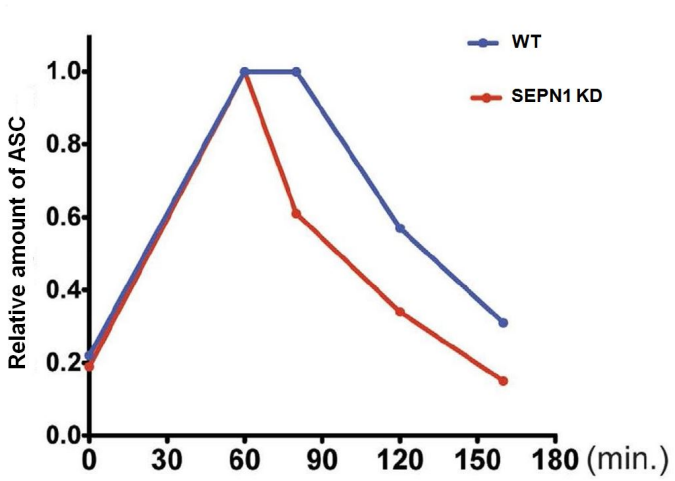

Figure 31 – Accelerated ASC turnover in SEPN1 KD cells. WT and SEPN1 KD cells were challenged with DHA and later the intracellular metabolism of the ASC examined by HPLC. Briefly, cells were supplemented with 25 µM of DHA for 30 minutes and then the ASC cellular content was measured at different time points after withdrawal of the oxidized vitamin from the cellular media. The height of the peaks at any time point is plotted after the arbitrary value of 1 that had been assigned to the highest peak.

3.1.2 –Mouse model

Unlike human and zebrafish, in which SEPN1 loss of function gives rise to an overt muscle phenotype, SEPN1 KO mouse does not show any apparent phenotypical alteration and thus seems to be protected by the possible existence of compensatory pathways.

The faster turnover of ASC in SEPN1 KD cells may suggest that this vitamin moderates hyperoxidation and thus may preserve muscle function in SEPN1 KO mouse. Accordingly, mice are still capable of producing ASC and thus can better cope with the lack of SEPN1, whereas human and zebrafish are ASC auxotrophs and thus may have a

limited amount of the protective ASC in muscle, showing an overt muscle phenotype following SEPN1 deficiency.

In order to test whether a limited amount of ASC in the skeletal muscle of SEPN1 KO mice compromises muscle homeostasis and exacerbates their phenotype, we used a mouse model that resembles the human condition of ASC auxotrophy.

Therefore, mice lacking L-Gulonolactone oxidase (Gulo KO mice), the enzyme of the last step of ASC biosynthesis, that depend on exogenous vitamin C for survival, were crossed with SEPN1 KO mice. Two sets of crosses were scheduled: female mice heterozygous for Gulo (Gulo Het mice) were crossed with male Gulo Het mice, and female SEPN1 KO, Gulo Het mice were crossed with male SEPN1 KO, Gulo Het mice, in order to recover all four informative genotypes (wt, SEPN1 KO, Gulo KO and SEPN1 KO, Gulo KO (DKO)) in the offspring. The DKO mice could not be obtained by crossing Gulo KO mice since the offspring did not survive the perinatal stage, although the mothers were receiving high-dosage of ASC regularly from the drinking water. Most likely, in our mouse model the ASC concentration in the milk produced by the mothers was not sufficient for the pups to survive the first days.

Mice with the double mutant genotype (DKO mice) were recovered with the frequency predicted by the Mendelian transmission of the mutant alleles, thus indicating the lack of any detrimental effect of both mutations on prenatal stages (Figure 32).

SEPN1 wt, Gulo Het **X** SEPN1 wt, Gulo Het

SEPN1 wt Offspring	Percentage Expected	Percentage Obtained	Number Expected	Number Obtained
Gulo Het	50	50	218	218
Gulo KO	25	25,7	109	112
Gulo wt	25	24,3	109	106

SEPN1 KO, Gulo Het **X** SEPN1KO, Gulo Het

SEPN1 KO Offspring	Percentage Expected	Percentage Obtained	Number Expected	Number obtained
Gulo Het	50	48.6	216	210
Gulo KO	25	24.1	108	104
Gulo wt	25	27.3	108	118

Figure 32 - DKO mice were recovered with the expected Mendelian frequency. SEPN1 wt, Gulo Het mice were crossed with SEPN1 wt, Gulo Het mice and SEPN1 KO, Gulo Het mice were crossed with SEPN1 KO, Gulo Het mice and the offspring genotyped at P14. The table indicates the expected and obtained distribution of genotypes at weaning.

Mice lacking GULO need to be supplemented with 330 mg/L of Ascorbate in water to thrive and reproduce normally (Maeda et al., 2000). Given the gender-related differences in ASC metabolism (Nakata and Maeda, 2002), male and female DKO mice and Gulo KO mice were separately randomised to three different dosages of ASC in water (330 mg/L [high dose], 110 mg/L [medium dose] or 66 mg/L [low dose]) at eight weeks of age, when the muscle is fully developed (Figure 33). The aim of this ASC titration was to find a dose of ASC that may reveal signs of SEPN1-RM without inducing the more serious condition of scurvy already in the counterpart of Gulo KO mice.

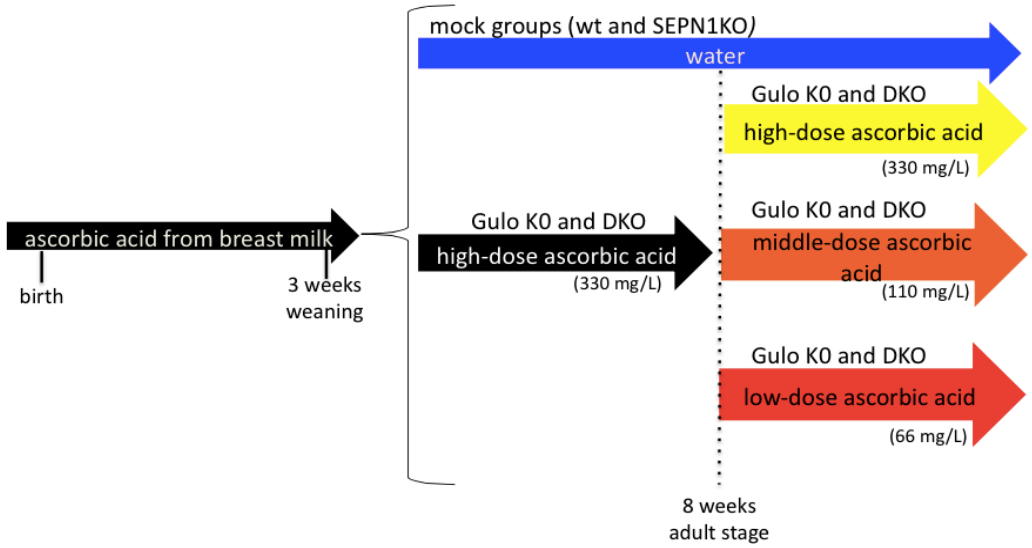

Figure 33 - Scheme of ASC supplementation in mice.

3.1.3 – ASC content in skeletal muscle is proportional to the dietary intake of ASC

The ASC content of the gastrocnemii of the male treated mice was measured by an HPLC method already after one month of treatment (Figure 34) and was proportional to the dietary ASC supplementation. Notably, the gastrocnemii of the mice receiving the high dose of ASC in their drinking water contained significantly less of this vitamin than those of the WT and SEPN1 KO mice, thus suggesting that this dose is sub-optimal (Figure 35).

Unfortunately, we failed to measure reliably ASC in the serum and plasma of these mice and therefore we cannot make any assessment on the correlation between the amount of ASC in the blood and in the skeletal muscle.

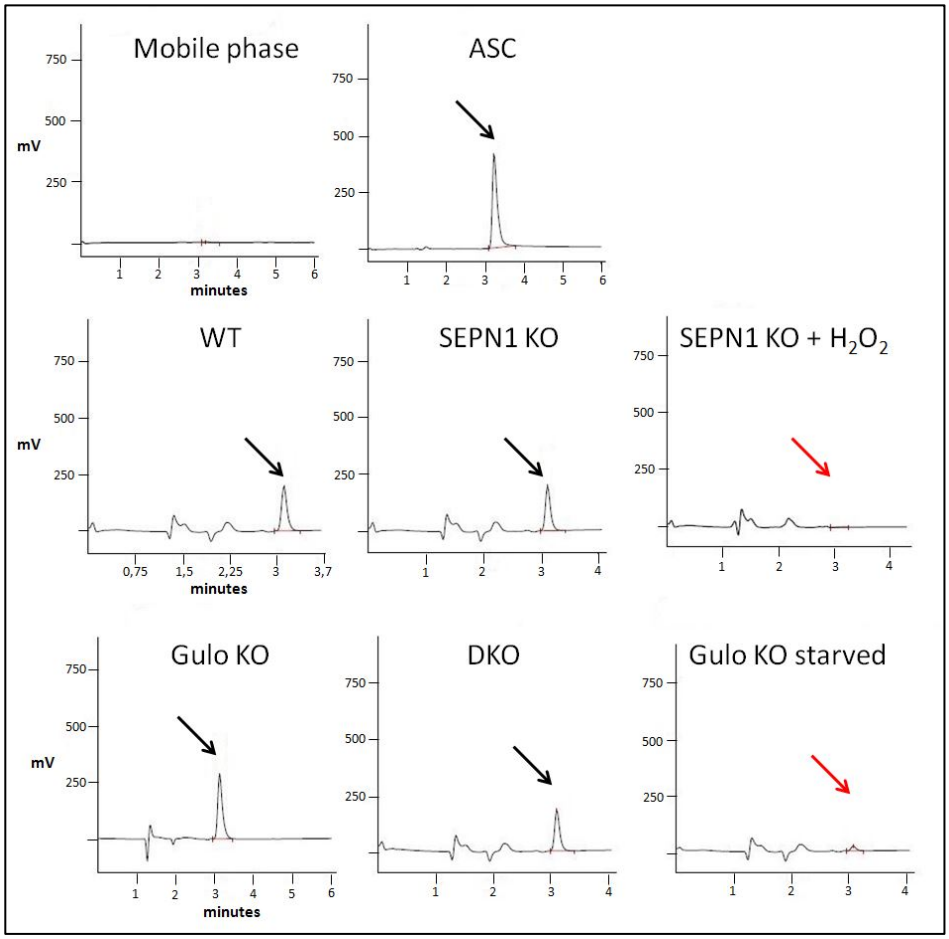

Figure 34 - Representative HPLC traces of the standard ASC and ASC in the gastrocnemii. The upper traces show a peak signal for the standard ASC that is not detected in the mobile phase indicating that the method is specific for the detection of ASC. The lower traces show a peak signal of ASC in the gastrocnemius of the indicated genotypes, that is absent after treatment with the oxidant H_2O_2 and is greatly reduced after one week of ASC starvation in Gulo KO mice. Black arrows indicate the ASC peak (elution time 3,12 - 3,25 min). Red arrows indicate the lack of ASC at the expected elution time.

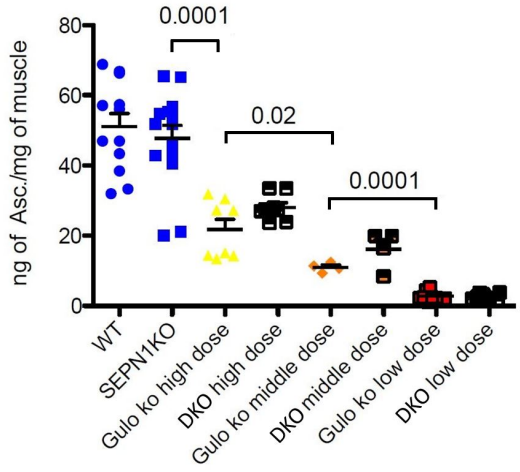

Figure 35 - ASC content in gastrocnemii. ASC content in gastrocnemius of male mice supplemented with the three different dosages of ASC. Each dot represents a single animal (means ± standard errors of the means (SEM), one-way ANOVA test and Bonferroni's post-test, p values are indicated on the graph).

3.1.4 – Limited ASC triggers myopathy in SEPN1 KO mice

The DKO mice supplemented with the low dose of ASC started losing weight after three months and by the fourth month had lost 10% of their original weight. As the weight loss of the DKO mice treated with the low dose of ASC indicated a selective effect on mice with the SEPN1 KO background, all muscles were examined after four months of treatment. In line with their reduced body weight, the mass of the gastrocnemii of the DKO mice treated with the low dose of ASC was reduced by 25%.

In addition, morphometric analysis of the muscle fibers by using “wheat-germ agglutinin” (WGA) staining and measuring the minimal Feret’s diameter (that is a reliable measurement of the fiber size) showed that muscles of DKO mice treated with the low dose of ASC had signs of atrophy (Figure 36).

ER stress response acts by inhibiting protein translation through the PERK pathway, thus analysing the amount of protein synthesis is a valid tool to point out the presence of ER stress due to the restricted availability of ASC. By means of the *in vivo* SUnSET puromycin technique we were able to notice that the atrophy of DKO mice treated with the low dose of ASC was also accompanied by an attenuation of new protein synthesis (Figure 37).

Despite the lack of atrophy, histochemical staining for the activity of the mitochondrial enzyme NADH dehydrogenase (NADH-TR) revealed a high number of minicores and less NADH-TR activity in the DKO mice treated with the medium dose of ASC than in the Gulo KO mice, thus indicating a functional defect in the mitochondria of DKO myofibers that may precede the atrophy noticed in the DKO mice treated with the low dose of ASC (Figure 38).

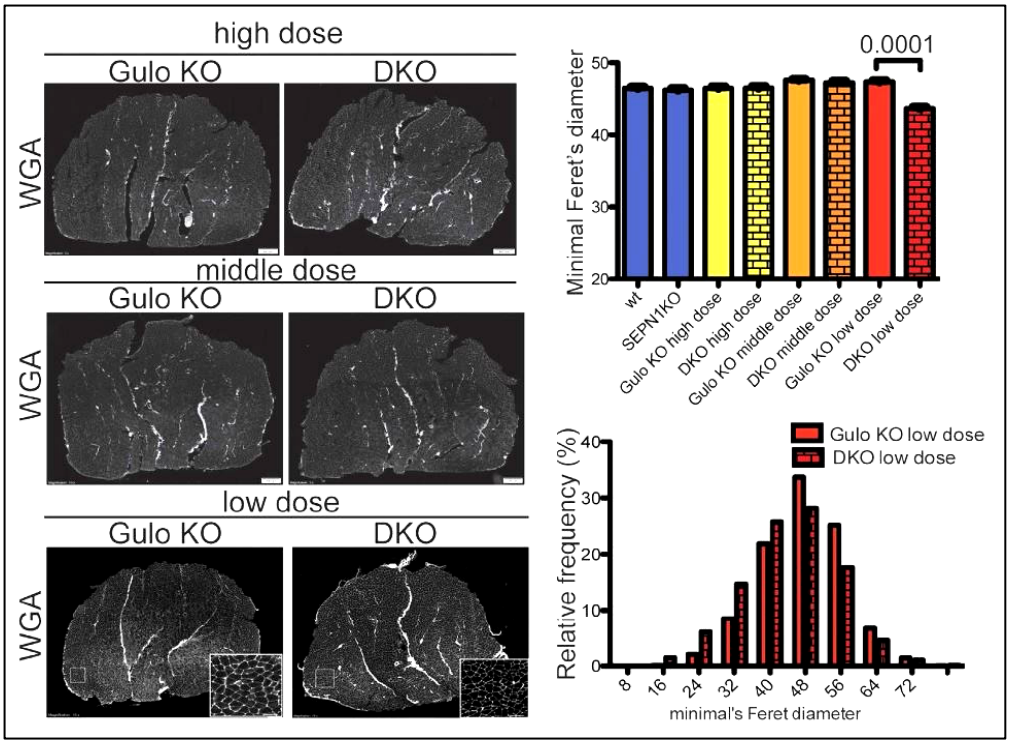

Figure 36 - Low levels of ASC trigger muscle atrophy in DKO mice. On the left, representative micrographs of gastrocnemii stained with wheat-germ agglutinin (WGA). On the right, quantitative measurements of the average size of muscle fibers (minimal Feret's diameter) (µm) and their frequency in gastrocnemii for n=4 muscles and 6000 fibers counted per condition (mean ± standard error of the mean) (two-tailed unpaired Student's t test, p value is indicated on the graph) (scale bar: 100 µm).

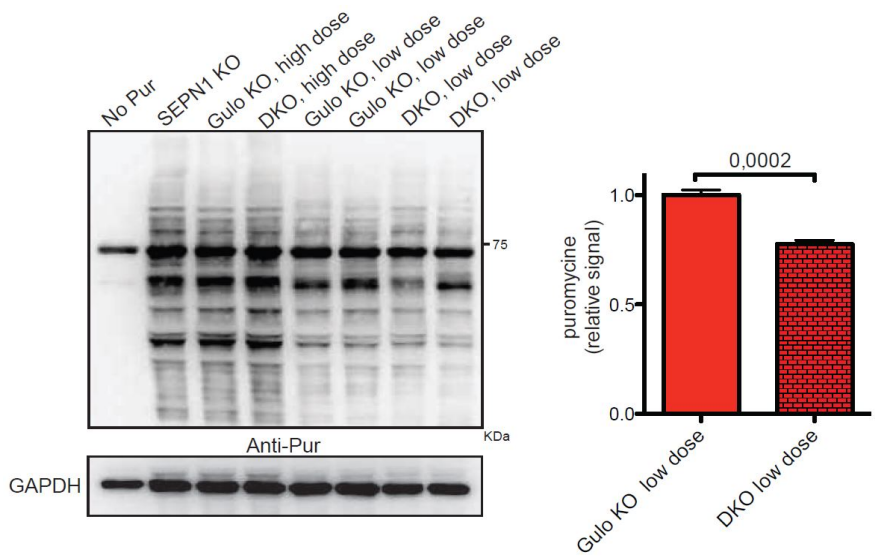

Figure 37 - Low levels of ASC affect the rate of new protein synthesis in DKO muscle. Western blotting analysis of the rate of new protein synthesis (SUnSET method) in the gastrocnemii of mice with the indicated genotype and ASC treatment. "No Pur" indicates a control mouse that was not injected with puromycin. Puromycin incorporation was detected with anti-puromycin (anti-Pur) antibody, and GAPDH was used as loading control. On the left, bar graph shows the quantified signal of puromycin in protein lysates of gastrocnemii. Results are represented as means ± standard errors of the means (SEM) (two-tailed unpaired Student's t test, p value is indicated on the graph) (n=4).

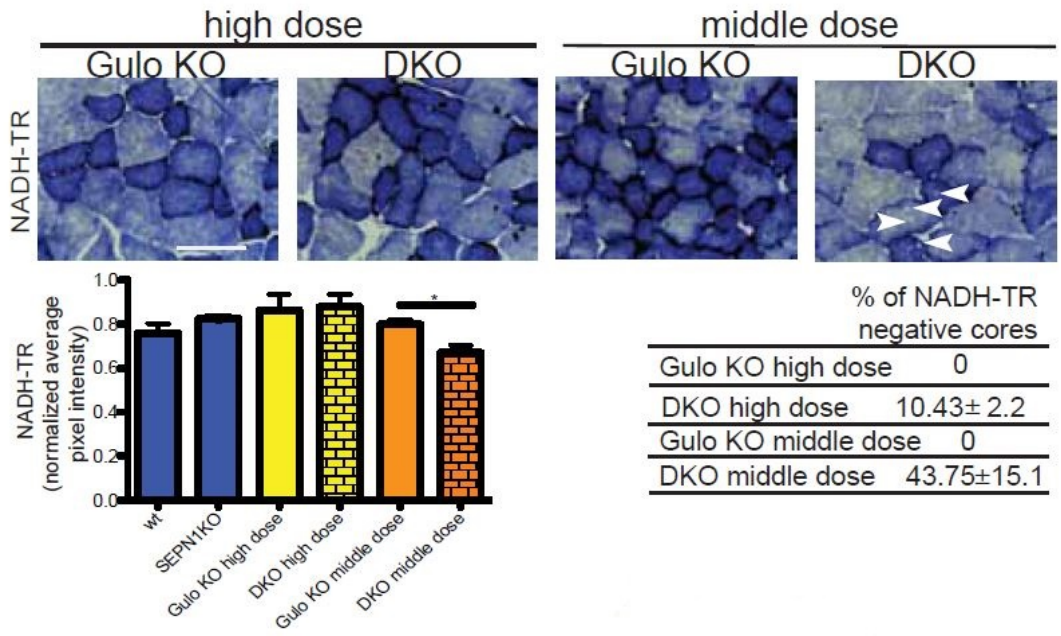

Figure 38 - A middle dose of ASC in DKO muscle is associated with a paler NADH-TR staining and the presence of minicores. Representative NADH-TR staining of gastrocnemii. White arrowheads indicate minicores (n=6 per group, scale bar: 50 µm). Table indicates the percentage of minicore-like structures in type I fibers of gastrocnemii as revealed by NADH-TR labelling (average value from 100 type I fibers). Bar graph indicating quantification of NADH-TR staining reporting for the NADH-TR activity. Results are represented as means ± standard errors of the means (SEM) for n *= 3 per group (two-tailed unpaired Student's t test, *p <0.05).*

In addition, a lower ASC level in muscle together with the lack of SEPN1 increased the expression of mRNA of some ER stress markers (GADD34, BIP, CHOP, ATF4) in DKO mice (as seen by semi quantitative real time PCR). Interestingly, the levels of CHOP, that is considered a maladaptive mediator of the ER stress response in conditions of chronic ER stress, are the highest in DKO mice fed with the lowest dose of ASC thus suggesting a role of ASC in defending ER homeostasis and coping with the lack of SEPN1 in muscle (Figure 39).

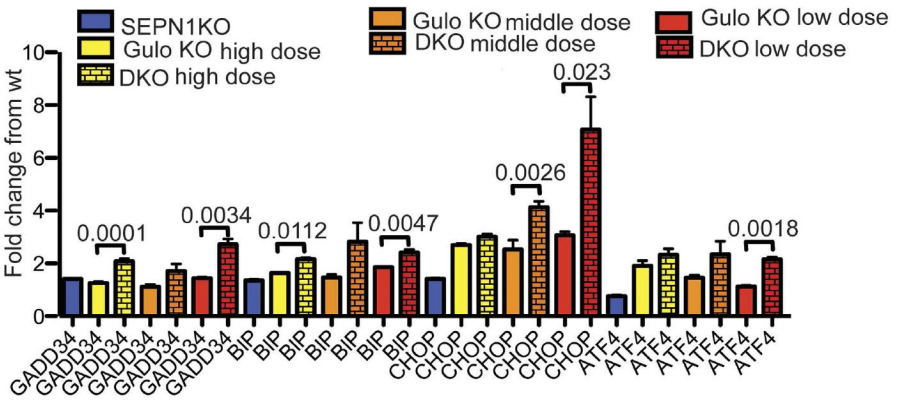

Figure 39 – Relative abundance of ER stress markers mRNAs measured by semi-quantitative real-time RT-PCR in cDNA from gastrocnemii (n=3 per each group). The bar graphs show mean values ±SEM, the differences were examined using a two-tailed unpaired Student's t-test. P values are indicated in the graph.

Importantly, the normalized maximal strength of the gastrocnemius muscle measured *in vivo* tended to be less in the DKO mice regardless of the ASC dose, but was significantly less only in those treated with the medium dose (Figure 40). The DKO muscle of mice treated with the lowest dose of ASC was atrophic and show only reduced absolute muscle strength as seen by the frequency/force graph (Figure 41).

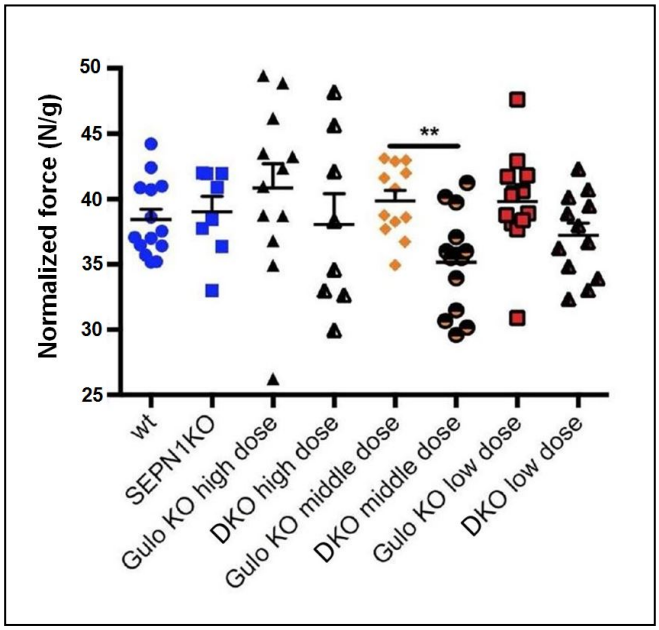

*Figure 40 - A middle dose of ASC affects muscle normalized force of DKO mice. Bar graphs representing the in vivo specific force of the gastrocnemius muscle of the indicated mice after four months of ASC treatment. Please, note the diminished muscle force of the DKO mice supplemented with the middle dose of ASC (110 mg/L). Results are represented as means ± standard errors of the means (SEM) (two-tailed unpaired Student's t test, **p<0.01).*

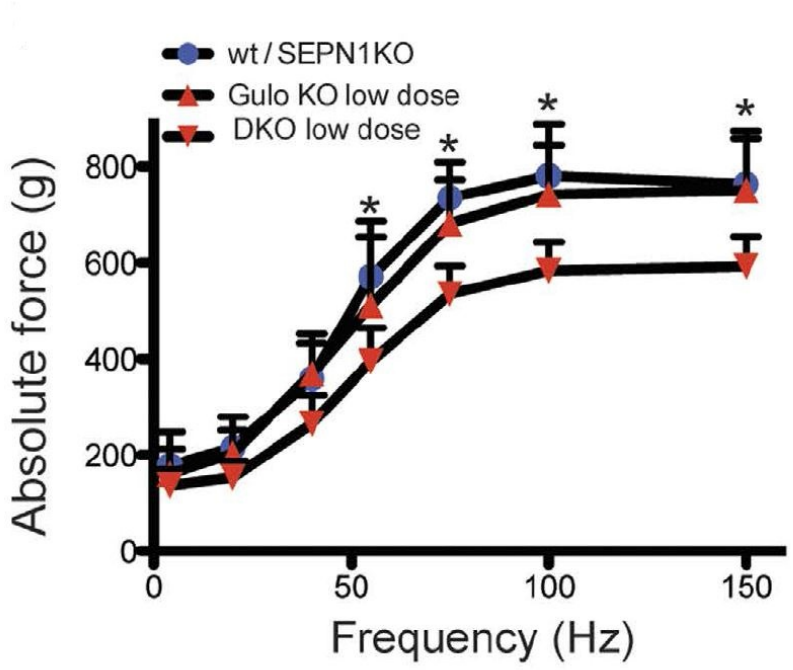

*Figure 41 - A low dose of ASC reduces muscle absolute force of DKO mice. Force-frequency curve of the absolute force (g stands for gram). in male Gulo KO and DKO mice after four months of ASC treatment at 66 mg/L. Results are represented as means ± standard errors of the means (SEM) for n = 12 per group (two-way Anova followed by Bonferroni's post-test, * p<0,05).*

3.1.5 –Conclusions

In this first part of my thesis project we exploited compound Gulo KO mice, which are unable to synthesize ASC, and SEPN1 KO mice in order to investigate whether reduced dietary levels of ASC affect muscle homeostasis. The double mutant mice were randomized and fed with three different concentrations of ASC. After four months of treatment the hind limb muscles were analysed. The reported findings show that a deficiency of vitamin C is associated with ER stress and induces a SEPN1-related pathological muscle phenotype in SEPN1 KO mice, whose severity is inversely proportional to the muscle concentration of the vitamin C: a medium dose of ASC impairs muscle fibers, as seen by the formation of the minicores, and the impaired normalized muscle force, whereas a lower dose triggers a more serious condition of muscle atrophy, thus leading to smaller muscle fibers that develop less absolute force.

This investigation regarding the role of ASC in SEPN1 KO mice was important to point out the role of ER stress in the development of a myopathic condition linked with the absence of SEPN1.

Also, it could be useful to evaluate a potential treatment with ASC in patients. While daily administration of ASC might not represent a cure for the SEPN1-RM, is tempting to assume that it could be helpful to mitigate the symptoms.

3.2 –Diaphragm dysfunction in SEPN1 KO mice

3.2.1 – Aim

Species that are auxotrophs for ASC, such as humans, express a different pattern of transporters for ASC compared to the species that retain the ability to produce endogenous ASC (Montel-Hagen et al., 2008). For these reasons, one of the subsequent steps in this line of investigation should consider an animal model that could resemble even more closely the human condition (such as guinea pigs).

The ASC investigation in the first part of this thesis has been crucial to understand that ER homeostasis is an important factor in the rise of myopathic signs in SEPN1 KO mice and we wanted to deepen the knowledge of this aspect using a less complex mouse model, not dependent on exogenous ASC. In fact, management of the ASC auxotrophic colony was a task that required great effort, due to constant genotyping of the offspring and taking care of the preparation of the vitamin in the drinking water.

Furthermore, diaphragm dysfunction has recently been detected in paediatric patients with SEPN1-RM and occurs when the patients are still ambulant (Caggiano et al., 2017). As the diaphragm is highly enriched in mitochondria which are defective in SEPN1-RM patients and in DKO (Gulo KO, SEPN1 KO) mice treated with the medium dose of ASC we decided to inspect the diaphragm of SEPN1 KO mice for pathological and ER stress signs.

3.2.2 – Diaphragm dysfunction in older SEPN1 KO mice

First of all, we examined mRNA levels of markers (ERO1, CHOP, BIP, GADD34, ATF4, XBP-1s) of the ER stress and ER stress response in the SEPN1 KO diaphragm of four-week-old mice. At this stage, there was a significant decrease of CHOP and an increase of BIP in the diaphragm muscle of SEPN1 KO mice (Figure 42). At twenty-four-week-old there was a significant and marked increase of mRNA levels of CHOP, ERO1, BIP, ATF4 and XBP-1s in SEPN1 KO diaphragm muscle (Figure 43). Higher protein levels of ERO1 and BIP were confirmed in SEPN1 KO diaphragm muscle by immunoblotting (Figure 43).

Despite the lack of substantial morphological defects, as indicated by the H&E staining, or fiber type switching, as indicated by immuno-staining with specific myosins (Figure 44), in SEPN1 KO diaphragm muscle of twenty-four-week-old mice, *ex-vivo* force measurements on isolated strips showed significant impairment in the normalized force (not detected in leg muscles), which was also accompanied by a modest increase of relaxation time (Figure 45).

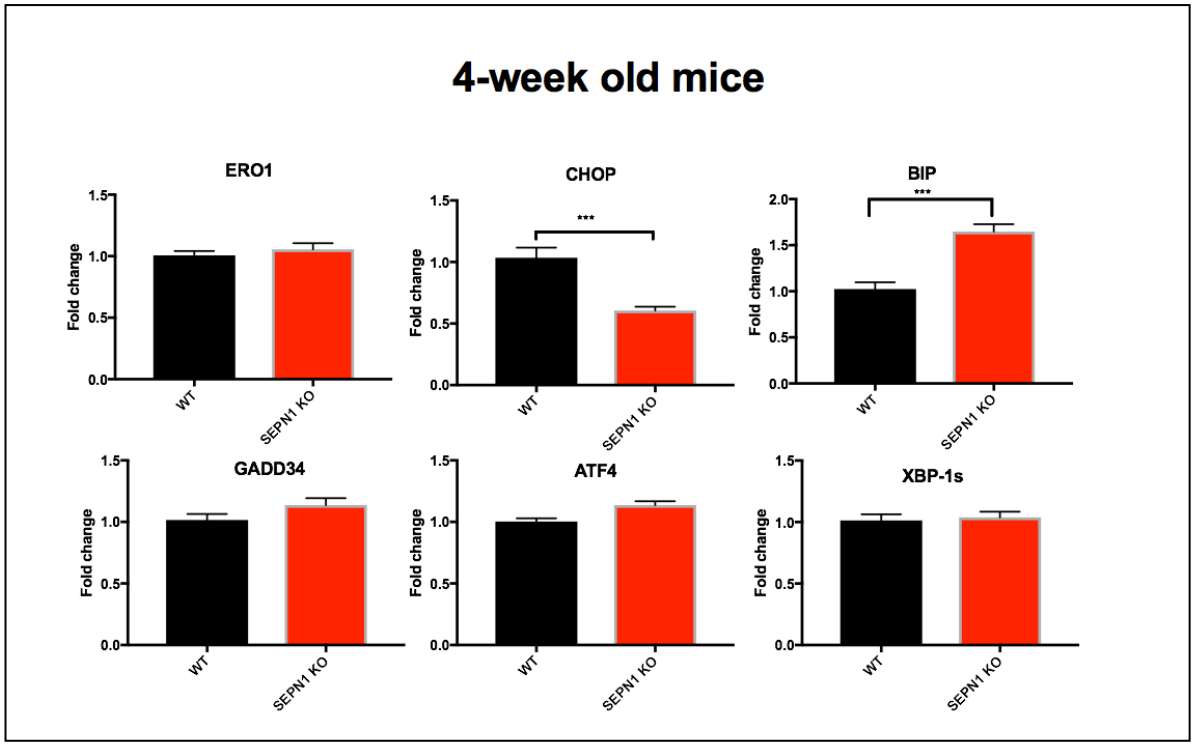

*Figure 42 – Levels of ER stress markers in SEPN1 KO diaphragm of 4-week old mice. Semi-quantitative real-time RT-PCR analysis of ER stress markers of diaphragms from four-week old mice (means ± standard errors of the means (SEM) for n = 4 per group, two-tailed unpaired Student's t test, ***p <0.001).*

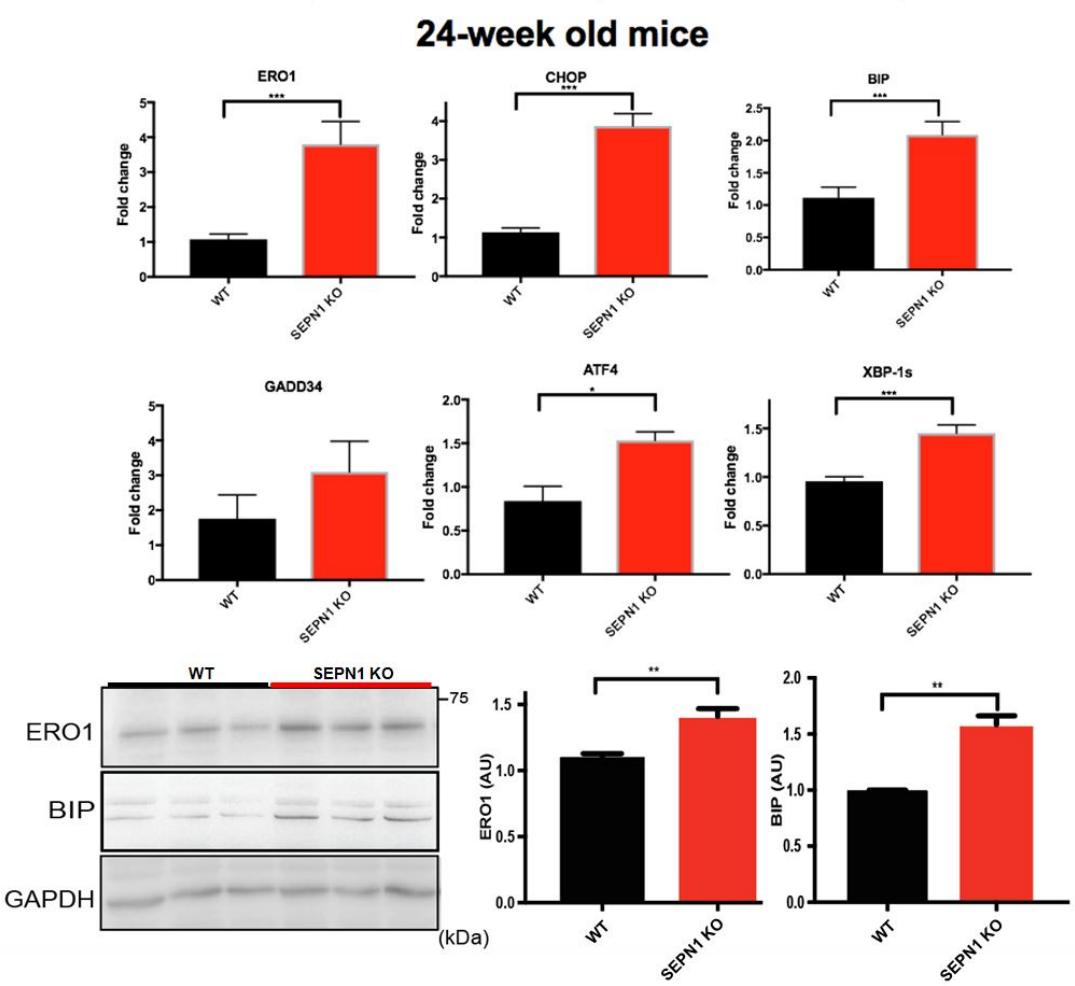

*Figure 43 - Lack of SEPN1 exacerbates ER stress in diaphragm of 24-week old mice. Semi-quantitative real-time RT-PCR analysis of ER stress markers from diaphragms of 24-week old mice (n=6) (means ± standard errors of the means (SEM), two-tailed unpaired Student's t test, * p<0,05, ** p<0,01, ***p <0.001). Bottom: Immunoblots and quantification of relative signals of ERO1 and BIP in diaphragm lysates. GAPDH is used as a loading control.*

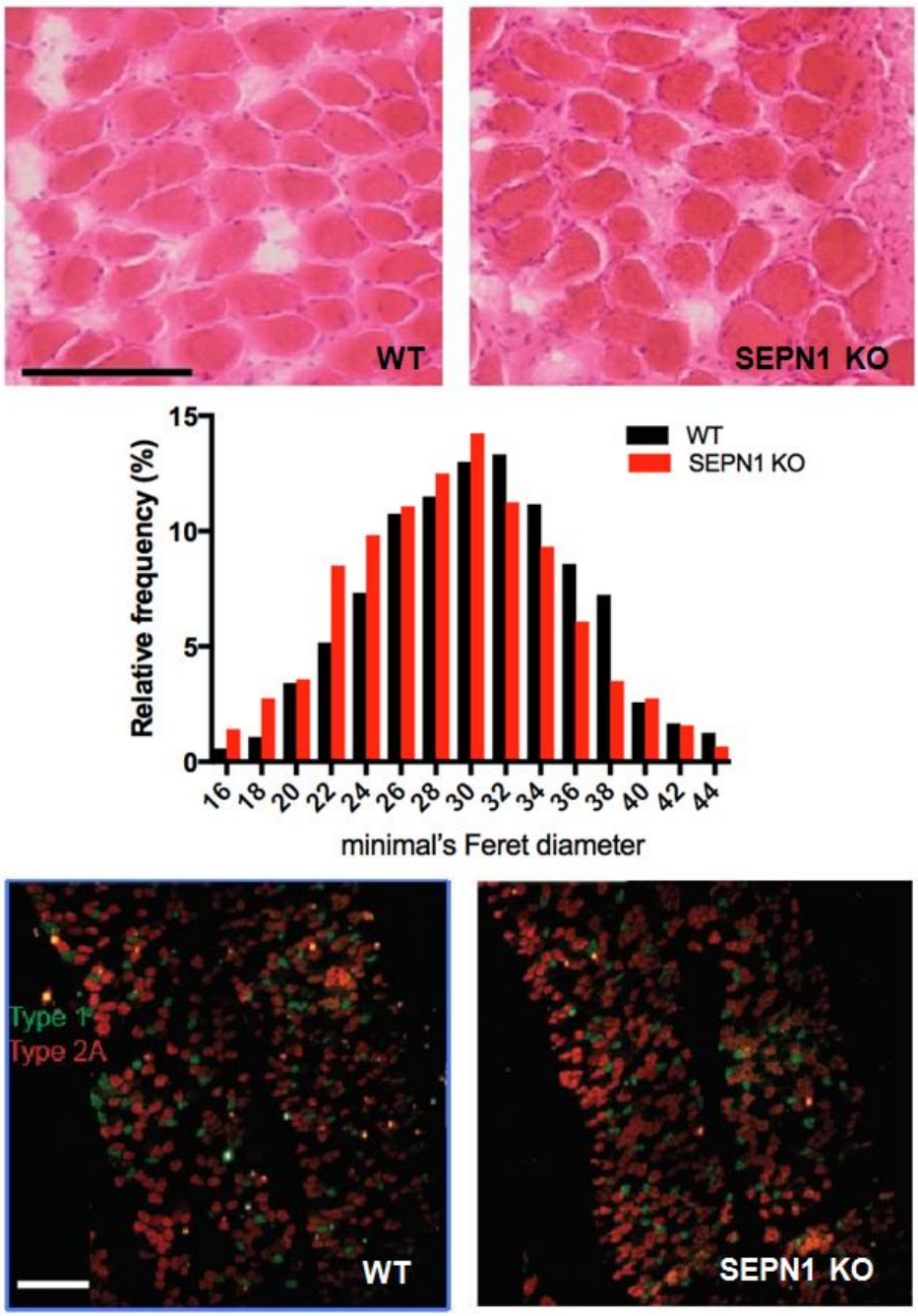

Figure 44 - Lack of SEPN1 does not impair muscle morphometry. Up: H&E staining of WT and SEPN1 KO mice diaphragm. Middle: minimal Feret's diameter (µm) (n=1200 total fibers from 3 different animals for each genotype) of WT and SEPN1 KO mice diaphragms. Bottom: fiber type immunostaining images of diaphragms using specific myosin heavy chain antibodies (scale bars = 100 µm).

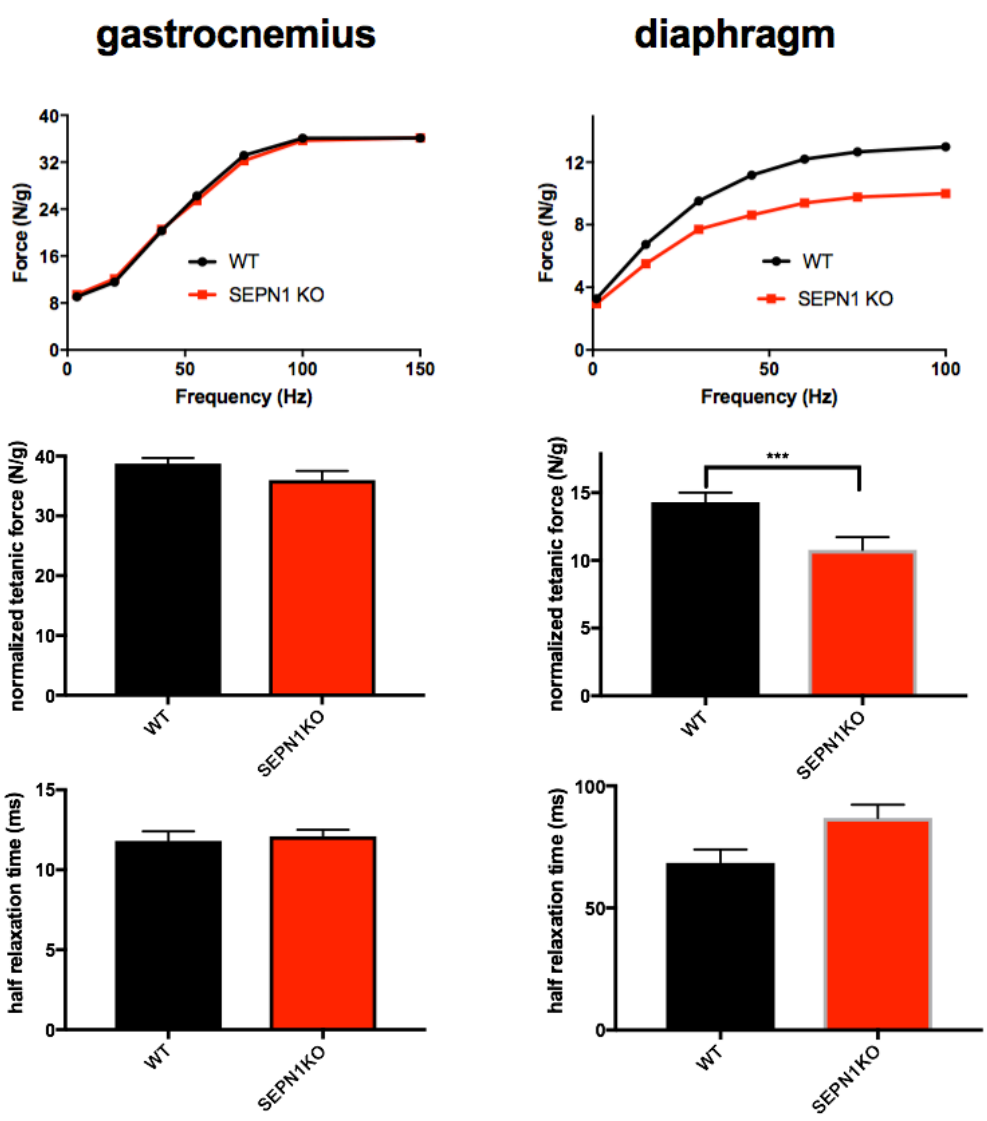

*Figure 45 – Contractile diaphragm dysfunction in SEPN1 KO mice. Frequency curves, tetanic force and half relaxation time (stimulation frequency at 100 Hz) observed in-vivo in the gastrocnemii (left half of the panel) (n=12) and ex-vivo in diaphragm strips (right half of the panel) (n=20) (means ± SEM, two-tailed unpaired Student's t test, ***p <0.001).*

3.2.3 – Ablation of CHOP rescues diaphragm impairment in SEPN1 KO mice

It was shown recently that the genetic deletion of the ER stress mediator CHOP preserves tissue function after a chronic ER stress (Marciniak et al., 2004; Pennuto et al., 2008; Song et al., 2008). CHOP is a pro-apoptotic gene that is activated due to persistent and unresolved ER stress by the UPR program (Ron and Walter, 2007). CHOP KO mice don't show any pathological phenotype, and they don't differ from wild type in terms of lifespan, fertility and thriving ((Zinszner et al., 1998).

Inspired by these studies we decided to test whether CHOP ablation is also beneficial to SEPN1 KO muscle. To this purpose CHOP KO mice (Zinszner et al., 1998) were crossed with SEPN1 KO mice, and diaphragm function tested in mice with the four informative genotypes: WT, CHOP KO, SEPN1 KO, and double SEPN1/CHOP KO (DKO) mice. The contemporary deletion of CHOP and SEPN1 lowered ERO1 mRNA levels and those of other ER stress markers in diaphragms (Figure 46).

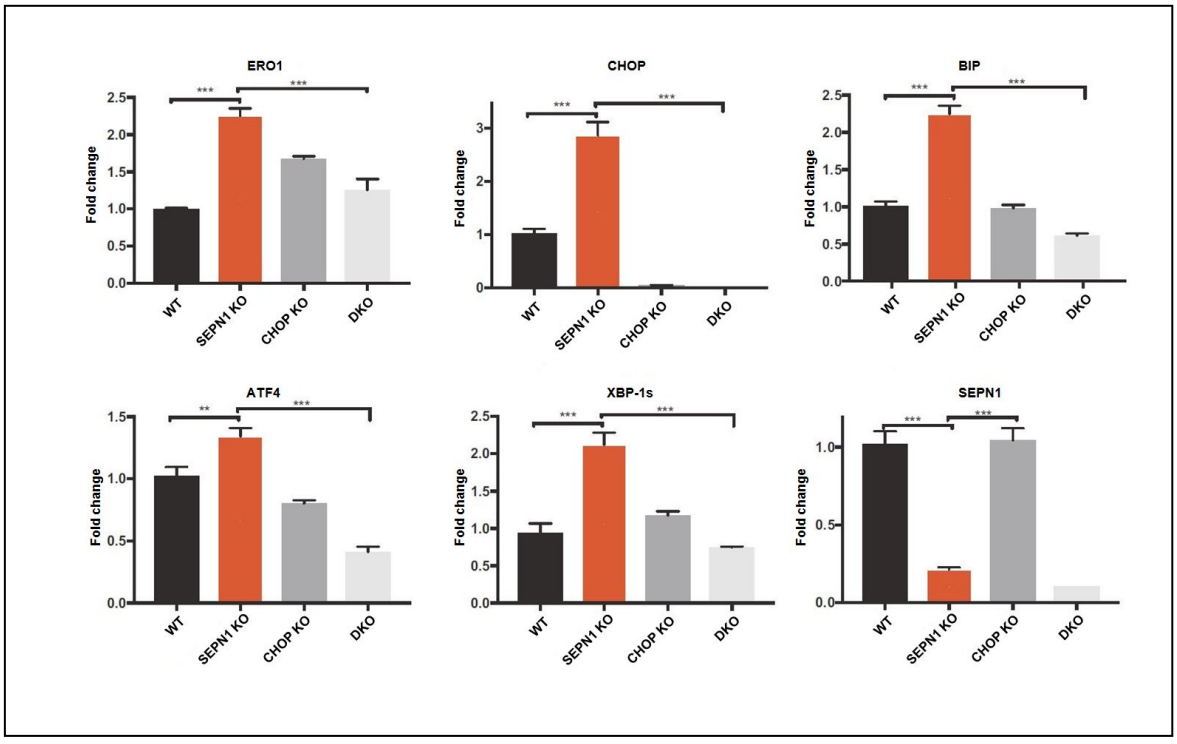

*Figure 46 - Deletion of CHOP in mice lacking SEPN1 decreases ER stress. Semi-quantitative real-time RT-PCR of ER stress response markers in mRNA obtained from WT, SEPN1 KO, CHOP KO and DKO mice diaphragms (n=8) (means ± standard error of the mean (SEM), one-way ANOVA multiple comparison test and Sidak's post test, **p <0.01, ***p <0.001).*

As one consequence of ER stress is the attenuation of protein synthesis, we examined the levels of protein translation in the diaphragms of WT, CHOP KO, SEPN1 KO and DKO mice by injecting puromycin in mice and using the SUnSET puromycin assay. The results of this assay show that the rate of protein synthesis was lower in SEPN1 KO diaphragms when compared to the WT and restored in DKO mice (Figure 47).

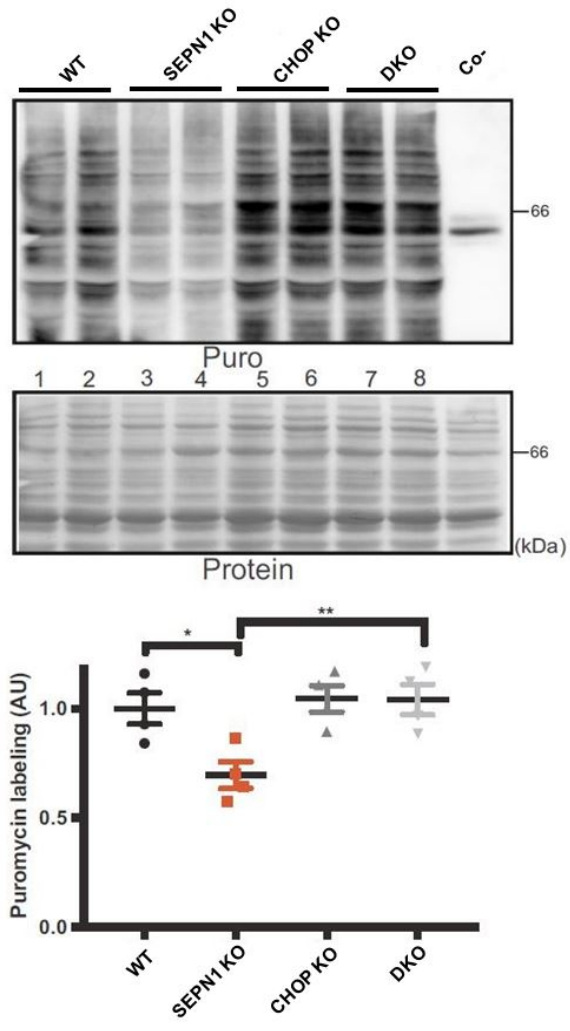

*Figure 47 - Deletion of CHOP rescues the impaired protein synthesis in diaphragms of SEPN1 KO mice. Immunoblot and quantification (with arbitrary units) of puromycin-tagged proteins (newly synthesised proteins) in WT, SEPN1 KO, CHOP KO and DKO mice diaphragm. Below, it is shown a ponceau (Protein) of the loaded proteins. "Co-" indicates a control mice not injected with puromycin. (means ± standard error of the mean (SEM), one-way ANOVA multiple comparison test and Sidak's post test, **p <0.01).*

Importantly, *ex vivo* measurements of diaphragm force of WT, CHOP KO, SEPN1 KO and DKO mice show a significant recovery of this force in the DKO mice indicating that the deletion of CHOP in a SEPN1 KO diaphragm improves muscle physiology (Figure 48).

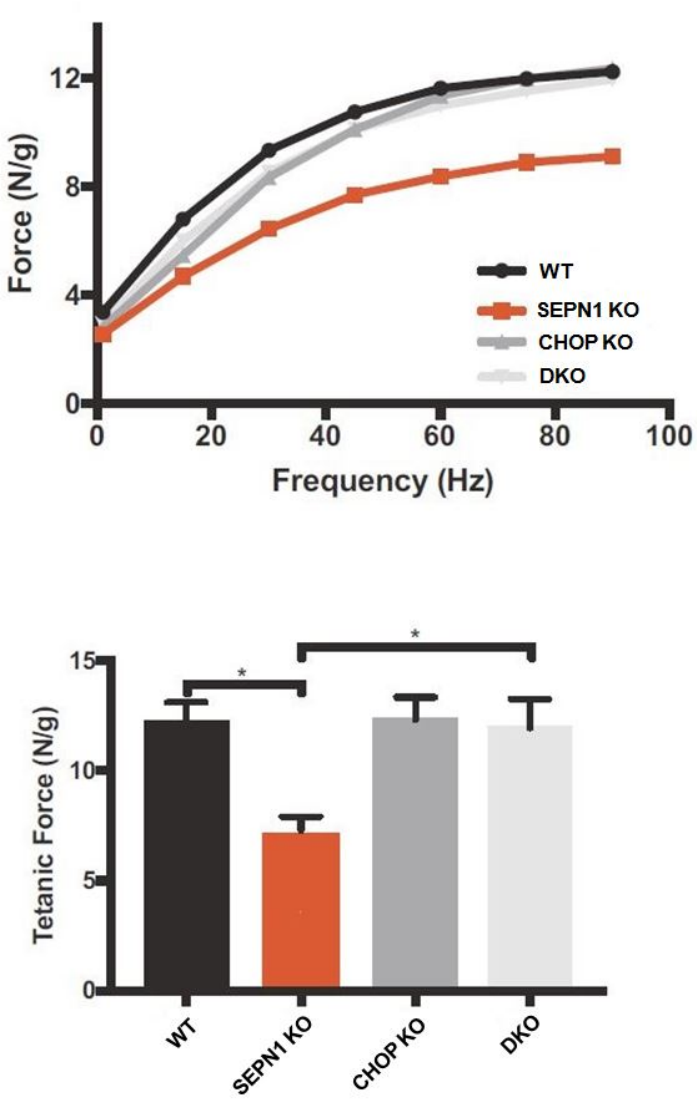

*Figure 48 - Deletion of CHOP in mice lacking SEPN1 rescues diaphragm dysfunction. Representative force frequency curves and below bar graphs of tetanic force of ex-vivo diaphragm strips from WT, SEPN1 KO, CHOP KO and DKO mice (n=8) (means ± standard error of the mean (SEM), one-way ANOVA multiple comparison test and Sidak's post test, *p <0.05).*

3.2.4 – Ablation of CHOP reduces exercise-induced ER stress in SEPN1 KO muscle

Although we and others have shown that the hind limb muscles of SEPN1 KO mice have no gross alterations in muscle histology, physiology or in the levels of the ER stress markers, we reasoned that SEPN1 function may be important when activity levels rise during muscle activity. Therefore, we investigated the expression of the mRNA of the ER stress markers in soleus and gastrocnemius muscles (two different hind limb muscles) isolated from mice after exhaustive running, during which the muscle contractile activity significantly increases (Wu et al., 2011). ER stress markers (ERO1, BIP, XBP-1s, ATF4 and GADD34) were more upregulated after running in SEPN1 KO soleus, that is an oxidative muscle, when are compared to those of the WT. Milder differences in the levels of ER stress markers were also seen in the gastrocnemius, that is mainly a glycolytic muscle. Interestingly, ERO1 levels, and those of the other ER stress markers, were down-regulated in the DKO soleus after running (Figure 49 and 50).

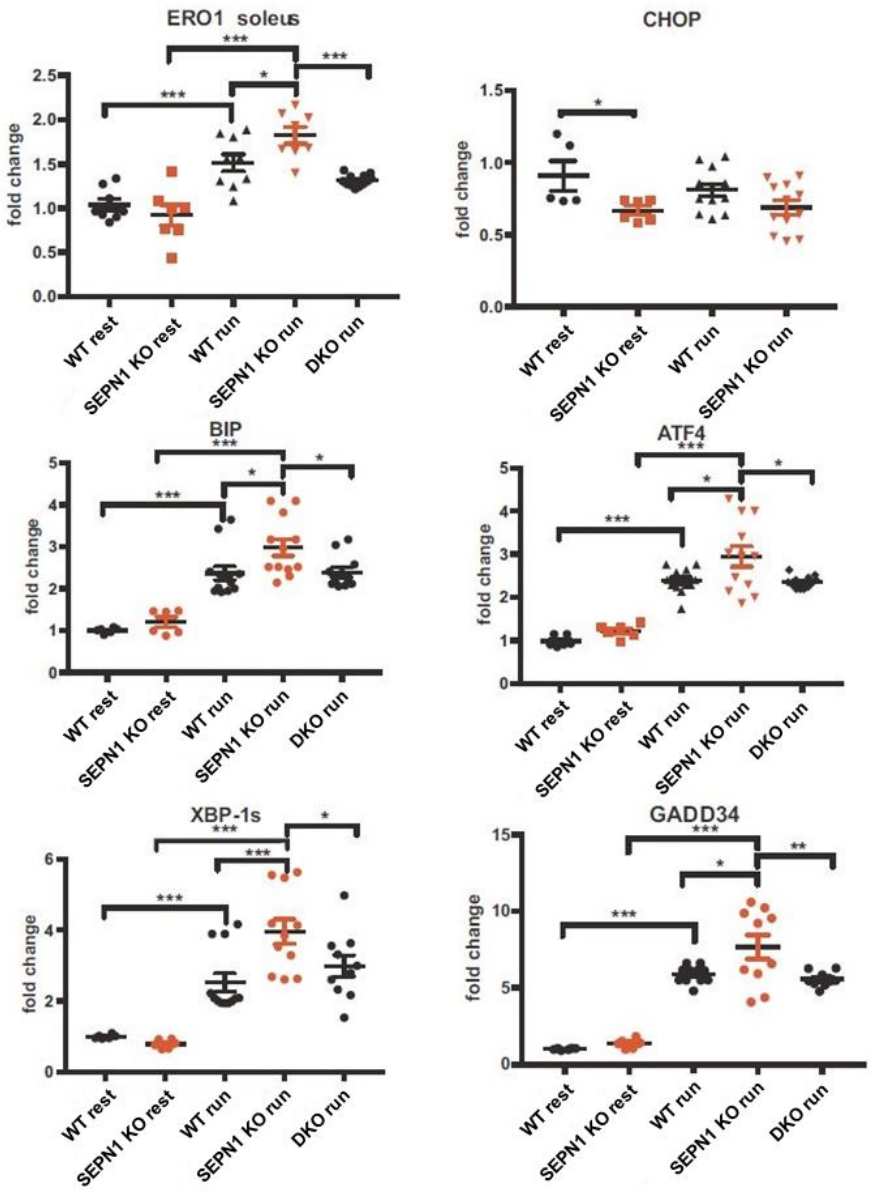

*Figure 49 - Deletion of CHOP reduces ER stress in the soleus of SEPN1 KO mice after an intensive bout of exercise. Semi-quantitative Real-time RT-PCR analysis of ER stress markers in mRNA obtained from soleus of 24-week old sedentary (rest) and exhausted (run) mice (means ± standard error of the mean (SEM), one-way ANOVA multiple comparison test and Sidak's post test, *p <0.05, **p<0.01, ***p <0.001).*

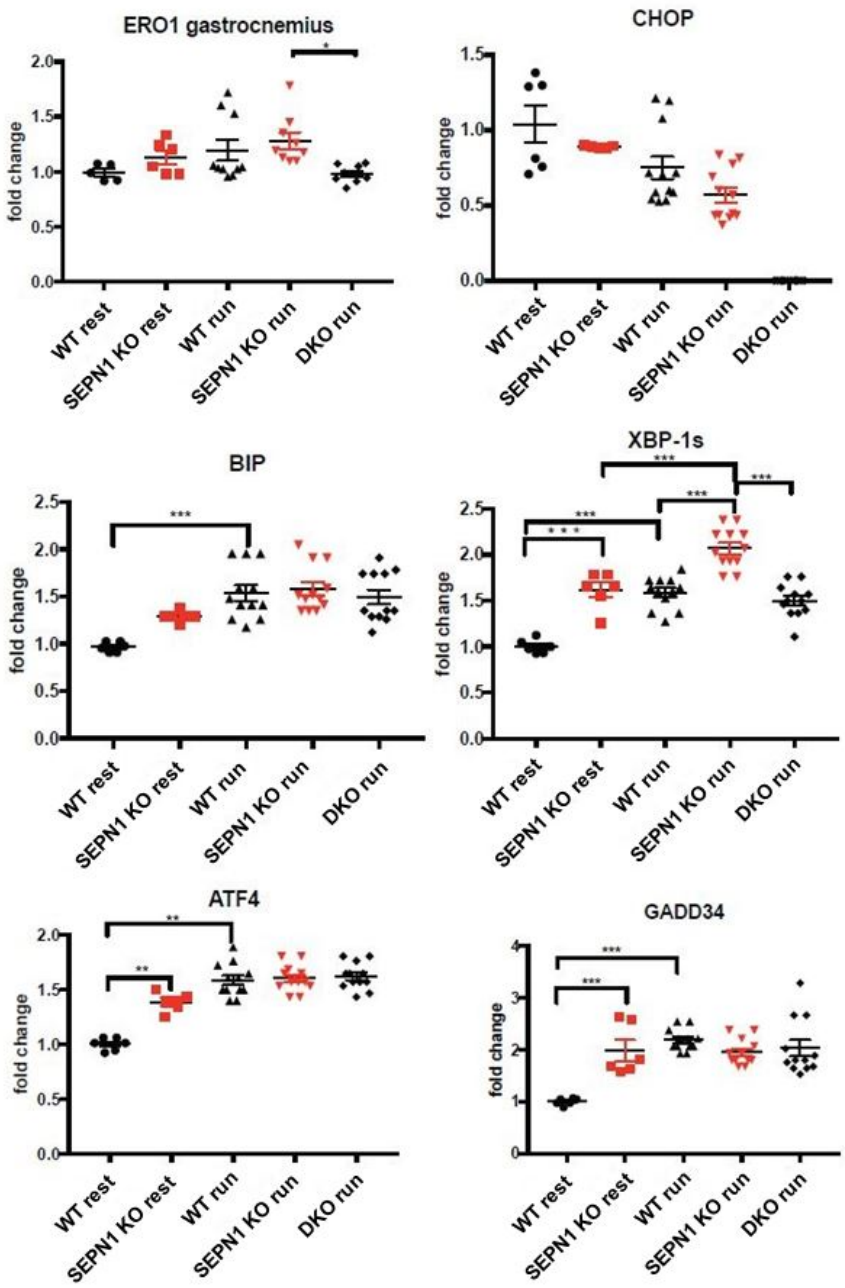

*Figure 50 - Deletion of CHOP reduces ER stress in the gastrocnemius of SEPN1 KO mice after an intensive bout of exercise. Semi-quantitative Real-time RT-PCR analysis of ER stress response markers in mRNA obtained from WT, SEPN1 KO and DKO gastrocnemius of 24-week old sedentary (rest) and exhausted (run) mice (means ± standard error of the mean (SEM), one-way ANOVA multiple comparison test and Sidak's post test, *p <0.05, **p<0.01, ***p <0.001).*

3.2.5 – Conclusions

The reason for a major effect of SEPN1 deficiency on the diaphragm and the relative preservation of the leg muscle is still object of study, but likely it is related to the high oxidative metabolism of the diaphragm in addition to its increased activity. SEPN1 KO mice resemble the phenotype of patients with SEPN1-RM, insofar as they do not show major myopathic signs at the level of the leg muscles under normal cage conditions but the force of the diaphragm muscle is impaired. This correlates with higher levels of ER stress markers CHOP and its target ERO1.

Therefore, we investigated whether the ER stress mediator CHOP is involved in SEPN1 KO muscle phenotype by crossing SEPN1 KO with CHOP KO mice and analysing the muscle phenotype of the compound mutant mice. The ablation of CHOP restored diaphragm function in SEPN1 KO mice, indicating that the CHOP branch of the ER stress response is an important pathogenic cause in SEPN1 KO mice.

In the end, the deletion of CHOP limited the activation of the maladaptive branch of the UPR and the activation of the apoptotic program in the DKO mice, relieving the skeletal muscle from the development of a detrimental ER stress in case SEPN1 is not present.

3.3 – Lipotoxicity and ER stress in SEPN1 KO mice

3.3.1 - Aim

Autosomal recessive mutations of the SEPN1 gene cause SEPN1-RM, a rare congenital myopathy typically associated with insulin resistance. In the third part of my project thesis we investigated the mechanisms that are involved in the development of the insulin resistance in SEPN1-devoid models. Specifically, we pursued the hypothesis that insulin resistance may be triggered by the augmented ER stress due to lipid accumulation in skeletal muscle of SEPN1 KO mouse.

3.3.2 –Palmitate-induced ER stress in SEPN1 devoid myotubes

Insulin resistance has been already connected to the accumulation of lipid droplets in skeletal muscle (Unger and Scherer, 2010). Furthermore, overload of palmitate, a saturated fatty acid, has been reported to generate ER stress in myotubes, although the mechanisms underlying this connection remain unclear (Perry et al., 2018). For these reasons, we decided to start testing the effect of palmitate on SEPN1-devoid myotubes. In order to avoid cellular adaptation issues, we decided to work with C2C12 myotubes where an acute knock down of SEPN1 (by an adenovirus that delivers SEPN1 shRNA) was triggered and compare these myotubes with mock-infected isogenic, except for SEPN1, WT myotubes. Three days after adenoviral infection, semi-quantitative real time RT-PCR showed that mRNA SEPN1 levels were 70% lower when compared to WT cells. Unfortunately, the polyclonal antibody that we used to recognize SEPN1 (SAB210211, SIGMA) suddenly stopped working and thus we have to

rely only on the RT-PCR data to estimate SEPN1 expression levels. To assess whether lipid accumulation affects the viability of the cells, WT and SEPN1 KD C2C12 cells were exposed to palmitate at concentrations between 5 and 500 μM or its vehicle. The colorimetric viability MTS assays showed that SEPN1 KD cells were less viable than WT cells at concentration of palmitate higher than 50 μM, which suggests a greater lipotoxicity of palmitate in SEPN1 KD cells (Figure 51).

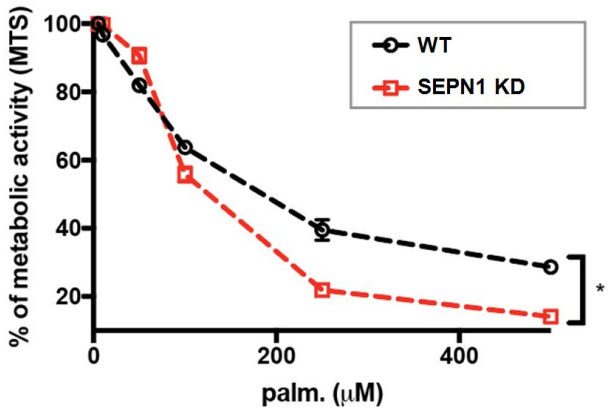

*Figure 51 - SEPN1 defends myotubes from the consequence of a lipotoxic stimulus. Metabolic activity (MTS) of WT and SEPN1 KD C2C12 cells treated with the indicated concentrations of palmitate for 24 h. Metabolic activity is expressed as the relative reduction in MTS signal in palmitate-exposed cells compared to that of vehicle-treated cells (arbitrarily set at 100%) (n= 4) (means ± standard error of the mean (SEM), two-way ANOVA multiple comparison test and Sidak's post test, *p <0.05) (this experiment was done in collaboration with my labmate Ersilia Varone).*

In order to determine whether the lower viability induced by palmitate in SEPN1 KD myotubes is due to increased ER stress, we examined the mRNA levels of ER stress markers in WT and SEPN1 KD cells after challenging the cells with the two concentrations of palmitate of 100 and 200 μM. Interestingly, the levels of the ER stress markers CHOP, ERO1, GADD34, ATF4 and BIP were increased in SEPN1 KD cells challenged with both concentrations of palmitate, thus indicating increased ER stress in SEPN1 KD cells (Figure 52).

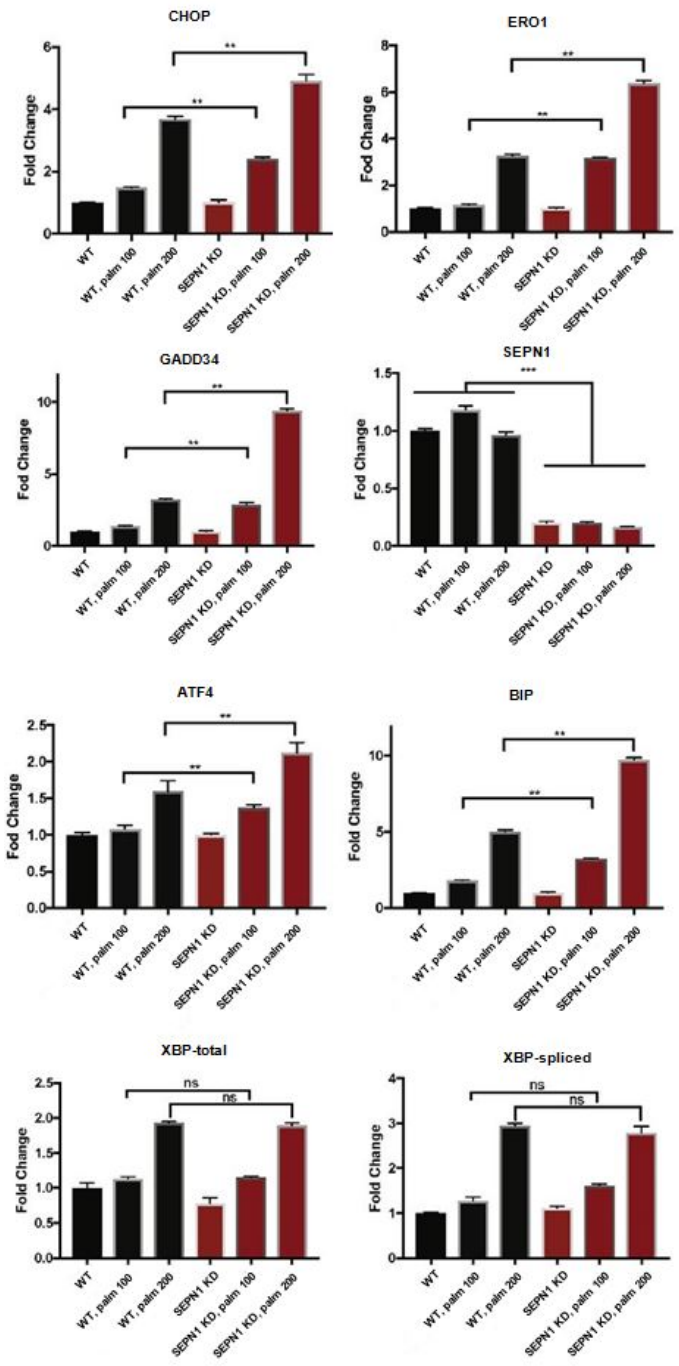

*Figure 52 - Lack of SEPN1 and palmitate treatment trigger ER stress in C2C12 cells. Semi-quantitative Real-time RT-PCR analysis of ER stress markers in mRNA of WT and SEPN1 KD cells treated with BSA (vehicle condition) or palmitate at the concentrations of 100 µm or 200 µm (means ± standard error of the mean (SEM), one-way ANOVA multiple comparison test and Sidak's post test, **p <0.01, ***p<0,001) (this experiment was done in collaboration with my labmate Ersilia Varone).*

3.3.3 – Lipotoxicity affects insulin sensitivity in SEPN1 devoid myotubes

As ER stress may affect insulin-dependent glucose uptake (Panzhinskiy et al., 2013) we investigated whether SEPN1 deficiency increases the susceptibility to insulin resistance of myotubes. To this end, WT and SEPN1 KD myotubes were tested for insulin-dependent glucose uptake in the presence of vehicle or palmitate (100 μM) by using metabolic tracings of H^3-2-deoxyglucose (2DG). As expected WT and SEPN1 KD myotubes showed reduced uptake of 2DG following palmitate treatment when compared to the vehicle-treated counterpart but the uptake of 2DG was less in SEPN1 KD than in WT suggesting that SEPN1 deficiency significantly contributes to the impairment of the insulin-mediated glucose uptake (Figure 53).

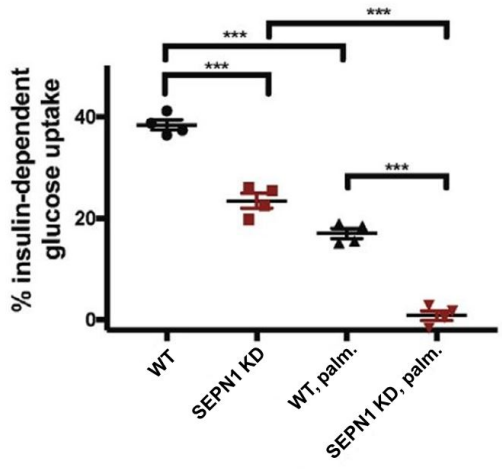

*Figure 53 - SEPN1 KD C2C12 cells treated with palmitate are less responsive to insulin-dependent glucose uptake. Dot blots representing the percentage increase of glucose uptake in the insulin -treated groups compared to the untreated counterpart (n=4) (means ± standard error of the mean (SEM), one-way ANOVA multiple comparison test and Sidak's post test, ***p <0.001).*

3.3.4 –High- fat fed SEPN1 KO mice are insulin resistant and myopathic

In order to study the direct consequences of fatty acid-induced lipotoxicity on SEPN1 KO skeletal muscle, we fed 9-week-old adult male WT and SEPN1 KO mice a high-fat

diet (HFD, 40% of calories from fat) for nine weeks and compared them with their counterparts fed a standard diet.

The WT and SEPN1 KO mice fed the standard diet showed no statistically significant difference in weight gain, but the SEPN1 KO mice on HFD showed a tendency to gain less weight even though their food intake was similar to that of the WT mice (Figure 54). Glucose tolerance tests showed that glycemic control was comparable between WT and SEPN1 KO on standard diet but, despite the lower weight gain of SEPN1 KO mice on HFD, these mice displayed moderately greater glucose intolerance than the WT mice (Figure 55).

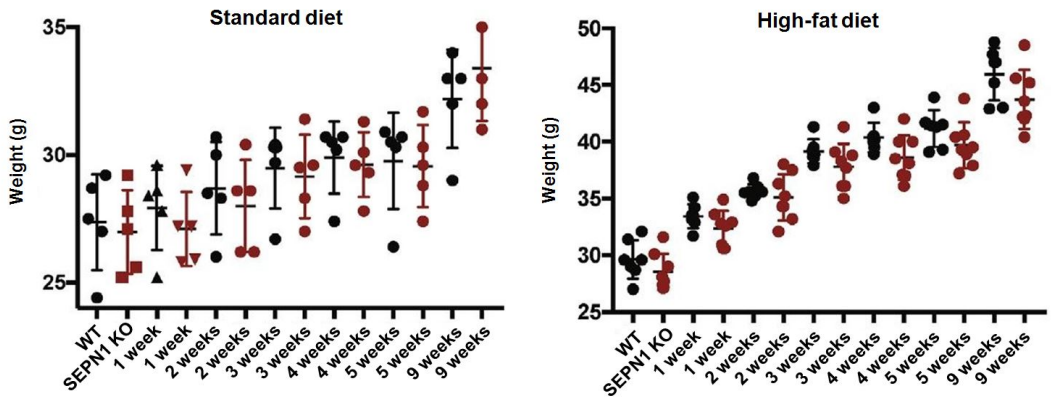

Figure 54 - Body weight of standard and HFD fed WT and SEPN1 KO mice. Body weight of WT and SEPN1 KO mice under standard diet (left panel) (n=5) or HFD (right panel) (n=6) for 9 weeks (means ± standard error of the mean (SEM).

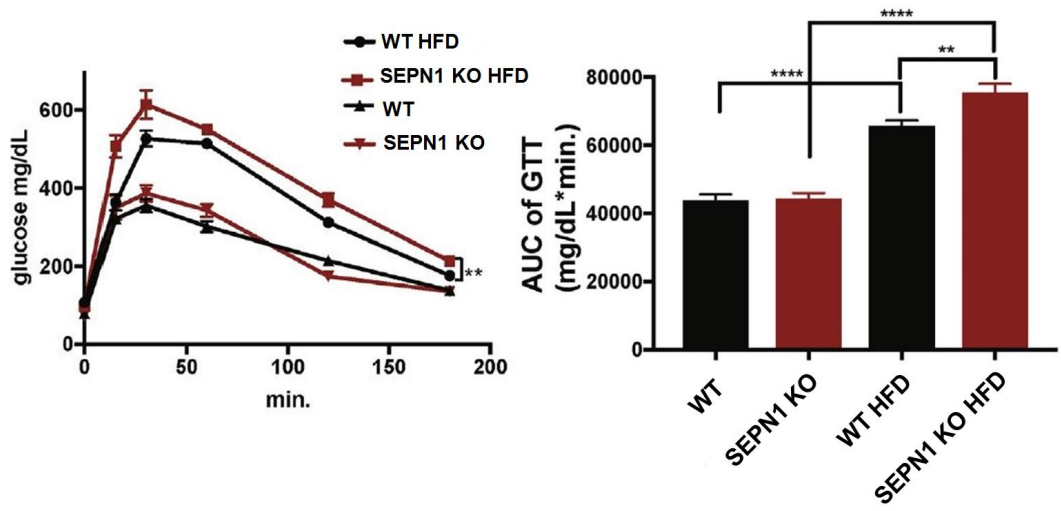

*Figure 55 – Higher glucose intolerance in HFD fed SEPN1 KO mice. Left: Blood glucose trace of GTTs in WT and SEPN1 KO mice fed a standard diet (n=5) or a HFD (n=6) for nine weeks. The time-points represent the times of 15, 30, 60, 120 and 180 min after the intraperitoneal injection of glucose. Right: bar graphs of the Area Under the Curve (AUC) of the glycemic curve (means ± standard error of the mean (SEM), two-way ANOVA multiple comparison test and Sidak's post-test, **p <0.01, ****p<0, 0001).*

This modest impairment of SEPN1 KO glucose tolerance was not associated with a decrease in plasma and pancreatic insulin levels thus suggesting that the defective glucose tolerance of the SEPN1 KO mice was not due to defects in insulin secretion by the endocrine pancreas (Figure 56).

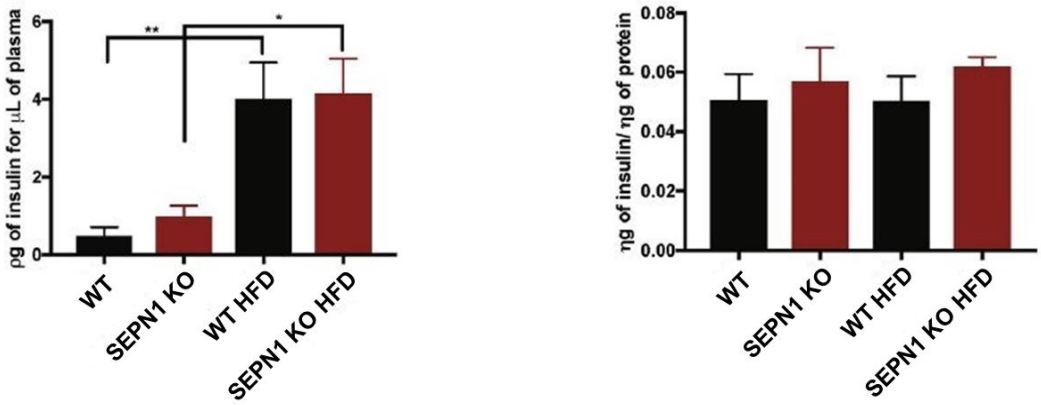

*Figure 56 - HFD and lack of SEPN1 do not impair insulin secretion. Left: bar graphs representing insulin levels in the plasma of WT and SEPN1 KO mice fed a regular diet (n=5) or a HFD (n=6) for nine weeks. Right: bar graphs showing insulin levels in pancreatic lysates of the previously described experimental groups (means ± standard error of the mean (SEM), one-way ANOVA multiple comparison test and Sidak's post test, *p<0,05, **p <0.01).*

Subsequently, given the correlation between ER stress and insulin resistance, we analysed the mRNA levels of ER stress markers in the gastrocnemius muscle. In qualitative agreement with our findings in palmitate-treated SEPN1 KD myotubes, the levels of ER stress markers CHOP, ERO1 and GADD34 were higher in the gastrocnemii of the SEPN1 KO mice fed a HFD (Figure 57).

Despite these defects, the gastrocnemius of the SEPN1 KO mice fed a HFD did not show significant alterations in H&E staining but the NADH-TR staining, that reports for oxidative activity, as well as the PAS staining, that reports for glycogen levels, were paler. On the contrary, Oil Red O staining showed an increase/accumulation in lipid droplets of high-fat-fed SEPN1 KO gastrocnemius (Figure 58).

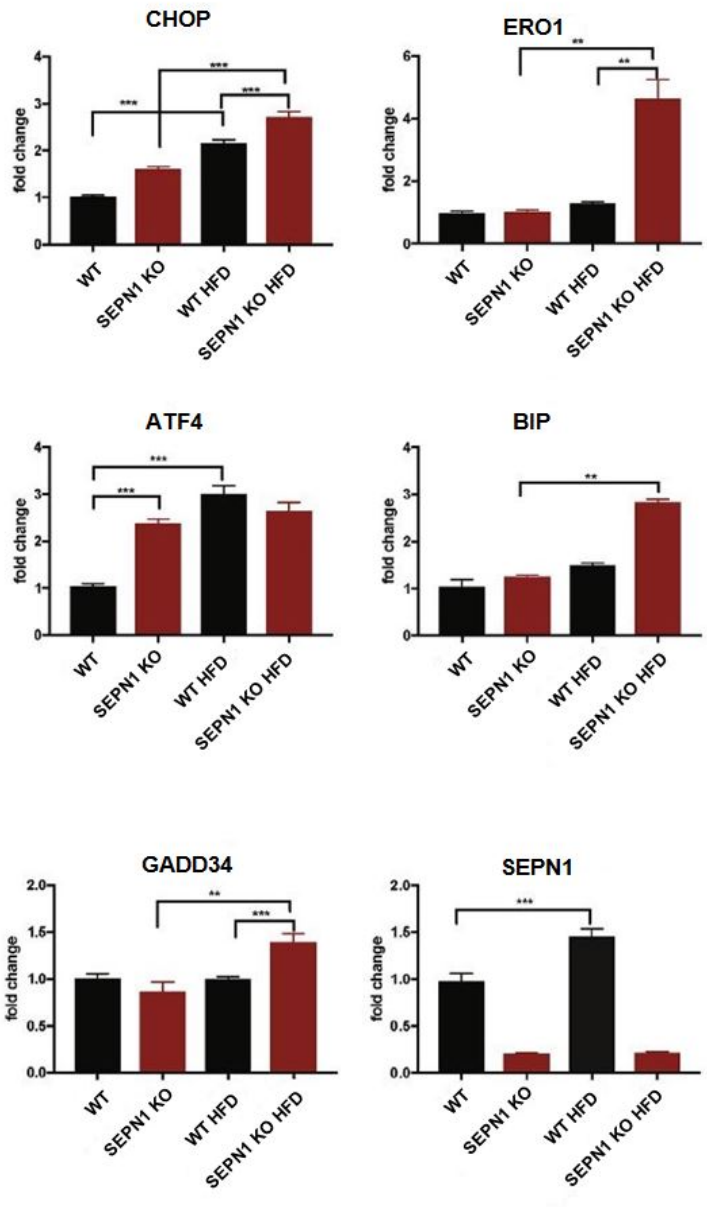

*Figure 57 - HFD and lack of SEPN1 enhance ER stress. Semi-quantitative real-time RT-PCR analysis of ER stress markers from WT and SEPN1 KO mice gastrocnemii fed a regular diet (n=5) or a HFD (n=6) (means ± standard error of the mean (SEM), one-way ANOVA multiple comparison test and Sidak's post test, **p<0,01, ***p <0,001.*

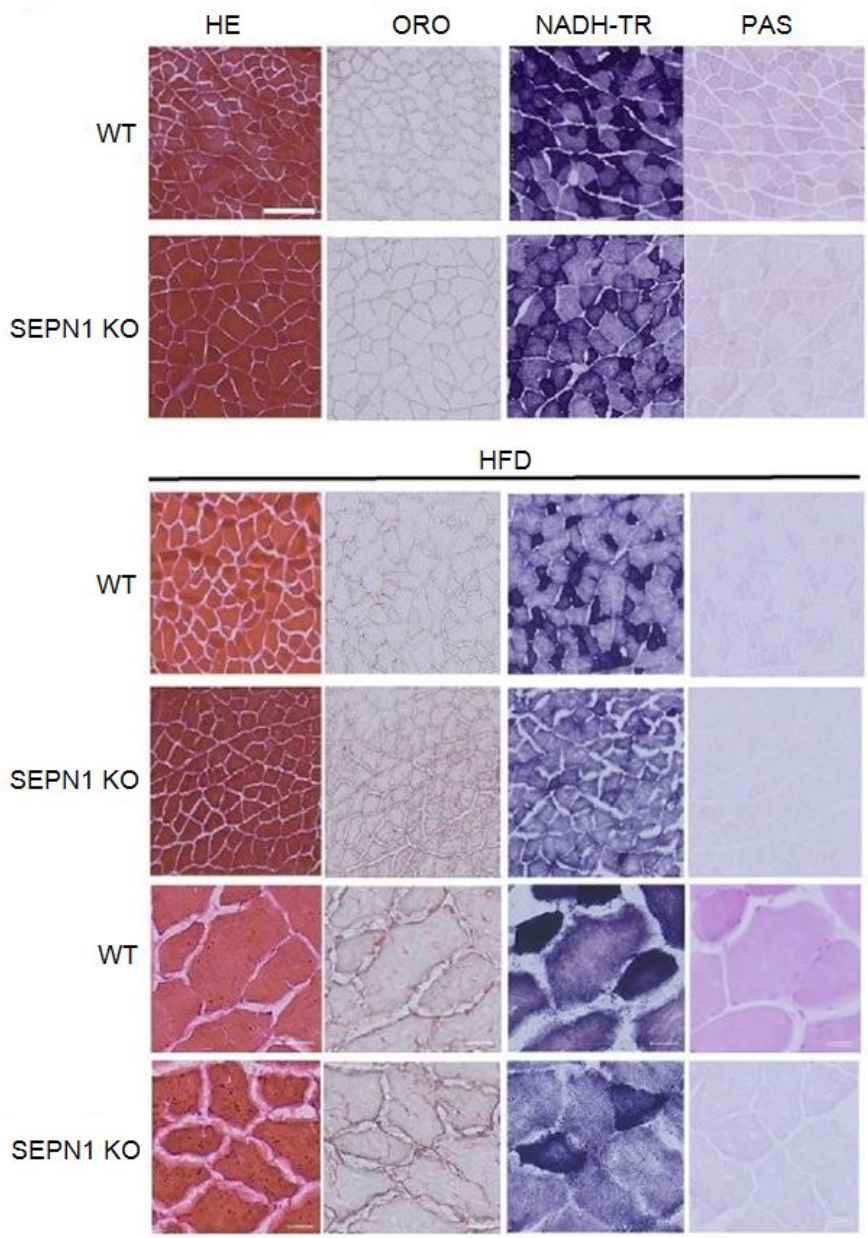

Figure 58 - Lack of SEPN1 together with HFD triggers accumulation of lipids, reduces oxidative activity and glycogen in muscle. Representative H&E, Oil Red O (ORO), NADH-TR and periodic acid-Schiff (PAS) stainings in WT and SEPN1 KO gastrocnemii from mice fed a standard (up) or HFD (below) diet. Scale bar 40 µm (below, 20 µm for the high magnification acquisitions) (n=4) (this experiment was done in collaboration with my labmate Simona di Modica).

The similar weight between gastrocnemii of HFD fed WT and SEPN1 KO indicated lack of atrophy in the SEPN1 KO muscle.

Despite lack of atrophy in the HFD fed SEPN1 KO muscle, the force was depressed and the force generated was significantly less during tetanic stimulation (100 Hz) (Figure 59).

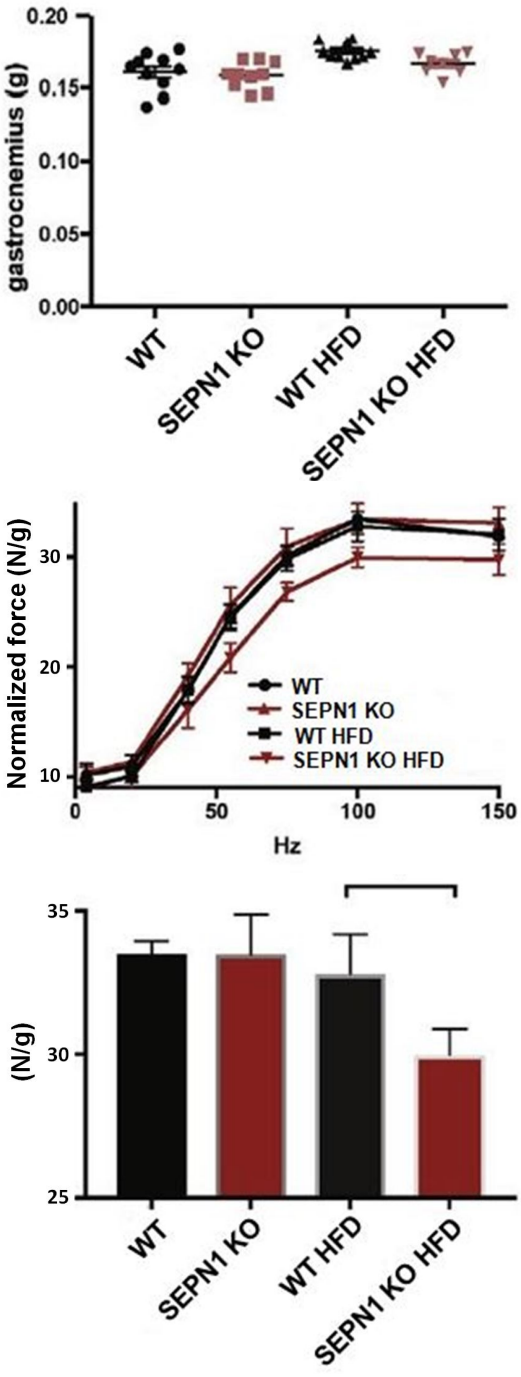

Figure 59 - Lack of SEPN1 together with HFD impair skeletal muscle force. Up: dot plot of the weight of gastrocnemii from mice fed a chow normal diet and a HFD.

Middle: normalized force/frequency graph of hind limb muscle (that mainly reports for the force of the gastrocnemius) in the indicated groups.

*Bottom: Bar graph of the tetanic in-vivo force (stimulation frequency of 100 Hz) in the indicated groups (means ± standard error of the mean (SEM), one-way ANOVA multiple comparison test and Sidak's post test, *p<0,05).*

3.3.5 – Conclusions

ER stress can be activated by a saturated fatty acid overload that is also linked to the insulin resistance. We have explored the hypothesis that SEPN1 deficiency sensitizes muscle cells to the consequences of ER stress and therefore increases the lipotoxicity of saturated fatty acids impairing insulin sensitivity. We have seen that SEPN1 deficiency increases palmitate-induced lipotoxicity, thus eliciting ER stress and blunting insulin-dependent glucose uptake in myotubes.

SEPN1 KO triggers glucose intolerance in mice on a HFD despite their trend towards gaining less weight than their WT counterparts but no overt abnormalities in plasma or pancreatic insulin content were detected, suggesting that the glucose intolerance is not caused by a defect in endocrine pancreatic insulin secretion.

In qualitative agreement with findings in SEPN1-devoid myotubes, HFD in SEPN1 KO mice leads to chronic ER stress in muscle, which suggests a correlation between reduced body glucose tolerance, insulin activity and increased ER stress in the muscles of SEPN1 KO mice fed a HFD (Figure 60). These abnormalities in SEPN1 KO mice triggered by a HFD reduce hind limb skeletal muscle strength, which is instead preserved in these mice fed a standard chow diet. Therefore, we propose a model in which the lack of SEPN1 sensitizes skeletal muscle to the consequences of chronic ER stress induced by palmitate treatment in cells or a HFD in mice, thus impairing insulin signalling and affecting force-frequency responses in skeletal muscle. What is therapeutically important is that these findings suggest that environmental cues eliciting ER stress in skeletal muscle (such as HFD) affect the pathological phenotype of SEPN1-RM, and can therefore contribute beyond simple genotype-phenotype correlations to the prognosis of SEPN1-RM patients.

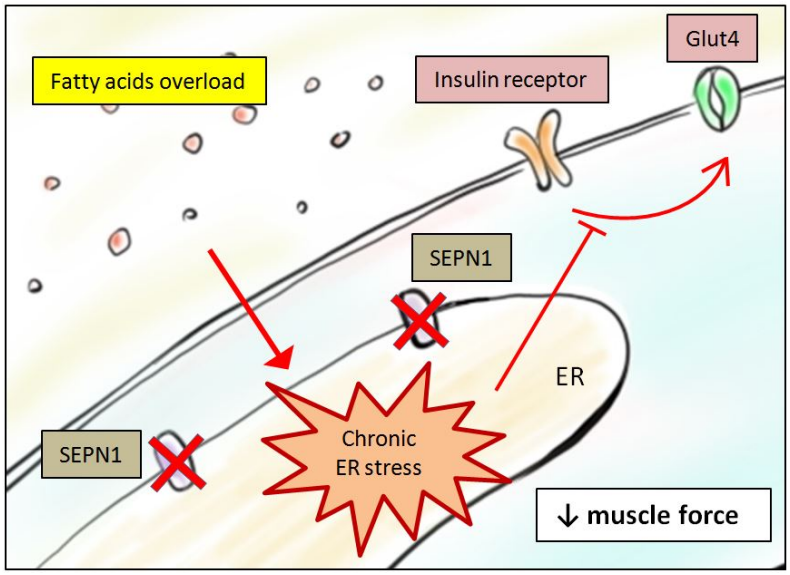

Figure 60 – Lack of SEPN1 impairs muscle force. Without SEPN1, fatty acids accumulation (either caused by palmitic acid or HFD) triggers a chronic ER stress that reduces glucose tolerance and the force generated by the skeletal muscle.

Chapter 4 – General Discussion

SEPN1-RM is a rare congenital disorder arising from loss-of-function mutations in the SEPN1 gene that affects the muscle system, and leads to life-threatening respiratory malfunction, requiring assisted ventilation with relative preservation of limb muscles and ambulation. No FDA-approved drugs are available for SEPN1-RM, so clarifying its pathogenic mechanism is an important step towards developing a pharmacological treatment.

SEPN1 KO mice are somehow protected from the effects of SEPN1 loss as they don't show an overt muscle phenotype. This suggests the existence of factors that compensate for the lack of SEPN1 in the murine muscle and leads us to test the hypothesis that the well placed, ER resident, ASC may contribute to this compensation. We therefore analysed the hind limb muscle phenotype of the offspring from the crosses between Gulo KO mice, unable to synthesize ASC, and SEPN1 KO mice to investigate whether reduced dietary levels of ASC affect muscle homeostasis of the SEPN1 KO mouse. Our findings demonstrate that, by inducing ER stress, a deficiency of vitamin C induces a SEPN1-related pathological muscle phenotype in SEPN1 KO mice, whose severity is inversely proportional to the muscle concentration of the vitamin: a medium dose of ASC impairs muscle fibers, as seen by the presence of minicores, and a reduced normalized muscle force, whereas a lower dose triggers the more serious

muscle atrophy, thus leading to smaller muscle fibers and reduced absolute muscle force. This part of the project was very informative not only to understand that deficiency of an anti-oxidant vitamin unveils the muscle phenotype in SEPN1 KO mice but also to reveal features of chronic ER stress in the SEPN1 KO muscle that can be an important part of the pathogenic mechanism of SEPN1-RM.

From a therapeutic point of view, it would be interesting to administer daily dosages of ASC to SEPN1-RM patients, in order to evaluate if the antioxidant action of ASC could ameliorate the symptoms of the disease also in human. While this treatment looks promising, it's necessary to first deepen the knowledge of ASC bioavailability depending on the type of administration. Oral administration, in fact, should be avoided since the majority of ASC would be absorbed by the gastro-intestinal tract and could not reach the skeletal muscles. Thus, in a possible clinical trial, Intravenous administration should be preferred.

In the second part of the thesis project we moved from the double mutant GULO, SEPN1 KO mice, to a simpler model – a mouse model that didn't require genotypization of the offspring and almost daily preparation of the ASC enriched drinking water - in order to acquire expertise in the phenotypical analysis of the diaphragm. The collaboration with the laboratory of Prof. Bert Blaauw and Prof. Stefano Schiaffino at the University of Padua, two experts in phenotypical characterisation of diaphragm, was instrumental to lead me to pinpoint a pathological phenotype of the diaphragm in adult SEPN1 KO mice. Although signs of atrophy were missed, reduced protein synthesis together with chronic ER stress were clear features of SEPN1 KO diaphragms. Importantly, the force of the muscle strips of diaphragms following electrical stimulation was impaired indicating a defective mechanism of excitation-contraction coupling in SEPN1 KO diaphragm. Given the higher levels of

CHOP, a maladaptive ER stress mediator in conditions of chronic ER stress, in the diaphragm of SEPN1 KO mice we decided to proceed with a genetic approach by crossing CHOP KO and SEPN1 KO mice and to test whether the lack of CHOP rescues the pathological phenotype of SEPN1 KO diaphragm by attenuating ER stress. CHOP loss attenuated ER stress and improved the contractile function of the diaphragm of SEPN1 KO mice suggesting that ER stress is an important component of the pathogenic mechanism underlying SEPN1-RM. The lack of CHOP avoids the activation of the maladaptive branch of the UPR and the pro-apoptotic program, sorting a beneficial effect in the SEPN1 KO mice, whose diaphragm activity would otherwise be impaired. Finally, in an attempt to dissect the mechanism behind the insulin resistance of SEPN1-RM patients we reasoned to test whether HFD, that triggers insulin resistance and ER stress in skeletal muscle, induced myopathy in the otherwise protected hind limb muscles of SEPN1 KO mice.

We saw that SEPN1 deficiency impairs glucose tolerance and leads to exaggerated ER stress and reduced hind limb skeletal muscle strength in SEPN1 KO mice fed a HFD.

These findings allowed us to propose a model in which the lack of SEPN1 sensitises skeletal muscle to the consequences of chronic ER stress induced by palmitate treatment in cells or HFD in mice, thus impairing insulin signalling and affecting force-frequency responses in skeletal muscle.

Our hypothesis is that SEPN1 protects the cells and the skeletal muscle from the development of ER stress due to a lipotoxic environment, although the mechanism underlying this protection is still unclear and needs to be further addressed.

What is therapeutically important is that HFD, by eliciting ER stress in skeletal muscle, affects the pathological phenotype of SEPN1-RM, and can therefore contribute beyond simple genotype-phenotype correlations in establishing a prognosis.

In this perspective, these results will lead to the intriguing idea of testing drugs as 4-PBA (4-phenylbutiric acid) and TUDCA (Tauroursodeoxycholic acid), two chemical chaperones, which are involved in attenuating ER stress and are already FDA approved, as a mean of treating diaphragm dysfunction and insulin resistance in SEPN1-RM.

Chapter 5 – Materials and methods

Transgenic mice

Procedures involving animals were conducted in conformity with the institutional guidelines at the IRCCS – Mario Negri Institute for Pharmacological Research in compliance with national (D.lgs 26/2014; Authorization n. 19/2008-A issued March 6, 2008 by Ministry of Health) and international laws (EEC Council Directive 2010/63/UE; the NIH Guide for the Care and Use of Laboratory Animals, 2011 edition). They were reviewed and approved by the Mario Negri Institute Animal Care and by an Ethical Committee that includes *ad hoc* members for the judgement of ethical issues, and by the Italian Ministry of Health (Decreto no. 381/2016-PR and 485/2018-PR).

SEPN1 KO mice were purchased from EMMA repository, GULO KO from MMRC repository and CHOP KO mice from Jackson laboratory. DNA preparation for PCR genotyping: partial mice phalanx (from pups until 10-14 days of age) or tail tips were lysed overnight in a mix composed of Direct PCR lysis reagent (Viagen) and proteinase K (SIGMA, P8044) 0,2 mg/mL, in a thermomixer at 55°C with shake. The day after, to inactivate the proteinase K, the temperature was raised at 85 C for 15 minutes and finally the samples stored at 4°C.

***Sepn1* locus genotyping protocol**

A PCR mix was prepared by mixing SEPN1 Forward primer (5'–3'): TCCAATGACGTCAGGCTGTGACTTGC, SEPN1 Reverse primer (5'-3'): GGATCAGTAGAAAGTACC primers at a final concentration of 0,35 µM, Quickload Taq 2x master mix (New England Biolabs, M0271S) and the tissue lysate that contains genomic DNA (1 µl).

The PCR cycle as follows: 94°C for 2 minutes, 94°C for 30 seconds, 56°C for 30 seconds, 72°C for 1 minute, repeat from step 2 to 4 for 35 times, final step at 72°C for 5 minutes. Horizontal gel electrophoresis was used to run the amplicons (1,5% agarose

gel with 0,3X Gel Red Nuclease Acid staining as a DNA-binding dye), for 25 minutes at 100 V that were visualized by using an UV transilluminator (Figure 61).

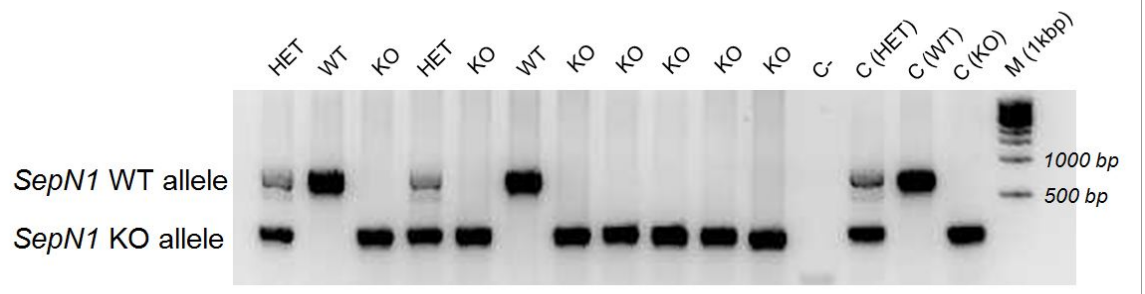

Figure 61 – Representative snapshot of an agarose gel with the amplicons of the genotype of Sepn1 locus of 11 different pups. "C-" refers to a blank, i.e. a sample without template DNA, C(HET) refers to a sample from an already known Sepn1 heterozygous mouse, C(WT) from a known Sepn1 wild-type mouse and C(KO) from a known SepN1 KO mouse. M 1 kbp is a DNA ladder (New England Biolabs – N0468S).

***L-Gulonolactone oxidase* locus genotype protocol**

GULO wild type and *GULO* knock out allele had to be amplified in two different PCR reactions with the same reagents of above.

The primer used were: GULO Forward primer (common) (5'–3'): GTC GTG ACA GAA TGT CTT GC,

GULO wild type reverse primer (5'-3'): CCC AGT GAC TAA GCA TAA GC, GULO KO reverse primer (5'-3'): CGC GCC TTA ATT AAG GAT CC. The PCR cycle as follows: 94°C for 2 minutes, 94°C for 30 seconds, 55°C for 30 seconds, 72°C for 1 minute, repeat from step 2 to 4 for 35 times, final step at 72°C for 5 minutes (Figure 62).

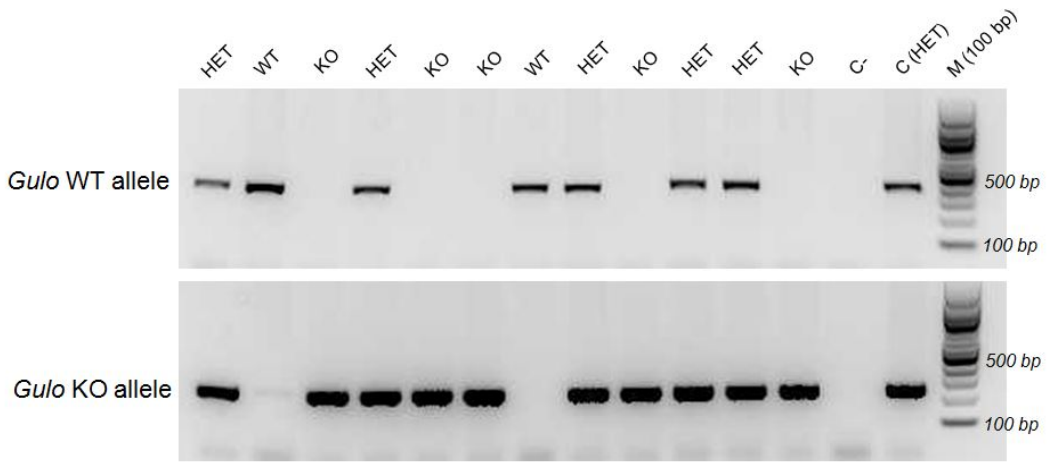

Figure 62 – Representative snapshot of an agarose gel with the amplicons of the genotype of Gulo locus of 12 different pups. Gulo WT and KO alleles had to be amplified in two different reactions. "C-" refers to a blank, i.e. a sample without template DNA, C(HET) refers to a sample from an already known Gulo heterozygous mouse. M = 100 bp DNA ladder (New England Biolabs – N3231S).

Chop locus genotype protocol

CHOP Forward primer (common) (5'–3'): ATGCCCTTACCTATCGTG, CHOP wild type reverse primer (5'-3'): GCAGGGTCAAGAGTAGTG and CHOP KO reverse primer (5'-3'): = AACGCCAGGGTTTTCCCAGTCA were added to the multiplex PCR master mix. The cycle as follows: 94°C for 2 minutes, 94°C for 30 seconds, 61°C for 30 seconds, 72°C for 1 minute, repeat from step 2 to 4 for 35 times, final step at 72°C for 5 minutes (Figure 63).

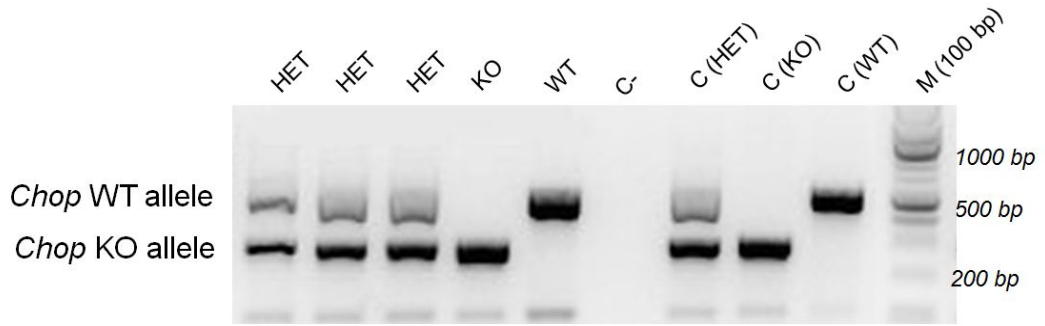

Figure 63 – Representative snapshot of an agarose gel with the amplicons of the genotype of Chop locus of 5 different pups. "C-" refers to a blank, i.e. a sample without template DNA, C(HET) refers to a known Chop heterozygous mouse, C(KO) to a known Chop KO mouse and C(WT) to a known Chop Wild-type mouse. M = 1 kbp DNA ladder (New England Biolabs – N0468S).

SUnSET protocol for quantification of new proteins

The rate of protein synthesis in the gastrocnemius and diaphragm of mice was analysed by using the *in vivo* "SUnSET" technique (Surface Sensing of Translation) (Schmidt et al., 2009). Briefly, mice were starved for 30 min, then injected in the peritoneum with puromycin (0.040 µmol/g), a drug that binds the nascent polypeptide and causes premature termination of the translation. After 30 minutes from the puromycin injection the muscles were homogenized with a Polytron homogenizer in an ice-cold buffer (40 mM TRis, pH7,5, 1mM EDTA, 5mM EGTA; 0,5% Triton X100 together to protease and phosphatase inhibitors). Protein concentrations were determined with a BCA kit and the amount of puromycin incorporation in the muscles determined by Immunoblot with a mouse anti-puromycin antibody (Merck Millipore).

Glucose Tolerance Test (GTT)

Mice were overnight fasted. The day after the basal level of the glycemia was measured from a blood drop from the tail and by using a glucometer. Then mice were intraperitoneally injected with 2 mg of glucose for each gram of mouse weight (Merck). After 15, 30, 60, 120 and 180 minutes from the injection the blood glucose levels were recorded. Mice were manipulated in an isolated room by the same operator to reduce the risk of stress-induced altered blood glucose levels.

Glucose uptake measurements

Cell glucose uptake was measured using a radioactive derivative of 2-deoxy-D-glucose radiolabeled with tritium at C1 and C2. This is a glucose analogue unidirectionally transported inside the cells where it's phosphorylated and remains trapped inside the cells.

C2C12 myotubes were serum starved for 1 h then incubated in Krebs-Ringer buffer (MgCl2: 0,0468 g/L, KCl: 0,34 g/L, Na2HPO4:0,1 g/L, NaH2PO4:0,18 g/L) with 0,3% BSA and with 0,5 µmol/L 2-deoxy-[3H]-D-glucose (4 µci/mL) for 30 min. Later insulin (100 nM) was added to the cell media for 30 minutes. Finally, cell medium was removed and cells were rapidly washed with cold Krebs-Ringer buffer, before lysing them in 0,2% SDS. Radioactivity was determined by liquid scintillation counting (Perkin Elmer 2800 TR, Courtaboeuf, France) and protein content by using the Bradford protein assay. Insulin-dependent glucose uptake was determined by comparison of the radioactive signal from insulin-treated cells and untreated cell.

ASC *in vivo* administration

ASC was prepared at a concentration of 8,24 g/L (with sterile water) using "L-Ascorbic acid" from SIGMA (A7506). This solution was then diluted to 0,33 g/L (High-dose), 0,11 g/L (Medium-dose) and 0,066 g/L (Low-dose) to which EDTA was added (at a final concentration of 0,01 mM). The ASC solution was added to the drinking bottles in mouse cages. ASC solution was changed twice a week.

HPLC (High-performance liquid chromatography) for ASC content in cells

ASC in the cells was extracted by a solution of 60% methanol and 1 mM EDTA from which the precipitated proteins were discarded by centrifugation (10,600 *g* for 5 min). ASC was analyzed by using reverse-phase HPLC with a Synergi 4 micron Fusion-RP 80 A column (Phenomenex) and coulometric detection. The chromatograph consisted of Shimadzu LC-10AD pump (Shimadzu, Italy), refrigerated (4 °C) 717 autosampler (Waters, Italy), Coulochem II electrochemical detector equipped with a 5014B electrochemical cell consisting of two in-series electrodes (ESA, Chelmsford, MA) and software for acquisition and calculation of chromatographic data (Azur 5.0; Datalys, France). Detector settings were electrode 2.200 mV; electrode 1.0 mV. Mobile phase contained 50 mM sodium phosphate monobasic, 50 Mm sodium acetate anhydrous, 0.5 mM acetyltrimethylammonium bromide dissolved in HPLC-grade water (pH 4.8). Methanol percentage was adjusted to 20% of final volume and the mobile phase was filtered through 0, 45 µ m membrane filter (Millipore) and degassed. The column was conditioned with mobile phase at 1 mL/min for two days and washed after every 30–50 biological samples with 50% methanol/ water for 12 hours at 1 mL/min. Oxidation potentials setting for the electrochemical cell were E1 0 mV; E2 + 200 mV. The assay

was calibrated daily with fresh solutions (2.5–40 ng of standard ASC) diluted in the mobile phase. Retention time of ASC was around 6.05 min.

HPLC (High-performance liquid chromatography) for ASC content in mice skeletal muscles

ASC in the muscles was extracted by a solution composed by 60% methanol and 1 mM EDTA then centrifuged to pellet the precipitated protein (10,600 *g* for 5 min).

The column of 4 mm particle size, 150 × 4.6 mm, Accucore X C18 (Thermo Scientific, Italy) was coupled with a drop-in 10 × 4.6 mm guard column (Thermo Scientific, Italy). The mobile phase was prepared by dissolving 50 mM NaH2PO4 and 50 mM CH3COONa in about 750 mL ultrapure water (Milli-Q; Millipore, Italy). Two-hundred mL methanol containing 0.5 mM N-cetyl-N,N,N, trymethylammonium bromide (CTMAB) were added to the buffer solution, the pH of the solution adjusted to 5.0 with concentrated H3PO4 and the volume brought to 1 L with ultrapure water. After filtration (with 0.45 mm membrane filters (Sartorius Stedim Biotech, Germany), and degassing under vacuum, the mobile phase was pumped through the HPLC system at a constant flow rate of 1 mL/min. The column and guard column were conditioned with mobile phase at 1 mL/min for 48 hours. Oxidation potentials for the electrochemical cell were set at E1 0 mV; E2 + 200 mV. ASC was read as the second electrode output signal. The column was calibrated every day with fresh solutions (2.5–40 ng of standard ASC) diluted in the mobile phase. Retention time of ASC was 3.20 min.

Histological analysis of muscles

Muscles were flash-frozen in isopentane pre-cooled in liquid nitrogen, embedded in optimal cutting temperature compound, and cross sections (8 µm thick) were cut with

a cryostat. Cryosections were processed for nicotinamide adenine dinucleotide-TR (NADH-TR) staining, hematoxylin and eosin (H&E) staining, Oil red-O (ORO) staining and periodic acid-Schiff (PAS) staining.

NADH-TR staining for the detection of type I myofibers

Several studies show that type I myofibers (oxidative) have a higher content of oxidative enzymes such as succinate dehydrogenase, reduced nicotinamide adenine dinucleotide tetrazolium reductase (NADH-TR) and reduced nicotinamide adenine dinucleotide phosphate-tetrazolium reductase than type II fibers (glycolytic).

NADH-TR is a staining for oxidative fibers and therefore leads to distinguish between oxidative and glycolytic fibers in sections of skeletal muscle.

Briefly, muscle sections were incubated with the two substrates of NADH-TR, tetrazolium and NADH. Tetrazolium is converted to a purple-blue pigment when is reduced by accepting electrons from NADH. Therefore, the oxidative fibers with a high enzymatic activity will be stained with an intense blue/purple color whereas the glycolytic fibers with a low enzymatic activity with a paler blue/purple color.

Practically, fresh cut cross sections were air dried for 15 minutes and incubated with a freshly- prepared staining solution containing TRIS-HCL 0,1 M pH 7.4, 25 mg of Nitro Blue tetrazolium (Sigma-Aldrich, N-6876) and 20 mg of β-Nicotinamide adenine dinucleotide (Sigma-Aldrich, N-8129) for 40 minutes at 37 °C. Solutions of 30, 60 and 90 % acetone were prepared and the sections were rinsed tree times in each of these solutions to remove the unbound tetrazolium. Finally, the sections were rinsed several times in deionized H2O and mounted with the aqueous mounting medium onto a labelled glass slide.

H&E protocol to evaluate the morphology of the fibers

Hematoxylin is a compound with positive charge that binds the anionic sites of the histones in the chromatin, hence hematoxylin stains in blue/violet the nuclei of the cells. Eosin binds positively charged components of the tissue, such as cytoplasmic and mitochondrial proteins and the extracellular matrix, resulting in a pink staining.

Fresh cut cross sections of muscles were air dried for 15 minutes and incubated with Harris' Hematoxylin (Bio-Optica, 05-06004) for 4 minutes, rinsed with tap water and incubated with eosin (Millipore Merck, 1.15935.0025) for 1 minute. At the end, sections were washed with tap water, dehydrated with increasing concentrations of ethanol (70-80-100%) and cleared with xylene. Finally, the sections were mounted with the aqueous mounting medium onto a labelled glass slide.

Periodic acid Schiff (PAS) protocol to evaluate glycogen accumulation

Periodic acid oxidizes glycols to aldehydes, then Schiff reagent reacts with the aldehydes giving rise to a purple-magenta color.

Briefly, fresh cut cross sections were air dried for 15 minutes and fixed with 10% formalin for 10 minutes, then washed with distilled H_2O. Sections were incubated with 0,5% periodic acid (Sigma-Aldrich, P0430) for 10 minutes at room temperature, rinsed in distilled water then incubated with Schiff reagent (Millipore Merck, 1.09033.0500) for 15 minutes at room temperature. Finally, sections were rinsed with distilled water, dehydrated with increasing concentration of ethanol (70-80-100%), cleared with xylene and mounted with the aqueous mounting medium onto a labelled glass slide. Some sections were pre-incubated with amylase (an enzyme that digests polysaccharides) to validate the specificity of the staining in recognizing glycogen.

Oil-Red O staining protocol to stain lipid droplets

Oil-Red O is a fat-soluble dye for triglycerides and neutral lipids that is transported inside cells using propylene glycol. Lipids are stained with a red color.

Fresh cut 12 µm cross sections were air dried for 30 minutes, fixed with ice cold 10% formalin for 10 minutes and rinsed with distilled water. Once completely air dried, sections were incubated with propylene glycol for 3 minutes then with pre-warmed Oil Red O (Sigma-Aldrich, O0625) solution for 15 minutes at 60°C. Then, sections were incubated with 85% propylene glycol (Sigma-Aldrich, 398039) for 3 minutes and rinsed twice in distilled water. Finally, sections are rinsed in Harris' Hematoxylin for 3 minutes, washed with distilled water and mounted with a non-aqueous mounting medium.

For immunofluorescence analysis, muscle cryosections were incubated with a solution of PBS containing 10% bovine serum albumin (BSA) and mounted with aqueous mounting medium (Fluorescence Mounting Medium, Dako). Muscle section were acquired at 10X by Olympus BX-61 Virtual Stage microscope.

The fiber size diameter (minimal Feret's diameter) was determined on 8 µm frozen muscle sections stained with Alexa Fluor ®488 conjugate of wheat-germ agglutinin (WGA), a lectin that binds sialic acid and *N*-acetyl-glucosaminyl residues in the connective tissue.

***In vivo* muscle force measurements**

In vivo muscle force was measured using a 305B muscle lever system (Aurora Scientific Inc.) in mice anesthetized with a mixture of Xylotine and Zoletil. Mice were placed on a thermostatically controlled table, the knee was kept stationary and the foot was firmly fixed to a footplate, which was connected to the shaft of the motor. Contraction was

elicited by an electrical stimulation of the sciatic nerve. Teflon-coated 7 multistranded steel wires (AS 632, Cooner Sales, Chatsworth, CA, U.S.A.) were implanted with sutures on either side of the sciatic nerve close to the knee. At the distal ends of the two wires the insulation was removed, while the proximal ends were connected to a stimulator (Grass S88). In order to avoid recruitment of the dorsal flexor muscles, the common peroneal nerve was cut.

***Ex vivo* diaphragm force measurements**

Force development measurements in the diaphragm were made in an *ex vivo* setting. Small strips of diaphragms were cut and mounted between a force transducer and a micro manipulated shaft, in an oxygenated organ bath. Optimal length was determined through the length-tension curve at 100 Hz stimulation frequency. Tetanic force was determined after stimulation with trains of 500 ms once every two seconds at 100 Hz (Blaauw et al., 2009).

Protein lysate from muscles

The muscles were frozen and rapidly pulverized with liquid nitrogen. The obtained powder was mechanically lysed using an Ultra Turrax homogeniser in RIPA buffer (except for SunSET). The insoluble material was isolated by centrifugation of the samples at a 10.000 rpm for 5 minutes. The protein lysate was recovered and quantified using the BCA method.

Treadmill

Mice were trained on an open treadmill (TSE-Systems Phenomaster/Labmaster) for two days. The third day mice started to run at a speed of 10 m/min for forty minutes,

then the speed was increased of 1 m/min every 10 min for a total of 30 min and finally the speed was increased by 1 m/min every five minutes until the mice were exhausted. Exhaustion was defined as the point at which mice spent more than five seconds at the start of the lane despite air stimulation (provided by an air puff). The muscles were isolated five hours after the treadmill running.

Antibodies

The following antibodies were used for Western blotting: monoclonal mouse anti-beta Actin from Santa Cruz, mouse anti-GAPDH from Sigma, mouse anti-puromycin from Merck Millipore, mouse anti- KDEL (to recognize BIP) from Enzo Life Sciences and polyclonal rabbit anti-ERO1α. The following antibodies were used for Immunostaining: monoclonal BA-D5 (to stain type1 fiber) and SC71-S D5 (to stain type 2 A fiber) from Iowa Hybridoma bank.

High-fat diet and palmitate treatment

Male WT and SEPN1 KO mice were fed a regular diet or a high-fat diet (HFD) (MD. 88137, 42% from fat prepared by ENVIGO).

C2C12 cells were incubated with palmitic acid (P0500 SIGMA), that was previously conjugated with fatty-acid free BSA and compared with vehicle (BSA)-treated cells.

Insulin measurements

Plasma insulin levels were measured by means of an enzyme-linked immunosorbent assay (ELISA) (Abcam, ab100578) using mouse insulin as the standard. The pancreata were removed and immediately frozen in liquid nitrogen. Protein extracts were

prepared using the acid/ethanol method. The protein in tissue extracts was determined using the Bradford method.

C2C12, SEPN1 knockdown and lentiviral transduction

C2C12 cells were cultured in DMEM supplemented with 25 mM glucose and 10% foetal calf serum (FCS). SEPN1 was knocked down using Mission™ shRNA-encoding lentiviruses against mouse *SEPN1* mRNA (SHCLND-NM_029100.2, Sigma) following the manufacturer's instructions: knockdown pooled KD was targeted with shRNA TRCN0000247860. Mock cells were obtained by means of a lentivirus driving *puro*-resistance. After transduction and selection with puromycin at 5 µg/ml for 7 days, the cells were used for ascorbate measurements.

SEPN1 KD recombinant adenovirus and acute SEPN1 knock down in C2C12

The SEPN1 shRNA sequence TRCN0000247860 was sub-cloned under a U6 promoter together a GFP under a CMV promoter in an adenoviral-Type5 (dE1/E3) backbone and the adenovirus was produced by Vector BIOLABS (Malvern, PA, USA) (titer 2.7×1010 PFU/mL). Similarly, a GFP adenovirus (Ad-CMV-GFP, titer 1×1010 PFU/mL) was produced as a control. The adenoviruses were used at 200 multiplicity of infection (MOI) to infect low passages C2C12 cells at a 50% of confluence in differentiation media (DMEM high glucose, 5% horse serum). After 3 days in differentiation media the cells were harvested and the levels of SEPN1 were analysed by Real-Time quantitative PCR. After additional three days of differentiation (six days of differentiation) glucose uptake was assessed.

MTS assay

Six thousand C2C12 cells/well were plated in 96-well plates. A day later, the media was replaced and the cells incubated with complete media with palmitate (24 h). Later cells were incubated in MTS [3-(4,5-dimetiltiazolo-2-il)-5-(3-carbossimetossifenil)-2-(4-solfofenil)-2H-tetrazolio] and PMS (Phenazine methosulfate) as indicated in CellTiter 96® Aqueous Non-Radioactive Cell Proliferation Assay (Promega). Acquisitions were made by TECAN infinite M200 using excitation wavelengths at 490 nm.

Real-time quantitative RT-PCR analysis

Total RNA was isolated from the cells and muscle tissue using the RNeasy Mini Kit (Qiagen). One microgram of total RNA was reverse-transcribed and analysed using the Applied Biosystems' real-time PCR System and the ΔΔCt method. Relative gene expression in cells was normalized to beta-actin or cyclophilin, and relative gene expression in muscle was normalized to cyclophilin or GAPDH mRNA levels.

The real-time primers were:

mGADD34 F: GAGGGACGCCCACAACTTC R: TTACCAGAGACAGGGGTAGGT

mCHOP F: CCACCACACCTGAAAGCAGAA R: AGGTGAAAGGCAGGGACTCA

mBIP F: TCATCGGACGCACTTGGAA R: CAACCACCTTGAATGGCAAGA

mATF4 F: ATGGCCGGCTATGGATGAT R: CGAAGTCAAACTCTTTCAGATCCATT

mERO1 F: CATACTCAGCATCGGGGGAC R: GAATGTGAGCAAGCTGAGCG

mSEPN1 F: GCTTTCCTGTAGAGATGATG R:GCCCCGCCGGAGTCCTTC

mXBP1s F: GAGTCCGCAGCAGGTG R: GTGTCAGAGTCCATGGGA

mXBP1 total F: GGAGTGGAGTAAGGCTGGTG R: CCAGAATGCCCAAAGGATA

Statistics

All results were analysed using Prism 5 and 6 software (Graphpad). N was indicated in the figure legend except for dot plots. One asterisk was used for $p < 0.05$, two for $p < 0.01$, three for $p < 0.001$, and four for $p < 0.0001$.

Chapter 6 - Appendix

Publications by the candidate originated from the work described in this thesis:

- Diego Pozzer, Mariagrazia Favellato, Marco Bolis, Roberto William Invernizzi, Francesca Solagna, Bert Blaauw, Ester Zito

"Endoplasmic reticulum oxidative stress triggers tgf-beta-dependent muscle dysfunction by accelerating ascorbic acid turnover"

Scientific reports, 2017. January 20. https://doi.org/10.1038/srep40993

- Diego Pozzer, Ersilia Varone, Alexander Chernorudskiy, Silvia Schiarea, Sonia Missiroli, Carlotta Giorgi, Paolo Pinton, Marta Canato, Elena Germinario, Leonardo Nogara, Bert Blaauw, Ester Zito

"A maladaptive ER stress response triggers dysfunction in highly active muscles of mice with SELENON loss"

Redox biology, 2019, January 1. https://doi.org/10.1016/j.redox.2018.10.017

- Ersilia Varone, Diego Pozzer, Simona Di Modica, Alexander Chernorudskiy, Leonardo Nogara, Martina Baraldo, Mario Cinquanta, Stefano Fumagalli, Rocio Nur Villar-Quiles, Maria-Grazia De Simoni, Bert Blaauw, Ana Ferreiro, Ester Zito

"SELENON (SEPN1) protects skeletal muscle from saturated fatty acid-induced ER stress and insulin resistance"

Redox biology, 2019. June 1. https://doi.org/10.1016/j.redox.2019.101176

Chapter 7 - Bibliography

Abrams, C.K., Siram, S.M., Galsim, C., Johnson-Hamilton, H., Munford, F.L., Mezghebe, H., 1992. Selenium Deficiency in Long-Term Total Parenteral Nutrition. Nutrition in Clinical Practice 7, 175–178. https://doi.org/10.1177/0115426592007004175

Addinsall, A.B., Wright, C.R., Shaw, C.S., McRae, N.L., Forgan, L.G., Weng, C.-H., Conlan, X.A., Francis, P.S., Smith, Z.M., Andrikopoulos, S., Stupka, N., 2018. Deficiency of selenoprotein S, an endoplasmic reticulum resident oxidoreductase, impairs the contractile function of fast-twitch hindlimb muscles. American Journal of Physiology-Regulatory, Integrative and Comparative Physiology 315, R380–R396. https://doi.org/10.1152/ajpregu.00244.2017

Allamand, V., Richard, P., Lescure, A., Ledeuil, C., Desjardin, D., Petit, N., Gartioux, C., Ferreiro, A., Krol, A., Pellegrini, N., Urtizberea, J.A., Guicheney, P., 2006. A single homozygous point mutation in a 3'untranslated region motif of selenoprotein N mRNA causes SEPN1-related myopathy. EMBO reports 7, 450–454. https://doi.org/10.1038/sj.embor.7400648

Arbogast, S., Beuvin, M., Fraysse, B., Zhou, H., Muntoni, F., Ferreiro, A., 2009. Oxidative stress in *SEPN1* -related myopathy: From pathophysiology to treatment. Annals of Neurology 65, 677–686. https://doi.org/10.1002/ana.21644

Bai, J., 1980. [The combined effect of selenium deficiency and viral infection on the myocardium of mice (preliminary study) (author's transl)]. Zhongguo Yi Xue Ke Xue Yuan Xue Bao 2, 29–31.

Bánhegyi, G., Marcolongo, P., Puskás, F., Fulceri, R., Mandl, J., Benedetti, A., 1998. Dehydroascorbate and Ascorbate Transport in Rat Liver Microsomal Vesicles. Journal of Biological Chemistry 273, 2758–2762. https://doi.org/10.1074/jbc.273.5.2758

Blaauw, B., Canato, M., Agatea, L., Toniolo, L., Mammucari, C., Masiero, E., Abraham, R., Sandri, M., Schiaffino, S., Reggiani, C., 2009. Inducible activation of Akt increases skeletal muscle mass and force without satellite cell activation. The FASEB Journal 23, 3896–3905. https://doi.org/10.1096/fj.09-131870

Bode, A.M., Cunningham, L., Rose, R.C., 1990. Spontaneous decay of oxidized ascorbic acid (dehydro-L-ascorbic acid) evaluated by high-pressure liquid chromatography. Clin. Chem. 36, 1807–1809.

Boyle, P.E., Irving, J.T., 1951. Skeletal Muscle Changes in Scurvy with a Note on the Mechanism of the Attachment of Myofibrils to Tendon. Science 114, 572–573. https://doi.org/10.1126/science.114.2970.572

Caggiano, S., Khirani, S., Dabaj, I., Cavassa, E., Amaddeo, A., Arroyo, J.O., Desguerre, I., Richard, P., Cutrera, R., Ferreiro, A., Estournet, B., Quijano-Roy, S., Fauroux, B., 2017. Diaphragmatic dysfunction in SEPN1-related myopathy. Neuromuscular Disorders 27, 747–755. https://doi.org/10.1016/j.nmd.2017.04.010

Calcutt, G., 1951. The formation of hydrogen peroxide during the autoxidation of ascorbic acid. Experientia 7, 26–26. https://doi.org/10.1007/BF02165477

Callewaert, B.L., Willaert, A., Kerstjens-Frederikse, W.S., De Backer, J., Devriendt, K., Albrecht, B., Ramos-Arroyo, M.A., Doco-Fenzy, M., Hennekam, R.C.M., Pyeritz,

R.E., Krogmann, O.N., Gillessen-kaesbach, G., Wakeling, E.L., Nik-zainal, S., Francannet, C., Mauran, P., Booth, C., Barrow, M., Dekens, R., Loeys, B.L., Coucke, P.J., De Paepe, A.M., 2008. Arterial tortuosity syndrome: clinical and molecular findings in 12 newly identified families. Human Mutation 29, 150–158. https://doi.org/10.1002/humu.20623

Castets, P., Bertrand, A.T., Beuvin, M., Ferry, A., Le Grand, F., Castets, M., Chazot, G., Rederstorff, M., Krol, A., Lescure, A., Romero, N.B., Guicheney, P., Allamand, V., 2011. Satellite cell loss and impaired muscle regeneration in selenoprotein N deficiency. Human Molecular Genetics 20, 694–704. https://doi.org/10.1093/hmg/ddq515

Castets, P., Lescure, A., Guicheney, P., Allamand, V., 2012. Selenoprotein N in skeletal muscle: from diseases to function. Journal of Molecular Medicine 90, 1095–1107. https://doi.org/10.1007/s00109-012-0896-x

Chambers, I., Frampton, J., Goldfarb, P., Affara, N., McBain, W., Harrison, P.R., 1986. The structure of the mouse glutathione peroxidase gene: the selenocysteine in the active site is encoded by the 'termination' codon, TGA. The EMBO Journal 5, 1221–1227. https://doi.org/10.1002/j.1460-2075.1986.tb04350.x

Chatterjee, I.B., 1973. Evolution and the Biosynthesis of Ascorbic Acid. Science 182, 1271–1272. https://doi.org/10.1126/science.182.4118.1271

Chen, Xiaoshu, Yang, G., Chen, J., Chen, Xuecun, Wen, Z., Ge, K., 1980. Studies on the relations of selenium and Keshan disease. Biological Trace Element Research 2, 91–107. https://doi.org/10.1007/BF02798589

Clarke, N.F., Kidson, W., Quijano-Roy, S., Estournet, B., Ferreiro, A., Guicheney, P., Manson, J.I., Kornberg, A.J., Shield, L.K., North, K.N., 2006. *SEPN1* : Associated with congenital fiber-type disproportion and insulin resistance. Annals of Neurology 59, 546–552. https://doi.org/10.1002/ana.20761

Deldicque, L., Cani, P.D., Philp, A., Raymackers, J.-M., Meakin, P.J., Ashford, M.L.J., Delzenne, N.M., Francaux, M., Baar, K., 2010. The unfolded protein response is activated in skeletal muscle by high-fat feeding: potential role in the downregulation of protein synthesis. American Journal of Physiology-Endocrinology and Metabolism 299, E695–E705. https://doi.org/10.1152/ajpendo.00038.2010

Delesalle, C., de Bruijn, M., Wilmink, S., Vandendriessche, H., Mol, G., Boshuizen, B., Plancke, L., Grinwis, G., 2017. White muscle disease in foals: focus on selenium soil content. A case series. BMC Veterinary Research 13. https://doi.org/10.1186/s12917-017-1040-5

Deniziak, M., Thisse, C., Rederstorff, M., Hindelang, C., Thisse, B., Lescure, A., 2007. Loss of selenoprotein N function causes disruption of muscle architecture in the zebrafish embryo. Experimental Cell Research 313, 156–167. https://doi.org/10.1016/j.yexcr.2006.10.005

Dentice, M., Ambrosio, R., Damiano, V., Sibilio, A., Luongo, C., Guardiola, O., Yennek, S., Zordan, P., Minchiotti, G., Colao, A., Marsili, A., Brunelli, S., Del Vecchio, L., Larsen, P.R., Tajbakhsh, S., Salvatore, D., 2014. Intracellular Inactivation of Thyroid Hormone Is a Survival Mechanism for Muscle Stem Cell Proliferation and Lineage Progression. Cell Metabolism 20, 1038–1048. https://doi.org/10.1016/j.cmet.2014.10.009

Dentice, M., Marsili, A., Ambrosio, R., Guardiola, O., Sibilio, A., Paik, J.-H., Minchiotti, G., DePinho, R.A., Fenzi, G., Larsen, P.R., Salvatore, D., 2010. The FoxO3/type 2 deiodinase pathway is required for normal mouse myogenesis and muscle

regeneration. Journal of Clinical Investigation 120, 4021–4030. https://doi.org/10.1172/JCI43670
Drouin, G., Godin, J.-R., Page, B., 2011. The Genetics of Vitamin C Loss in Vertebrates. Current Genomics 12, 371–378. https://doi.org/10.2174/138920211796429736
Dumitrescu, A.M., Cosmo, C.D., Liao, X.-H., Weiss, R.E., Refetoff, S., 2010. The Syndrome of Inherited Partial SBP2 Deficiency in Humans. Antioxidants & Redox Signaling 12, 905–920. https://doi.org/10.1089/ars.2009.2892
Fain, O., 2005. Musculoskeletal manifestations of scurvy. Joint Bone Spine 72, 124–128. https://doi.org/10.1016/j.jbspin.2004.01.007
Ferreiro, A., Quijano-Roy, S., Pichereau, C., Moghadaszadeh, B., Goemans, N., Bönnemann, C., Jungbluth, H., Straub, V., Villanova, M., Leroy, J.-P., Romero, N.B., Martin, J.-J., Muntoni, F., Voit, T., Estournet, B., Richard, P., Fardeau, M., Guicheney, P., 2002a. Mutations of the Selenoprotein N Gene, Which Is Implicated in Rigid Spine Muscular Dystrophy, Cause the Classical Phenotype of Multiminicore Disease: Reassessing the Nosology of Early-Onset Myopathies. The American Journal of Human Genetics 71, 739–749. https://doi.org/10.1086/342719
Ferreiro, A., Quijano-Roy, S., Pichereau, C., Moghadaszadeh, B., Goemans, N., Bönnemann, C., Jungbluth, H., Straub, V., Villanova, M., Leroy, J.-P., Romero, N.B., Martin, J.-J., Muntoni, F., Voit, T., Estournet, B., Richard, P., Fardeau, M., Guicheney, P., 2002b. Mutations of the Selenoprotein N Gene, Which Is Implicated in Rigid Spine Muscular Dystrophy, Cause the Classical Phenotype of Multiminicore Disease: Reassessing the Nosology of Early-Onset Myopathies. The American Journal of Human Genetics 71, 739–749. https://doi.org/10.1086/342719
Finno, C.J., Valberg, S.J., 2012. A Comparative Review of Vitamin E and Associated Equine Disorders. Journal of Veterinary Internal Medicine 26, 1251–1266. https://doi.org/10.1111/j.1939-1676.2012.00994.x
Fohe, L., Gzler, W.A., 1973. Glutathione peroxidase: a selenoenzyme. FEBS Letters 3.
Fradejas-Villar, N., 2018. Consequences of mutations and inborn errors of selenoprotein biosynthesis and functions. Free Radical Biology and Medicine 127, 206–214. https://doi.org/10.1016/j.freeradbiomed.2018.04.572
Franzini-Armstrong, C., 2018. The relationship between form and function throughout the history of excitation–contraction coupling. The Journal of General Physiology 150, 189–210. https://doi.org/10.1085/jgp.201711889
Frontera, W.R., Ochala, J., 2015. Skeletal Muscle: A Brief Review of Structure and Function. Calcified Tissue International 96, 183–195. https://doi.org/10.1007/s00223-014-9915-y
Gamberucci, A., Marcolongo, P., Németh, C., Zoppi, N., Szarka, A., Chiarelli, N., Hegedűs, T., Ritelli, M., Carini, G., Willaert, A., Callewaert, B., Coucke, P., Benedetti, A., Margittai, É., Fulceri, R., Bánhegyi, G., Colombi, M., 2017. GLUT10—Lacking in Arterial Tortuosity Syndrome—Is Localized to the Endoplasmic Reticulum of Human Fibroblasts. International Journal of Molecular Sciences 18, 1820. https://doi.org/10.3390/ijms18081820
Ge, K., Xue, A., Bai, J., Wang, S., 1983. Keshan disease-an endemic cardiomyopathy in China. Pathol Anat 15.
Gladyshev, V.N., Arnér, E.S., Berry, M.J., Brigelius-Flohé, R., Bruford, E.A., Burk, R.F., Carlson, B.A., Castellano, S., Chavatte, L., Conrad, M., Copeland, P.R., Diamond, A.M., Driscoll, D.M., Ferreiro, A., Flohé, L., Green, F.R., Guigó, R., Handy, D.E.,

Hatfield, D.L., Hesketh, J., Hoffmann, P.R., Holmgren, A., Hondal, R.J., Howard, M.T., Huang, K., Kim, H.-Y., Kim, I.Y., Köhrle, J., Krol, A., Kryukov, G.V., Lee, B.J., Lee, B.C., Lei, X.G., Liu, Q., Lescure, A., Lobanov, A.V., Loscalzo, J., Maiorino, M., Mariotti, M., Sandeep Prabhu, K., Rayman, M.P., Rozovsky, S., Salinas, G., Schmidt, E.E., Schomburg, L., Schweizer, U., Simonović, M., Sunde, R.A., Tsuji, P.A., Tweedie, S., Ursini, F., Whanger, P.D., Zhang, Y., 2016. Selenoprotein Gene Nomenclature. Journal of Biological Chemistry 291, 24036–24040. https://doi.org/10.1074/jbc.M116.756155

Glancy, B., Willis, W.T., Chess, D.J., Balaban, R.S., 2013. Effect of Calcium on the Oxidative Phosphorylation Cascade in Skeletal Muscle Mitochondria. Biochemistry 52, 2793–2809. https://doi.org/10.1021/bi3015983

Higo, T., Hattori, M., Nakamura, T., Natsume, T., Michikawa, T., Mikoshiba, K., 2005. Subtype-Specific and ER Lumenal Environment-Dependent Regulation of Inositol 1,4,5-Trisphosphate Receptor Type 1 by ERp44. Cell 120, 85–98. https://doi.org/10.1016/j.cell.2004.11.048

Hoekstra, W.G., 1975. Biochemical function of selenium and its relation to vitamin E. Fed. Proc. 34, 2083–2089.

Johansson, L., Gafvelin, G., Arnér, E.S.J., 2005. Selenocysteine in proteins—properties and biotechnological use. Biochimica et Biophysica Acta (BBA) - General Subjects 1726, 1–13. https://doi.org/10.1016/j.bbagen.2005.05.010

Jurynec, M.J., Xia, R., Mackrill, J.J., Gunther, D., Crawford, T., Flanigan, K.M., Abramson, J.J., Howard, M.T., Grunwald, D.J., 2008. Selenoprotein N is required for ryanodine receptor calcium release channel activity in human and zebrafish muscle. PNAS 105, 12485–12490. https://doi.org/10.1073/pnas.0806015105

Kraemer, W.J., Fleck, S.J. & Deschenes, M.R., 2012. Exercise physiology: integrating theory and application. Philadelphia Lippincott Williams & Wilkins.

Kryukov, G.V., Castellano, S., Nosolev, S.V., Lobanov, A.V., Zehtab, O., Guigó, R., Gladyshev, V.N., 2003. Characterization of Mammalian Selenoproteomes. Science 300, 1439–1443. https://doi.org/10.1126/science.1083516

Lauretani, F., Semba, R.D., Bandinelli, S., Ray, A.L., Guralnik, J.M., Ferrucci, L., 2007. Association of low plasma selenium concentrations with poor muscle strength in older community-dwelling adults: the InCHIANTI Study1Ƹ3 6.

Lescure, A., Gautheret, D., Carbon, P., Krol, A., 1999. Novel Selenoproteins Identified in Silico andin Vivo by Using a Conserved RNA Structural Motif. J. Biol. Chem. 274, 38147–38154. https://doi.org/10.1074/jbc.274.53.38147

Lescure, A., Rederstorff, M., Krol, A., Guicheney, P., Allamand, V., 2009. Selenoprotein function and muscle disease. Biochimica et Biophysica Acta (BBA) - General Subjects 1790, 1569–1574. https://doi.org/10.1016/j.bbagen.2009.03.002

Levander, O.A., Beck, M.A., 1997. Interacting nutritional and infectious etiologies of Keshan disease: Insights from coxsackie virus B-induced myocarditis in mice deficient in selenium or vitamin E. Biological Trace Element Research 56, 5–21. https://doi.org/10.1007/BF02778980

Levine, M., Conry-Cantilena, C., Wang, Y., Welch, R.W., Washko, P.W., Dhariwal, K.R., Park, J.B., Lazarev, A., Graumlich, J.F., King, J., Cantilena, L.R., 1996. Vitamin C pharmacokinetics in healthy volunteers: evidence for a recommended dietary allowance. Proceedings of the National Academy of Sciences 93, 3704–3709. https://doi.org/10.1073/pnas.93.8.3704

Levine, M., Padayatty, S.J., Espey, M.G., 2011. Vitamin C: A Concentration-Function Approach Yields Pharmacology and Therapeutic Discoveries. Advances in Nutrition 2, 78–88. https://doi.org/10.3945/an.110.000109

Li, Y., Camacho, P., 2004. Ca $^{2+}$ -dependent redox modulation of SERCA 2b by ERp57. The Journal of Cell Biology 164, 35–46. https://doi.org/10.1083/jcb.200307010

Lilley, B.N., Ploegh, H.L., 2004. A membrane protein required for dislocation of misfolded proteins from the ER. Nature 429, 834–840. https://doi.org/10.1038/nature02592

Lin, L., Shen, S., Tye, A., Cai, J.J., Jiang, P., Davidson, B.L., Xing, Y., 2008. Diverse Splicing Patterns of Exonized Alu Elements in Human Tissues. PLoS Genetics 4, e1000225. https://doi.org/10.1371/journal.pgen.1000225

Lippman, S.M., Klein, E.A., Goodman, P.J., Lucia, M.S., Thompson, I.M., Ford, L.G., Parnes, H.L., Minasian, L.M., Gaziano, J.M., Hartline, J.A., Parsons, J.K., Bearden, J.D., Crawford, E.D., Goodman, G.E., Claudio, J., Winquist, E., Cook, E.D., Karp, D.D., Walther, P., Lieber, M.M., Kristal, A.R., Darke, A.K., Arnold, K.B., Ganz, P.A., Santella, R.M., Albanes, D., Taylor, P.R., Probstfield, J.L., Jagpal, T.J., Crowley, J.J., Meyskens, F.L., Baker, L.H., Coltman, C.A., 2009. Effect of Selenium and Vitamin E on Risk of Prostate Cancer and Other Cancers: The Selenium and Vitamin E Cancer Prevention Trial (SELECT). JAMA 301, 39. https://doi.org/10.1001/jama.2008.864

Loflin, J., Lopez, N., Whanger, P.D., Kioussi, C., 2006. Selenoprotein W during development and oxidative stress. Journal of Inorganic Biochemistry 100, 1679–1684. https://doi.org/10.1016/j.jinorgbio.2006.05.018

Loscalzo, J., 2014. Keshan Disease, Selenium Deficiency, and the Selenoproteome. New England Journal of Medicine 370, 1756–1760. https://doi.org/10.1056/NEJMcibr1402199

Low, M., Sandoval, D., Avilés, E., Pérez, F., Nualart, F., Henríquez, J.P., 2009. The ascorbic acid transporter SVCT2 is expressed in slow-twitch skeletal muscle fibres. Histochemistry and Cell Biology 131, 565–574. https://doi.org/10.1007/s00418-008-0552-2

Lu, C., Qiu, F., Zhou, H., Peng, Y., Hao, W., Xu, J., Yuan, J., Wang, S., Qiang, B., Xu, C., Peng, X., 2006. Identification and characterization of selenoprotein K: An antioxidant in cardiomyocytes. FEBS Letters 580, 5189–5197. https://doi.org/10.1016/j.febslet.2006.08.065

Lu, J., Berndt, C., Holmgren, A., 2009. Metabolism of selenium compounds catalyzed by the mammalian selenoprotein thioredoxin reductase. Biochimica et Biophysica Acta (BBA) - General Subjects 1790, 1513–1519. https://doi.org/10.1016/j.bbagen.2009.04.013

Maeda, N., Hagihara, H., Nakata, Y., Hiller, S., Wilder, J., Reddick, R., 2000. Aortic wall damage in mice unable to synthesize ascorbic acid. Proceedings of the National Academy of Sciences 97, 841–846. https://doi.org/10.1073/pnas.97.2.841

Makałowski, W., Mitchell, G.A., Labuda, D., 1994. Alu sequences in the coding regions of mRNA: a source of protein variability. Trends in Genetics 10, 188–193. https://doi.org/10.1016/0168-9525(94)90254-2

Marciniak, S.J., Yun, C., Oyadomari, S., Novoa, I., Zhang, Y., Jungreis, R., Nagata, K., Harding, H.P., Ron, D., 2004. CHOP induces death by promoting protein synthesis and oxidation in the stressed endoplasmic reticulum. Genes & Development 18, 3066–3077. https://doi.org/10.1101/gad.1250704

Marino, M., Stoilova, T., Giorgi, C., Bachi, A., Cattaneo, A., Auricchio, A., Pinton, P., Zito, E., 2015. SEPN1, an endoplasmic reticulum-localized selenoprotein linked to skeletal muscle pathology, counteracts hyperoxidation by means of redox-regulating SERCA2 pump activity. Human Molecular Genetics 24, 1843–1855. https://doi.org/10.1093/hmg/ddu602

Marsili, A., Larsen, P.R., Zavacki, A.M., 2016. Tissue-Specific Regulation of Thyroid Status by Selenodeiodinases, in: Hatfield, D.L., Schweizer, U., Tsuji, P.A., Gladyshev, V.N. (Eds.), Selenium. Springer International Publishing, Cham, pp. 487–498. https://doi.org/10.1007/978-3-319-41283-2_41

Moghadaszadeh, B., Petit, N., Jaillard, C., Brockington, M., Roy, S.Q., Merlini, L., Romero, N., Estournet, B., Desguerre, I., Chaigne, D., Muntoni, F., Topaloglu, H., Guicheney, P., 2001. Mutations in SEPN1 cause congenital muscular dystrophy with spinal rigidity and restrictive respiratory syndrome. Nature Genetics 29, 17–18. https://doi.org/10.1038/ng713

Moghadaszadeh, B., Rider, B.E., Lawlor, M.W., Childers, M.K., Grange, R.W., Gupta, K., Boukedes, S.S., Owen, C.A., Beggs, A.H., 2013. Selenoprotein N deficiency in mice is associated with abnormal lung development. The FASEB Journal 27, 1585–1599. https://doi.org/10.1096/fj.12-212688

Montel-Hagen, A., Kinet, S., Manel, N., Mongellaz, C., Prohaska, R., Battini, J.-L., Delaunay, J., Sitbon, M., Taylor, N., 2008. Erythrocyte Glut1 Triggers Dehydroascorbic Acid Uptake in Mammals Unable to Synthesize Vitamin C. Cell 132, 1039–1048. https://doi.org/10.1016/j.cell.2008.01.042

Muñoz-Montesino, C., Roa, F.J., Peña, E., González, M., Sotomayor, K., Inostroza, E., A. Muñoz, C., González, I., Maldonado, M., Soliz, C., Reyes, A.M., Vera, J.C., Rivas, C.I., 2014. Mitochondrial ascorbic acid transport is mediated by a low-affinity form of the sodium-coupled ascorbic acid transporter-2. Free Radical Biology and Medicine 70, 241–254. https://doi.org/10.1016/j.freeradbiomed.2014.02.021

Myllyharju, J., 2008. Prolyl 4-hydroxylases, key enzymes in the synthesis of collagens and regulation of the response to hypoxia, and their roles as treatment targets. Annals of Medicine 40, 402–417. https://doi.org/10.1080/07853890801986594

Nakata, Y., Maeda, N., 2002. Vulnerable Atherosclerotic Plaque Morphology in Apolipoprotein E–Deficient Mice Unable to Make Ascorbic Acid. Circulation 105, 1485–1490. https://doi.org/10.1161/01.CIR.0000012142.69612.25

Noctor, G., Foyer, C.H., 1998. ASCORBATE AND GLUTATHIONE: Keeping Active Oxygen Under Control. Annual Review of Plant Physiology and Plant Molecular Biology 49, 249–279. https://doi.org/10.1146/annurev.arplant.49.1.249

Noh, O.J., Park, Y.H., Chung, Y.W., Kim, I.Y., 2010. Transcriptional Regulation of Selenoprotein W by MyoD during Early Skeletal Muscle Differentiation. Journal of Biological Chemistry 285, 40496–40507. https://doi.org/10.1074/jbc.M110.152934

Omaye, S.T., Schaus, E.E., Kutnink, M.A., Hawkes, W.C., 1987. Measurement of Vitamin C in Blood Components by High-Performance Liquid Chromatography.: Implication in Assessing Vitamin C Status. Annals of the New York Academy of Sciences 498, 389–401. https://doi.org/10.1111/j.1749-6632.1987.tb23776.x

Panzhinskiy, E., Hua, Y., Culver, B., Ren, J., Nair, S., 2013. Endoplasmic reticulum stress upregulates protein tyrosine phosphatase 1B and impairs glucose uptake in cultured myotubes. Diabetologia 56, 598–607. https://doi.org/10.1007/s00125-012-2782-z

Papp, L.V., Holmgren, A., Khanna, K.K., 2010. Selenium and Selenoproteins in Health and Disease. Antioxidants & Redox Signaling 12, 793–795. https://doi.org/10.1089/ars.2009.2973

Pennuto, M., Tinelli, E., Malaguti, M., Del Carro, U., D'Antonio, M., Ron, D., Quattrini, A., Feltri, M.L., Wrabetz, L., 2008. Ablation of the UPR-Mediator CHOP Restores Motor Function and Reduces Demyelination in Charcot-Marie-Tooth 1B Mice. Neuron 57, 393–405. https://doi.org/10.1016/j.neuron.2007.12.021

Perry, B.D., Rahnert, J.A., Xie, Y., Zheng, B., Woodworth-Hobbs, M.E., Price, S.R., 2018. Palmitate-induced ER stress and inhibition of protein synthesis in cultured myotubes does not require Toll-like receptor 4. PLOS ONE 13, e0191313. https://doi.org/10.1371/journal.pone.0191313

Petit, N., Lescure, A., Rederstorff, M., Krol, A., Moghadaszadeh, B., Wewer, U., Guicheney, P., 2003. Selenoprotein N: an endoplasmic reticulum glycoprotein with an early developmental expression pattern. Human Molecular Genetics 12, 1045–1053. https://doi.org/10.1093/hmg/ddg115

Pollard, M.G., Travers, K.J., Weissman, J.S., 1998. Ero1p: a novel and ubiquitous protein with an essential role in oxidative protein folding in the endoplasmic reticulum. Mol. Cell 1, 171–182.

Porter, K.R., 1945. A STUDY OF TISSUE CULTURE CELLS BY ELECTRON MICROSCOPY: METHODS AND PRELIMINARY OBSERVATIONS. Journal of Experimental Medicine 81, 233–246. https://doi.org/10.1084/jem.81.3.233

Rayman, M.P., 2008. Food-chain selenium and human health: emphasis on intake. British Journal of Nutrition 100, 254–268. https://doi.org/10.1017/S0007114508939830

Rayman, M.P., 2004. The use of high-selenium yeast to raise selenium status: how does it measure up? British Journal of Nutrition 92, 557. https://doi.org/10.1079/BJN20041251

Rederstorff, M., Castets, P., Arbogast, S., Lainé, J., Vassilopoulos, S., Beuvin, M., Dubourg, O., Vignaud, A., Ferry, A., Krol, A., Allamand, V., Guicheney, P., Ferreiro, A., Lescure, A., 2011. Increased Muscle Stress-Sensitivity Induced by Selenoprotein N Inactivation in Mouse: A Mammalian Model for SEPN1-Related Myopathy. PLoS ONE 6, e23094. https://doi.org/10.1371/journal.pone.0023094

Rocha, J.B., Piccoli, B.C., Oliveira, C.S., 2016. Biological and chemical interest in selenium: a brief historical account. Arkivoc 2017, 457–491. https://doi.org/10.24820/ark.5550190.p009.784

Ron, D., Walter, P., 2007. Signal integration in the endoplasmic reticulum unfolded protein response. Nature Reviews Molecular Cell Biology 8, 519–529. https://doi.org/10.1038/nrm2199

Rumsey, S.C., Daruwala, R., Al-Hasani, H., Zarnowski, M.J., Simpson, I.A., Levine, M., 2000. Dehydroascorbic acid Transport by GLUT4 in Xenopus Oocytes and Isolated Rat Adipocytes. Journal of Biological Chemistry. https://doi.org/10.1074/jbc.M000988200

Savini, I., Valeria Catani, M., Duranti, G., Ceci, R., Sabatini, S., Avigliano, L., 2005. Vitamin C homeostasis in skeletal muscle cells. Free Radical Biology and Medicine 38, 898–907. https://doi.org/10.1016/j.freeradbiomed.2004.12.009

Schmid, C., Jelinek, W., 1982. The Alu family of dispersed repetitive sequences. Science 216, 1065–1070. https://doi.org/10.1126/science.6281889

Schmidt, E.K., Clavarino, G., Ceppi, M., Pierre, P., 2009. SUnSET, a nonradioactive method to monitor protein synthesis. Nature Methods 6, 275–277. https://doi.org/10.1038/nmeth.1314

Segade, F., 2010. Glucose transporter 10 and arterial tortuosity syndrome: The vitamin C connection. FEBS Letters 584, 2990–2994. https://doi.org/10.1016/j.febslet.2010.06.011

Shchedrina, V.A., Zhang, Y., Labunskyy, V.M., Hatfield, D.L., Gladyshev, V.N., 2010. Structure–Function Relations, Physiological Roles, and Evolution of Mammalian ER-Resident Selenoproteins. Antioxidants & Redox Signaling 12, 839–849. https://doi.org/10.1089/ars.2009.2865

Song, B., Scheuner, D., Ron, D., Pennathur, S., Kaufman, R.J., 2008. Chop deletion reduces oxidative stress, improves β cell function, and promotes cell survival in multiple mouse models of diabetes. Journal of Clinical Investigation 118, 3378–3389. https://doi.org/10.1172/JCI34587

Sun, Q.-A., Hess, D.T., Nogueira, L., Yong, S., Bowles, D.E., Eu, J., Laurita, K.R., Meissner, G., Stamler, J.S., 2011. Oxygen-coupled redox regulation of the skeletal muscle ryanodine receptor-Ca2+ release channel by NADPH oxidase 4. Proceedings of the National Academy of Sciences 108, 16098–16103. https://doi.org/10.1073/pnas.1109546108

Tavender, T.J., Springate, J.J., Bulleid, N.J., 2010. Recycling of peroxiredoxin IV provides a novel pathway for disulphide formation in the endoplasmic reticulum. The EMBO Journal 29, 4185–4197. https://doi.org/10.1038/emboj.2010.273

Unger, R.H., Scherer, P.E., 2010. Gluttony, sloth and the metabolic syndrome: a roadmap to lipotoxicity. Trends Endocrinol. Metab. 21, 345–352. https://doi.org/10.1016/j.tem.2010.01.009

Vinceti, M., Burlingame, B., Filippini, T., Naska, A., Bargellini, A., Borella, P., 2016. The Epidemiology of Selenium and Human Health, in: Hatfield, D.L., Schweizer, U., Tsuji, P.A., Gladyshev, V.N. (Eds.), Selenium. Springer International Publishing, Cham, pp. 365–376. https://doi.org/10.1007/978-3-319-41283-2_31

Weekley, C.M., Harris, H.H., 2013. Which form is that? The importance of selenium speciation and metabolism in the prevention and treatment of disease. Chemical Society Reviews 42, 8870. https://doi.org/10.1039/c3cs60272a

Wells, W.W., Xu, D.P., 1994. Dehydroascorbate reduction. Journal of Bioenergetics and Biomembranes 26, 369–377. https://doi.org/10.1007/BF00762777

Whanger, P.D., 2000. Selenoprotein W: a review: Cellular and Molecular Life Sciences 57, 1846–1852. https://doi.org/10.1007/PL00000666

Wilson, J.X., 2002. The physiological role of dehydroascorbic acid. FEBS Letters 527, 5–9. https://doi.org/10.1016/S0014-5793(02)03167-8

Wu, J., Ruas, J.L., Estall, J.L., Rasbach, K.A., Choi, J.H., Ye, L., Boström, P., Tyra, H.M., Crawford, R.W., Campbell, K.P., Rutkowski, D.T., Kaufman, R.J., Spiegelman, B.M., 2011. The Unfolded Protein Response Mediates Adaptation to Exercise in Skeletal Muscle through a PGC-1α/ATF6α Complex. Cell Metabolism 13, 160–169. https://doi.org/10.1016/j.cmet.2011.01.003

Yang, G.Q., 1985. Keshan disease: an endemic selenium-related deficiency disease. Nestle nutrition workshop series (USA).

Zinoni, F., Birkmann, A., Stadtman, T.C., Bock, A., 1986. Nucleotide sequence and expression of the selenocysteine-containing polypeptide of formate dehydrogenase (formate-hydrogen-lyase-linked) from Escherichia coli.

Proceedings of the National Academy of Sciences 83, 4650–4654. https://doi.org/10.1073/pnas.83.13.4650

Zinszner, H., Kuroda, M., Wang, X., Batchvarova, N., Lightfoot, R.T., Remotti, H., Stevens, J.L., Ron, D., 1998. CHOP is implicated in programmed cell death in response to impaired function of the endoplasmic reticulum. Genes Dev. 12, 982–995. https://doi.org/10.1101/gad.12.7.982

Zito, E., 2015. ERO1: A protein disulfide oxidase and H2O2 producer. Free Radical Biology and Medicine 83, 299–304. https://doi.org/10.1016/j.freeradbiomed.2015.01.011

Zito, E., 2013. PRDX4, an Endoplasmic Reticulum-Localized Peroxiredoxin at the Crossroads Between Enzymatic Oxidative Protein Folding and Nonenzymatic Protein Oxidation. Antioxidants & Redox Signaling 18, 1666–1674. https://doi.org/10.1089/ars.2012.4966

Zito, E., Hansen, H.G., Yeo, G.S.H., Fujii, J., Ron, D., 2012. Endoplasmic Reticulum Thiol Oxidase Deficiency Leads to Ascorbic Acid Depletion and Noncanonical Scurvy in Mice. Molecular Cell 48, 39–51. https://doi.org/10.1016/j.molcel.2012.08.010